A THEORETICAL AND NUMERICAL STUDY OF ELECTROTHERMAL INSTABILITIES AND NON-EQUILIBRIUM PHENOMENA IN A PARTIALLY IONIZED MAGNETIZED PLASMA

by

REGINALD JAMES UNCLES

A Thesis Submitted for the Degree of Doctor of Philosophy
in the University of London

Physics Department
Imperial College of Science & Technology
London SW7 2BZ

July 1972

CONTENTS

Page

ABSTRACT 1

ACKNOWLEDGEMENTS 3

CHAPTER I: INTRODUCTION 4

1.1 The MHD Concept
1.2 Simple Generator Systems
  (a) Continuous Electrode System
  (b) Segmented Electrode Generator
  (c) Hall Generator
1.3 Effective Conductivity and Effective Hall Parameter
1.4 Closed Cycle and Open Cycle Systems
1.5 Non-Equilibrium Ionization
  (a) Dependence of Non-Equilibrium Ionization on the Hall Parameter
  (b) The Electrothermal Instability
  (c) Non-Uniformities with Hall Effect
1.6 Motivation for Numerical Model

CHAPTER II: THEORETICAL DESCRIPTION OF NON-EQUILIBRIUM PLASMA 21

2.1 Introduction
2.2 Equations of Motion
  (a) Electron Continuity
  (b) Electron Momentum
  (c) Electron Energy Equation
  (d) Field Equations
2.3 Assumptions Involved in Treating as a Closed Set
2.4 Characteristics of Equations
  (a) Full Set Including Thermal Conductivity
  (b) Full Set Neglecting Thermal Conductivity
  (c) Full Set with the Assumption of Saha Equilibrium
  (d) Full Set with Assumption of Saha Equilibrium and Neglecting Thermal Conductivity
  (e) Neglect of Spatial Gradients in Energy Equation
2.5 Summary

CHAPTER III: CHARACTERISTIC TIMES AND LENGTHS OF THE ELECTROTHERMAL INSTABILITY 43

3.1 Introduction
3.2 Linear Perturbation of the Equations
3.3 Electrothermal Growth Rates
3.4 Electrothermal Modes
  (a) Fast-Thermal Mode
  (b) Ionization Mode
3.5 Simplified Model of Ionization Mode
  (a) Coulomb Collision Dominated Plasma
  (b) Binary Collision Dominated Plasma

Page

3.6 Effect of Boundaries on the Electrothermal Instability
(a) Linear Perturbation of Equations
(b) Hyperbolic Nature of the Equations
3.7 Non-Linear Effects of the Electrothermal Instability
(a) Effective Conductivity
(b) Effective Hall Parameter
3.8 Summary

CHAPTER IV: DYNAMIC STABILIZATION OF THE ELECTRO-THERMAL INSTABILITY 63

4.1 Introduction
4.2 The Stabilizing Fields
4.3 Stability Analysis
4.4 Discussion of Results
4.5 Summary

CHAPTER V: NUMERICAL SOLUTION OF THE ELECTROTHERMAL EQUATIONS 77

5.1 Introduction
5.2 Analysis of Time-Scales
(a) Continuity Equation
(b) Energy Equation
(c) Wave Processes
5.3 Time Differencing
(a) Stability to Local Terms
(b) Stability to Flux Terms
5.4 Treatment of Convective Terms
5.5 Solution of the Ohms Law
5.6 Inclusion of Circuit Effects
5.7 Boundary Conditions
(a) Open System
(b) Periodic System
5.8 Some Results for Segmented Electrodes
5.9 Difficulties with the Numerical Model
(a) Effect of Fast-Thermal Mode
(b) Mesh Uncoupling
5.10 Summary

CHAPTER VI: NUMERICAL SIMULATION OF ELECTROTHERMAL WAVES 105

6.1 Introduction
6.2 Removal of Fast-Thermal Mode from System
6.3 Growth Rates for Insulator Walls and Electrode Walls
6.4 Insulator Walls
(a) Temporal Behaviour of Averaged Parameters
(b) Steady State Structure and Wave Velocity
6.5 Effect of External Circuits on the Steady State
6.6 Inclusion of Thermal Conductivity and Radiation Damping
6.7 Growth of Waves in Continuous Electrode Geometry
6.8 Conclusions and Comparison with Experiment

Page

CHAPTER VII: CURRENT AND DENSITY DISTRIBUTIONS IN A SEGMENTED ELECTRODE GENERATOR 138

7.1 Introduction
7.2 The Uniform Generator
(a) Effective Conductivity and Hall Parameter
(b) Electrode Leakage
7.3 Effect of Non-Equilibrium on Conduction
(a) Temporal Behaviour of Averaged Parameters
(b) Quasi-Steady States
(c) Discussion of Results
(d) Velocity Effects
(e) Effect of Reducing L/H
7.4 Multisegment Systems
7.5 Conclusions and Comparison with Experiment

SUMMARY 173

A Note on Nomenclature 176

REFERENCES 177

ABSTRACT

The purpose of this thesis is to investigate theoretically the behaviour of low-temperature, highly magnetized, partially ionized plasmas in the context of the closed cycle MHD application.

The growth of large amplitude electrothermal instabilities in this type of plasma is considered, and the effects of experimental configuration and instabilities on the current conduction discussed.

The equations of the electrothermal system, and the assumptions involved in them, are discussed in Chapter II. The mathematical 'type' of these equations is discussed under various approximations to provide a basis for the choice of boundary conditions.

In Chapter III, a simple linear theory is used to derive analytic formulae for the electrothermal growth rates, both for the infinite and bounded plasma. Expressions for the effective electrical conductivity and Hall parameter are obtained in the case of one-dimensional non-uniformities.

A method of stabilizing the electrothermal instability is suggested in Chapter IV. A linear theory is used to show that applied oscillatory electric fields, of sufficiently large amplitude and frequency, can lead to stabilization of the wave.

In Chapter V, a numerical model for the solution of the electrothermal system is presented. Conditions for numerical stability are discussed and the results of some preliminary calculations given.

In Chapter VI, a modified version of this model is used to follow the growth of electrothermal instabilities, in simple configurations, to their final large amplitude state. The interaction of the waves with external circuits is considered and comparisons with experimental results are made.

The growth and behaviour of non-uniformities in segmented electrode configurations are discussed in Chapter VII. It is shown that the assumption of periodic boundary conditions does not alter the essential physics, and the results obtained are compared with those for the uniform generator and experiment.

ACKNOWLEDGEMENTS

The work for this thesis was carried out while the author was a member of the Imperial College Plasma Physics Group.

He wishes to express his gratitude to Dr M G Haines, his supervisor, for many helpful and enlightening discussions during the course of this work.

The author also wishes to thank Dr D E Potter and Dr A H Nelson for numerous informal discussions.

Regarding the preparation of the thesis, the author thanks his wife, Glynnis, for typing the manuscript and for her help in the preparation of the figures.

During the course of this work the author was supported by a grant from the Science Research Council.

CHAPTER I

INTRODUCTION

1.1 The MHD Concept

In a magnetohydrodynamic (MHD) generator, an electrically conducting fluid is directed through a magnetic field at high velocity, $\underline{v}$, as shown in figures 1.1, 1.2, 1.3. The induced electric field, $\underline{v} \times \underline{B}$, generated in the fluid results in a current flow, $\underline{j}$, if a return path for the flow is provided, and the resultant $\underline{j} \times \underline{B}$ magnetomotive force retards the motion of the fluid. Electrical energy is therefore obtained at the expense of the internal energy of the fluid and kinetic energy of flow.

These are also, of course, the working principles of the electric dynamo. The important features of the MHD generator as a power source, however, are its ability to use very high temperature heat sources, and the fact that the induced electric field depends upon the flow velocity of a fluid, unlike the dynamo in which the induced electric field is related to the rate of rotation of a solid armature.

The working fluid of the MHD generator may be either a liquid metal or a plasma. Whilst the liquid metal generator may be attractive for certain applications, it will not be considered in this thesis. A general review of the plasma MHD generator has been provided by Brogan (1968).

If the generator is to extract a large proportion of the flow energy over a length, ℓ, then the magnetomotive force must satisfy

$$\int_0^{\ell} j_x B \, dy \sim \rho v^2$$

If, as in figure 1.2, the only component of current flow is normal to both $\underline{v}$ and $\underline{B}$, then $j_x \sim \sigma v B$, and the generator must satisfy

$$s = \sigma B^2 \ell / \rho v = R_M R_H \sim 1 \qquad (1.1)$$

for appreciable extraction of energy. Where R_m is the magnetic Reynolds number, and R_H is the ratio of magnetic to kinetic energy densities; for the plasma generator $R_m \ll 1$, and $R_H \gg 1$.

The source of plasma for the generator may be either a combustion process or heat exchange with a fission reactor. In either case electrical energy may be extracted by the MHD process at the high temperature end, whilst the generator exhaust may be used to drive a steam cycle. If one considers an interaction parameter, s, of 0.1 to be the minimum for the economic feasibility of such a system, then from equation (1.1) one requires $\sigma \gtrsim 10$ M m^{-1} for B = 1 T, $v = 10^3$ m sec^{-1}, $\rho = 1$ Kg m^{-3} and L = 10 m.

At the temperatures corresponding to the above heat sources, less than 3500°K for the combustion process, and less than 2000°K for the nuclear reactor, the latent electrical conductivity of generator fluids is very small, and is increased by seeding the fluid with a small amount of alkali metal. The first serious experiments on MHD power generation were performed by Karlovitz et al (1962), but these were unsuccessful due to the low values of electrical conductivity attained;

and much of the more recent research in generator fluids has been directed towards the attainment of large values of electrical conductivity in low temperature plasmas (Zauderer, 1968; Kerrebrock, 1964; Cool et al, 1968; Haines et al, 1968a).

The purpose of this thesis is to investigate theoretically the behaviour of low temperature, highly magnetized, partially ionized plasmas in the context of the closed cycle MHD application.

1.2 Simple Generator Systems

At the temperatures, densities and magnetic field strengths pertinent to the MHD process, the electron Hall parameter, β, typically lies in the range 1 to 10. The Hall effect is therefore an important consideration in determining the behaviour of the MHD plasma, and many of the difficulties experienced in power generation experiments can be attributed to the presence of the Hall effect. An Ohms law for the uniform plasma may be written

$$\underline{j} = \sigma \underline{\mathcal{E}} - \underline{j} \times \underline{\beta} \qquad (1.2)$$

with $\underline{\mathcal{E}} = \underline{E} + \underline{V} \times \underline{B}$

in which slip between ions and the other heavy particles is neglected, ie: negligible ion Hall parameter, and thermo-electric effects are neglected. The magnetic field is taken to be $\underline{B} = B\hat{\underline{z}}$ = constant. Equation (1.2) in component form is

$$\begin{aligned} j_x &= \frac{\sigma}{1+\beta^2}\left[\mathcal{E}_x - \beta \mathcal{E}_y\right] \\ j_y &= \frac{\sigma}{1+\beta^2}\left[\mathcal{E}_y + \beta \mathcal{E}_x\right] \\ j_z &= \sigma \mathcal{E}_z \end{aligned} \qquad (1.3)$$

For the two-dimensional systems considered in this thesis $j_z = 0 = \mathcal{E}_z$, and

$$\beta = \tan\theta = \left| \frac{\underline{j} \times \underline{\mathcal{E}}}{\underline{j} \cdot \underline{\mathcal{E}}} \right|$$

so that the current flow is always inclined to the total electric vector at the Hall angle; furthermore, for the uniform plasma, $\underline{\mathcal{E}}$ is just the sum of induced electric fields, and electric fields due to voltage drops across external circuitry.

In subsections (a)-(c) it is assumed that σ = constant and v = constant. This, in general, requires the current density to be independent of position, and the interaction length to greatly exceed the duct length.

(a) Continuous Electrode System

Figure 1.1 shows a continous electrode duct in which the plasma flows between parallel electrodes. The electrodes 'short' out the 'y' component of electric field $E_y = 0$, and the current therefore flows at an angle $\tan^{-1}\beta$ to the 'x' direction. The maximum power delivered to a matched load, per unit volume of generator, is thus

$$\left[j_x^2/\sigma_L \right]_{max} = \frac{\sigma}{4(1+\beta^2)} v^2 B^2$$

in which $\sigma_L = {}^{H}/_{R_L A}$, where H is the electrode separation, and A the electrode area. The output power saturates as a function of magnetic field, and this configuration is only useful for small values of the magnetic field. This result follows from the increased impedance of the device as the Hall parameter is increased, and the ensuing internal dissipation due to shorted Hall currents.

(b) Segmented Electrode Generator

In order to prevent the flow of Hall currents the electrodes can be segmented, as is shown in figure 1.2. This, in principle, prevents the flow of axial currents by formation of a space-charge field sufficient to maintain $j_y = 0$, ie: $\mathcal{E}_y = -\beta \mathcal{E}_x$, and allows a transverse current, j_x, to flow of magnitude $\sigma \mathcal{E}_x$. This is the case of infinite segmentation in which the segmentation period is considerably smaller than the cathode-anode separation, and there is no leakage current between electrode pairs. The maximum power output to a matched load, per unit volume of generator, is

$$\left[j_x^2 / \sigma_L \right]_{max} = \frac{1}{4} \sigma V^2 B^2$$

which increases quadratically with magnetic field. The majority of MHD experiments utilize this device, although the problems involved in maintaining an adequate Hall field, as discussed by Hoffmann (1968) and Kerrebrock (1966), are very great. Contributory features to the suppression of the Hall field include plasma to ground leakage, electrode-electrode leakage, plasma non-uniformities and so forth.

(c) Hall Generator

The Hall generator, shown in figure 1.3, shorts the induced currents and uses the Hall voltage to provide power to the external load. The maximum power output in this case is, assuming infinite segmentation,

$$\left[j_x^2 / \sigma_L \right]_{max} = \frac{1}{4} \sigma V^2 B^2 \left[\frac{\beta^2}{1 + \beta^2} \right]$$

which approaches the segmented electrode value at large Hall parameter.

1.3 Effective Conductivity and Effective Hall Parameter

The effective conductivity, σ_{eff}, and the effective Hall parameter, β_{eff}, are two properties of the MHD plasma which can be used to correlate plasma behaviour between different experiments. If $\langle \underline{j} \rangle$ is defined as the space averaged current density, then σ_{eff}, β_{eff} are defined as follows

$$|\langle \underline{j} \rangle| = \sigma_{eff} \langle \mathcal{E}_{\parallel} \rangle$$

and

$$\beta_{eff} = \langle \mathcal{E}_{\perp} \rangle / \langle \mathcal{E}_{\parallel} \rangle$$

where $\langle \mathcal{E}_{\parallel} \rangle$ and $\langle \mathcal{E}_{\perp} \rangle$ are the space averaged electric fields, parallel and perpendicular to the average current flow. For a uniform plasma, carrying a uniform current, it can be shown from equations (1.3) that $\sigma_{eff} = \sigma$ and $\beta_{eff} = \beta$. This is not so if an experimental configuration results in non-uniformities in the plasma, or if instabilities develop in an otherwise uniform plasma, and the values of $\sigma_{eff}/\langle\sigma\rangle$ and $\beta_{eff}/\langle\beta\rangle$ are an indication of the magnitude of such effects. In particular, for a segmented electrode generator a reduction in $\beta_{eff}/\langle\beta\rangle$ from unity will result in a degradation of performance, essentially by allowing partial shorting of the Hall field.

1.4 Closed Cycle and Open Cycle Systems

As mentioned in Section 1.1, the source of plasma heating for the system may be either a combustion process or heat exchange with a fission reactor. Whilst this does not affect the previous discussion, in practice the combustion process is always associated with open-cycle generators, in which the plasma is exhausted from the system; and the

latter with closed cycle systems, in which a noble gas is re-circulated through the system. In both cases the working fluid has to be seeded with a small fraction of alkali metal in order to achieve a sufficiently high electrical conductivity for power production.

In the open cycle case the electrons are strongly coupled thermally to the vibrational degrees of freedom of the polyatomic heavy particles, and the electron temperature and heavy particle temperature are approximately equal. In the closed cycle case, the monatomic noble-gas heavy particles do not present an efficient energy sink for the electrons, and any mechanism which preferentially feeds energy into the electrons will result in an elevated electron temperature. This case is discussed below.

1.5 Non-Equilibrium Ionization

The necessity for a large electrical conductivity was demonstrated in Section 1.1. The most attractive possibility for inducing non-equilibrium ionization in an MHD generator is through the Ohmic dissipation in the plasma, j^2/σ, as suggested by Kerrebrock (1964). The electrons are accelerated by the induced electric fields in the plasma, and thermalize by way of elastic collisions with the heavy particles. Owing to the large disparity between electron and heavy particle masses, the collisional energy loss mechanism is not very effective, and the electrons can achieve a temperature in excess of the heavy particle temperature. The principal inelastic energy loss from the electrons is due to the escape of resonance radiation, through

radiative recombination from the first excited state of the seed atoms, as discussed by Lutz (1967). The radiation can escape due to low seed pressure, line-broadening and small apparatus dimensions.

For the temperatures and densities of interest to MHD experments, mutual electronic interactions are sufficient to 'Maxwellianize' the electron distribution by removing the effects of perturbations due to elastic and inelastic collisions with the heavy particles; furthermore, when the electron density is sufficiently high, so that electronic collisions dominate atomic collisional and radiative processes, collisional equilibrium at the electron temperature follows, and the free electron density is determined by the Saha function at the electron temperature, ie:

$$n_e^2 = (n_s - n_e)\left[\frac{2\pi m_e k_B T_e}{h^2}\right]^{3/2} \exp\left[-\frac{T_P}{T_e}\right] \qquad (1.4)$$

These assumptions are borne out by experimental results (Kerrebrock, 1964; Cool et al, 1968; Zauderer, 1968), for sufficiently high electron densities, typically in excess of 10^{19} m^{-3}. In the regime for which electron-heavy particle interactions are dominated by binary collisions, $\sigma \propto n_e$ which is related to T_e through equation (1.4).

In the rest of the thesis the following plasma parameters have been used:

Argon buffer gas density, $n_n = 10^{25}$ m^{-3},

Cesium seed density, $n_s = 10^{22}$ m^{-3}.

The heavy particle temperature is taken to be $1500^{o}K$, except in Chapter V, where a value of $2000^{o}K$ is assumed.

In figure 1.4 the values of n_e/n_s and σ as functions of T_e, according to equation (1.4), are plotted for the above values of n_n and n_s. Similarly, figure 1.5 shows the ratio of binary to Coulomb electron-heavy particle collision frequencies as a function of T_e, and figure 1.6 the Hall parameter as a function of T_e. The functional forms for σ, β, ν_{eB} and ν_{ec} are given in Chapter 2.

(a) Dependence of Non-Equilibrium Ionization on the Hall Parameter

It is therefore envisaged that a steady-state of electron temperature will be reached in which the rate of energy gain by electrons in the induced electric fields, will balance the elastic collision losses to the heavy particles, ie:

$$j^2/\sigma = \underline{j}\cdot\underline{\mathcal{E}} = 3n_e K_B(T_e - T)\left[\frac{m_e}{m_n}\nu_{eB} + \frac{m_e}{m_s}\nu_{ec}\right] \qquad (1.5)$$

and that the electron density will then satisfy equation (1.4). The value of $|\underline{j}|$ corresponding to equation (1.5) is plotted in figure 1.7 as a function of T_e for $T = 1500^{\circ}K$ and the values of n_n, n_s given above.

Assuming that one of the electron-heavy particle collisional processes greatly dominates the other, equation (1.5) can be written, for Mach 1 flows,

$$\beta^2 \sim \frac{T_e}{T} - 1$$

in which it has been assumed that $j \sim \sigma vB$, $\beta = \frac{eB}{m_e\nu_{e\alpha}}$, $\sigma = \frac{n_e e^2}{m_e\nu_{e\alpha}}$ and $m_\alpha v^2 = 3\,kT$. For $T_e \gtrsim 2T$, the Hall parameter must satisfy $\beta > 1$.

The achievement of non-equilibrium ionization is therefore dependent upon the magnitude of the Hall parameter, for a $\underline{v} \times \underline{B}$ sustained discharge in which radiation losses are negligible.

(b) The Electrothermal Instability

It is shown in Chapter III that the uniform plasma state described above is not stable for $\beta > 2$, and in Chapter VI the stable state of the plasma, in this regime, is seen to consist of large amplitude non-uniformities in electron density and temperature. These non-uniformities are approximately one-dimensional, and move relative to the heavy particles. The existence of the instability was first suggested by Kerrebrock (1964); and a detailed account of the linear, and quasi-linear behaviour of the instability has been given by Nelson (1969).

The source of the instability is the enhanced Ohmic heating in the regions of increased electron density. If the energy loss mechanisms cannot remove the excess heating, the electron temperature will rise, leading through ionization, to a further increase in electron density. In this way an infinitesimal fluctuation in electron properties can lead to large amplitude non-uniformities. The fractional fluctuations in electron density and temperature, n_e^* and T_e^*, are related by equation (1.4). The result is

$$n_e^*/T_e^* \sim T_p/2T_e >> 1 \quad , \quad n_e^*, T_e^* << 1$$

so that small fluctuations in T_e lead to much larger fluctuations in n_e. It is shown in Chapter III that the characteristic time-scale for the growth of the instability is $\tau_E \sim \sigma_o n_{eo} I_p / j_o^2$. For $T_e = 3000^\circ K$, $j_o = 10^5 A\ m^{-2}$, $\sigma = 200\ M\ m^{-1}$ and $I_p = 5 \times 10^{-19}$ Joules in the case of Cs, this gives

$$\tau_E \sim 10^{-5}\ sec$$

In the case of a practical generator of length, say, 10 m, and a plasma velocity of 10^3 m sec^{-1}, an individual wave front could be resident in the duct for a time of the order of 10^3 e-fold times.

(c) Non-Uniformities with Hall Effect

The effect of plasma non-uniformities on the current conduction of MHD generators was first considered by Rosa (1962). He found that the presence of one-dimensional plasma non-uniformities resulted in an increased impedance of the plasma compared with its uniform value; and that this effect became more pronounced with increasing Hall parameter. In Chapter III this result is demonstrated by considering the effective conductivity and effective Hall parameter. For one-dimensional non-uniformities, whose orientation corresponds to the most unstable electrothermal waves in an infinite plasma, the expression for σ_{eff} becomes

$$\sigma_{eff}/\langle\sigma\rangle = \left[1+a_0/2\right]^{-1} \leqslant 1$$

in which

$$a_0 = \langle\sigma\rangle\left\langle\frac{1+\beta^2}{\sigma}\right\rangle - \left[1+\langle\beta\rangle^2\right] \geqslant 0$$

In the regime for which electron collisions are dominated by Coulomb interactions, $\sigma^* \approx 0$ and $\beta^* \approx -n_e^*$; assuming that $n_e^* = A \sin kx$, a_0 becomes

$$a_0 \approx \langle\beta\rangle^2 \langle n_e^{*2}\rangle = \frac{1}{2}\langle\beta\rangle^2 A^2$$

from which

$$\sigma_{eff}/\langle\sigma\rangle \approx \left[1+\frac{1}{4}\langle\beta\rangle^2 A^2\right]^{-1}$$

For large amplitude non-uniformities and at large $\langle\beta\rangle$, the effective conductivity is significantly reduced from its ideal value, and the plasma impedance is correspondingly increased.

The results of this section indicate that practical MHD generators, utilizing non-equilibrium ionization due to internal Ohmic dissipation at large β, will be constrained to operate in a region for which electrothermal instabilities are an important consideration. The effect of the resultant electronic non-uniformities will be to increase the internal impedance of the device, and lower its efficiency. The large amplitude behaviour of these waves is therefore of great interest in the field of MHD power generation, in particular, and in the physics of magnetized partially ionized plasmas in general.

1.6 Motivation for Numerical Model

The linear theories of the electrothermal instability for the infinite plasma (Nelson et al, 1969; Nelson, 1969; Zampaglione, 1972), have been successful in predicting the stability threshold, and the wave speeds observed experimentally. The inclusion of boundary effects (Nelson, 1969; Riedmüller, 1970) complicates the analytic description of the linear system, which can then only be solved for the simplest configurations.

The equations governing the plasma are non-linear. Highly simplified second-order theories for the instability have been explored (Nelson, 1971; Solbes, 1968), and these demonstrate some of the observed global properties of the instabilities. These analyses are essentially an extension of Rosa's theory, in which the non-uniformities are evaluated self-consistently with the current density, to second order, for the infinite plasma.

The temporal behaviour of the observed large amplitude non-uniformities, and their interaction with the boundaries and current field, presents a formidable problem. This is particularly true for the segmented electrode generator, in which complicated boundary conditions on the field variables are imposed. These conditions lead to non-uniform Ohmic heating in the duct, resulting in plasma non-uniformities and reductions in σ_{eff} and β_{eff} even in absence of instabilities. In this configuration, non-uniformities referred to as current streamers occur, together with electrothermal waves. The relationship between these phenomena has previously been unclear. It is also observed, under some conditions, that leakage currents can flow between neighbouring electrode pairs (Fischer, 1966).

It would therefore seem that the only method of obtaining realistic solutions to the electronic behaviour in complex configurations, is by way of numerical simulation. Several such simulations have been reported (Lengyel, 1969, 1970, 1971; Argyropoulos et al, 1967, 1969; Kim, 1969), although they have not, to date, answered many of the more interesting questions relating to non-equilibrium generators. The model presented here is more complete than those cited above, and has provided much physical data for values of β as large as 10.

Finally, the feasibility of the results presented in this thesis indicate the usefulness of numerical methods to the problem. It is hoped that the techniques used to overcome certain computational problems will be of assistance in the development of future numerical models, not only in the MHD power generation field, but also in other applications requiring an understanding of magnetized, partially ionized plasmas.

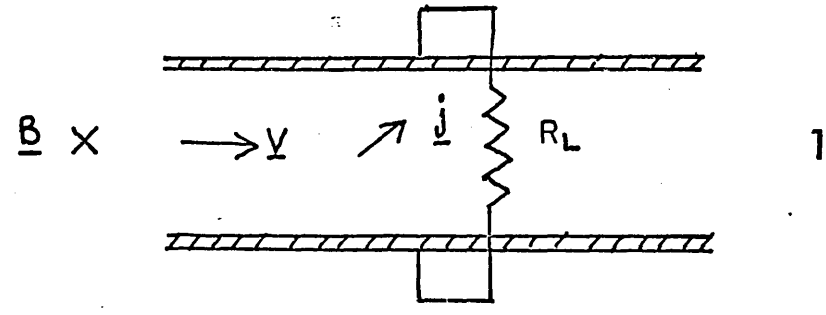

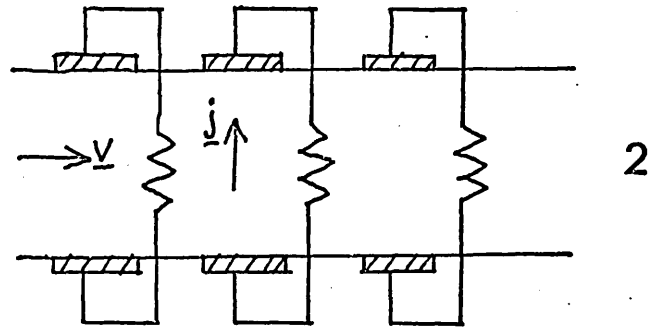

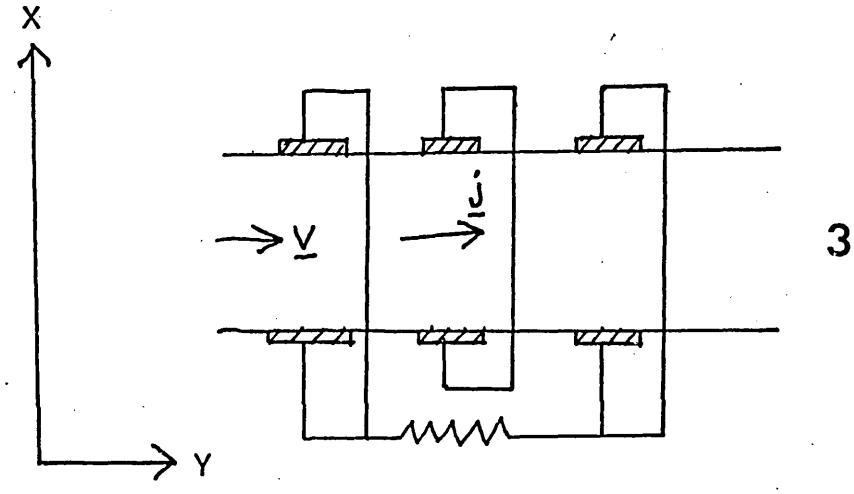

(1) Figure 1.1: Continuous Electrode Generator

(2) Figure 1.2: Segmented Electrode Generator

(3) Figure 1.3: Hall Generator

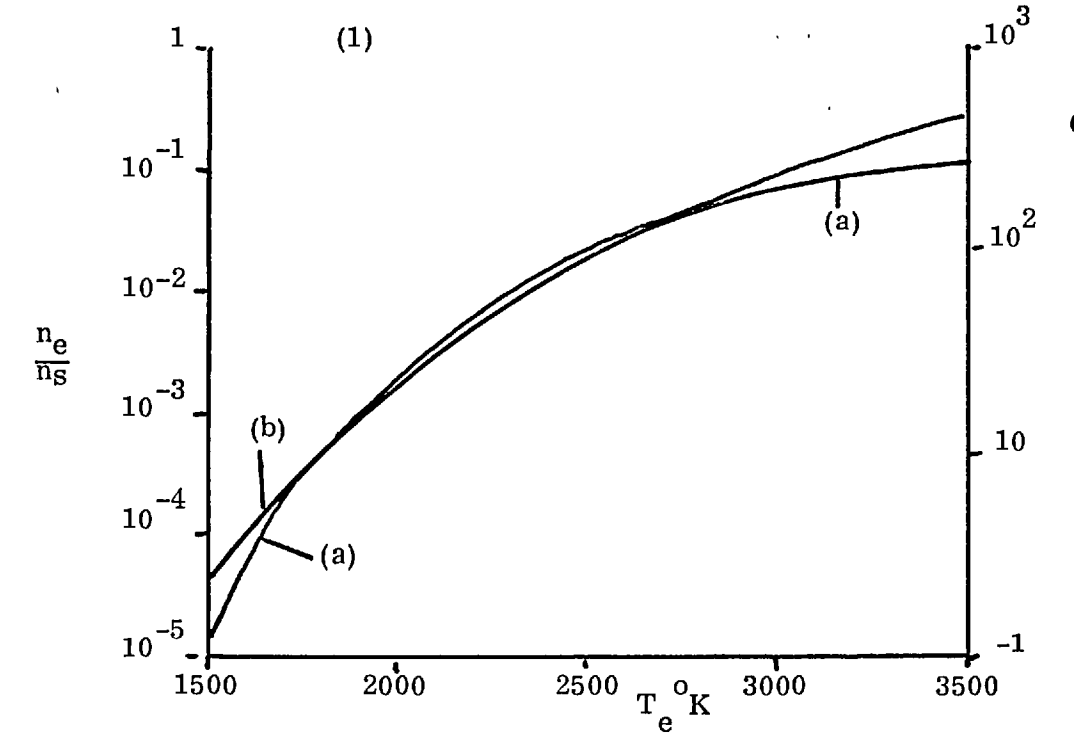

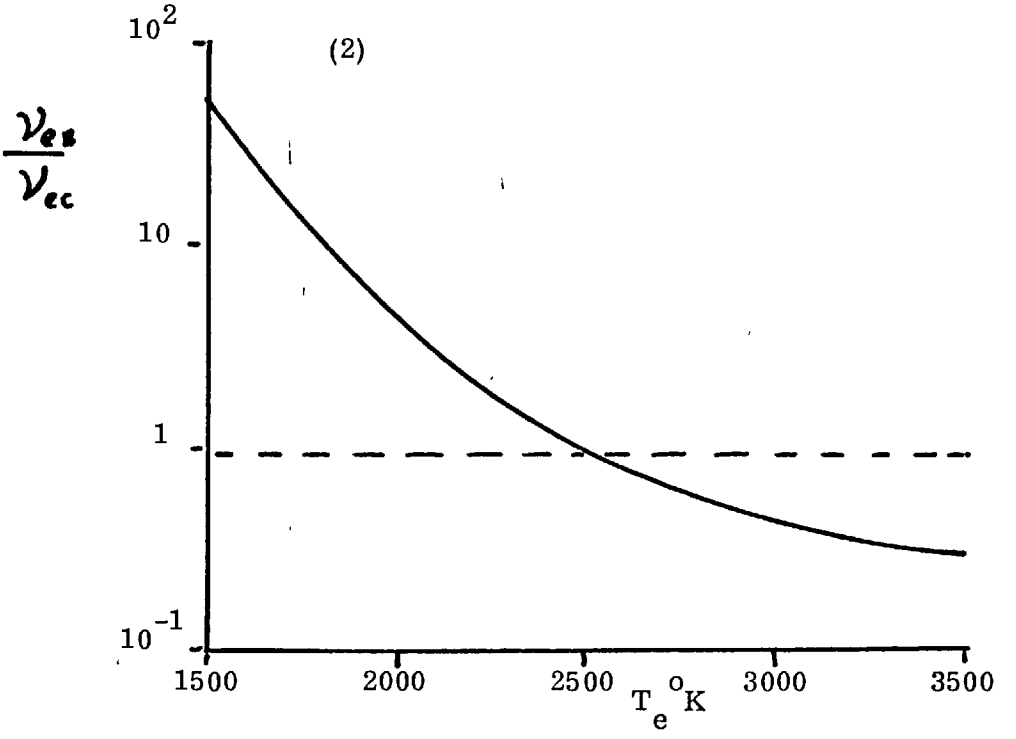

(1) Figure 1.4: (a) σ , (b) n_e/n_s against T_e

(2) Figure 1.5: ν_{eB}/ν_{ec} against T_e

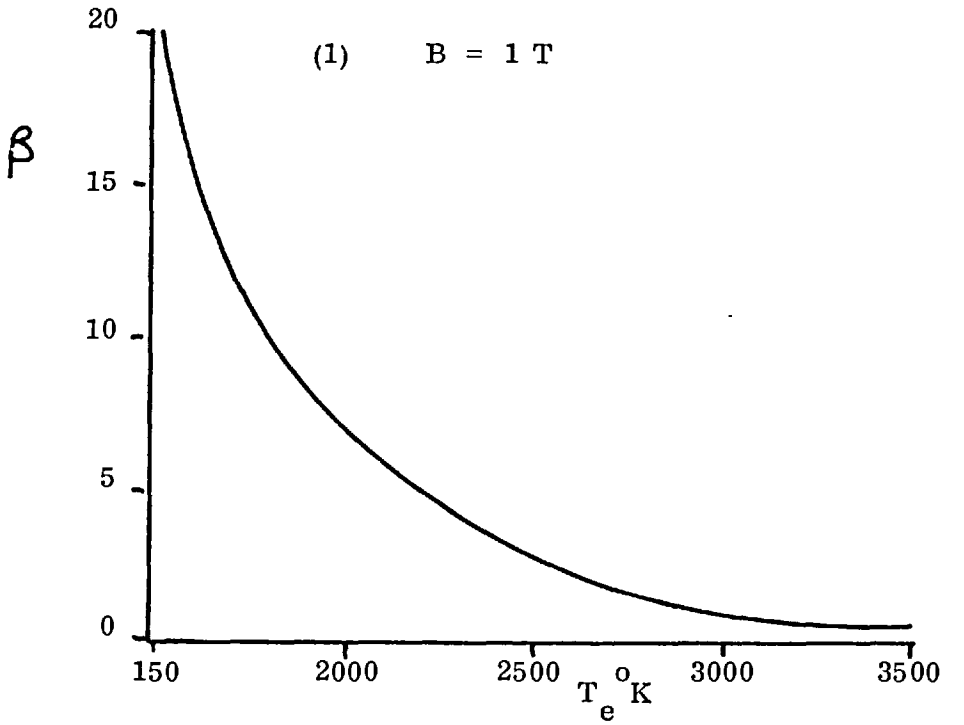

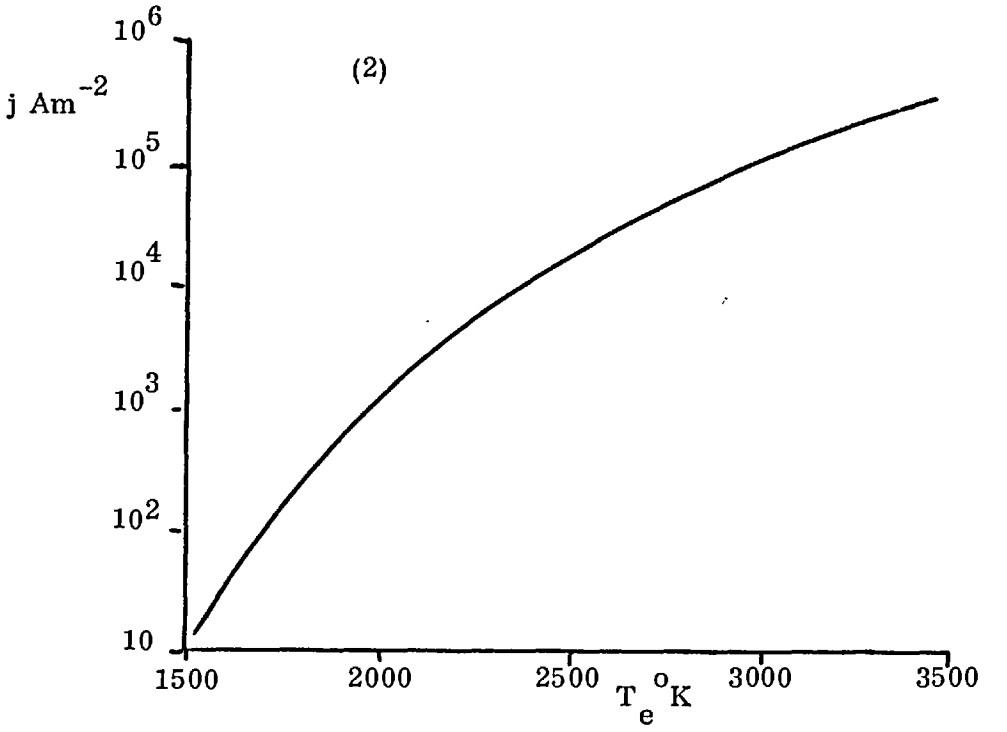

(1) Figure 1.6: β against T_e, B = 1 T

(2) Figure 1.7: j against T_e, T = 1500^{o}K

CHAPTER II

THEORETICAL DESCRIPTION OF NON-EQUILIBRIUM PLASMA

2.1 Introduction

This Chapter will be concerned with the theoretical description of the MHD plasma. The working fluid of the closed cycle generator consists of four components: (i) neutral buffer gas atoms, (ii) neutral seed atoms, (iii) ionized seed atoms and (iv) electrons. The complete description of this plasma is highly complex and requires the solution of the equations of fluid motion for each component, together with the solution of Maxwell's equation for the electric and magnetic fields, which in general are coupled to the fluid equations. The description is further complicated by the partially ionized nature of the fluid which introduces important features into the energy and mass conservation equations. In the two fluid approximation the description of the system is reduced to a consideration of the electron fluid, together with the heavy particles taken as a single, charged fluid. This description requires each of the heavy-particle fluids to possess equal temperatures, which is reasonable, since the heavy particles have roughly equal mass and are thus "tied" to one another thermally via collisions. Moreover, the features of the partially ionized nature of the plasma are restricted to the electron equations, since the local rate of ion production always balances seed atom "destruction", provided only single ionization occurs. In principle this latter set of

equations could therefore be solved to yield the heavy particle temperature, number density and flow velocity; together with electron temperature and number density and the local electric and magnetic fields. The above two-temperature model for the dense, alkali-vapour-seeded, noble gas plasma was first suggested by Kerrebrock (1964), and Cool et al (1968), amongst others, obtained experimental measurements of non-equilibrium electrical conductivity in seeded plasmas which showed substantial agreement with predicted values based upon the two-temperature plasma model.

Whilst the complete solutions of the two-temperature model are, of course, of interest, it is frequently permissible in the MHD regime to consider the heavy particle properties as fixed and solve for the electron fluid motion; this is a result of the long interaction length and the large disparity between electron and heavy particle masses. The latter approach has been adopted in this thesis and will be discussed in Section 2.3. Whilst bulk magneto-fluid effects have been neglected, the essential features of the non-equilibrium plasma are retained and with them the most difficult theoretical problems.

In Sections 2.2 and 2.3 the fundamental equations for the electron fluid are stated and the assumptions involved in them discussed; and in Sections 2.4 and 2.5 the mathematical characteristics and necessary boundary conditions considered.

2.2 Equations of Motion

These equations are obtained from successive moments of the Boltzmann equation, as discussed by Spitzer (1961), and include the production of electrons by ionization as discussed by De Groot and Mazur (1963) for example.

(a) Electron Continuity

This may be written in flux form

$$\frac{\partial n_e}{\partial t} + \nabla.(n_e \underline{v}_e) = \dot{n}_e \qquad (2.1)$$

$\dot{n}_e$ represents the local net rate of production of electrons by ionization of the seed atoms. In the heavy particle frame of reference the steady-state of equation (2.1) is assumed to correspond to Saha equilibrium at the electron temperature, ie:

$$\dot{n}_e = A_1 n_e(n_s - n_e) - A_2 n_e^3$$

where $A_2 = 1.1 \times 10^{-20} \times T_e^{-9/2}\ m^6\ sec^{-1}$

and $A_1 = \left[\frac{2\pi m_e k_B T_e}{h^2}\right]^{3/2} \exp\left[-\frac{T_p}{T_e}\right] \times A_2$

in which the recombination coefficient is obtained from the collisional-radiative theory of Hinnov et al (1962). These authors calculate the energy of an atomic level, i^*, such that the number of electrons transferred above it from the continuum, and which eventually recombine, equals the number transferred below it which subsequently ionize. This is the level where the probabilities of one-level transitions through collisional excitation and de-excitation are approximately equal. The ionization rate from the i^{th} level is then obtained for a given n_{ai}, the number of Cs atoms in the i^{th} excited state, using the classical Thomson

formula for energy transfer in electron-electron collisions. Assuming the inverse recombination rate is the same when n_{ai} is determined by the Saha function, a recombination rate into the i^{th} level is obtained. Summing this from $i = 1 \rightarrow i^*$ a total recombination rate, given by A_2, is obtained.

(b) Electron Momentum

In total differential form the electron momentum equation may be written

$$n_e m_e \frac{D\underline{v}_e}{Dt} = -n_e e(\underline{E} + \underline{v}_e \times \underline{B}) - \nabla p_e + m_e n_e \nu_e (\underline{v} - \underline{v}_e)$$

which omits thermo-electric effects and uses a simplified form for the Hall effect. The last term represents the frictional drag between electrons and heavy particles. The ∇p_e term cannot be neglected here because of the possibility of large gradients occurring in the solutions; and in Chapter VII it is shown that this term leads to an asymmetry between anode and cathode conduction. In the absence of ion-slip, and assuming quasi-neutrality, the current density may be written

$$\underline{j} = n_e e (\underline{v} - \underline{v}_e)$$

Since the time scales of interest are much longer than the collision time, one can neglect the inertia term in the above equation and write it in the form

$$\underline{j} = \sigma \underline{\mathcal{E}} - \underline{j} \times \underline{\beta} \tag{2.2}$$

In which

$$\underline{\mathcal{E}} = \underline{E} + \underline{v} \times \underline{B} + \frac{\nabla p_e}{n_e e} \tag{2.3}$$

and

$$\beta = e\underline{B}/m_e\nu_e \tag{2.4}$$

and

$$\sigma = n_e e^2/m_e\nu_e \tag{2.5}$$

Equation (2.2) therefore represents the Ohms law for the system.

The total electron-heavy particle collision frequency has two contributions, namely electron-neutral collisions and electron-ion collisions, so that $\nu_e = \nu_{eB} + \nu_{ec}$

where $$\nu_{ec} = \frac{1}{6} \cdot n_e (\pi k_B T_e)^{-3/2} \frac{e^4}{\epsilon_0^2 \sqrt{2m_e}} \ln \Lambda$$

and $$\Lambda = \frac{12\pi}{e^3} \left[\frac{\epsilon_0^3 k_B^3 T_e^3}{n_e}\right]^{1/2}$$

and where $$\nu_{eB} = n_n \left[\frac{8k_B T_e}{\pi m_e}\right]^{1/2} q_{en}$$

with (Ovcharienko, 1969)

$$q_{en} = \left[6.0 + 5.5 \times 10^{-3} (T_e - 2000)\right] \times 10^{-21} \text{ m}^2.$$

(c) Electron Energy Equation

In flux form this may be written

$$\frac{\partial U_e}{\partial t} + \nabla.(U_e \underline{v}_e) = j^2/\sigma - L - P_e \nabla.\underline{v}_e - I_p \dot{n}_e + \nabla.(K_e \nabla T_e) - \dot{Q}_R \tag{2.6}$$

with $P_e = n_e k_B T_e$ and $U_e = {}^3/_2\, n_e k_B T_e$

and $$K_e = \frac{n_e k_B^2 T_e}{m_e \nu_e} \cdot \frac{5/2}{1+\beta^2}$$

The right hand side of equation (2.6) comprises, from left to right: Ohmic heating, elastic collision losses to the heavy particles as given by equation (1.5), compressional heating or cooling, ionizational heating or cooling, heat conduction and radiation transfer. The latter two terms

are much smaller than those remaining, except for extremely fine scale structure (less than 10^{-3} m) as discussed by Nelson (1969), and are frequently omitted from calculations. The mathematical implications of this approximation are discussed in Section 2.4.

(d) Field Equations

Coupled with the above equations (2.1)-(2.6) are Maxwell's equations for the electric and magnetic fields. These are taken to be

$$\nabla \cdot \underline{j} = 0 \tag{2.7}$$

and

$$\nabla \times \underline{E} = 0 \tag{2.8}$$

Equation (2.7) is the equation of charge-conservation and assumes that deviations from neutrality are small, and that the time to set up space charge fields is considerably smaller than the time scales of interest. Equation (2.8) is Faraday's law in the limit of zero magnetic Reynolds number.

2.3 Assumptions Involved in Treating as a Closed Set

Provided n_n, n_s, T and $\underline{v}$ are prescribed, equations (2.1)-(2.8) form a closed set for the eight variables, n_e, T_e, $\underline{j}$ and $\underline{E}$. These equations are almost universally employed in the studies of non-equilibrium phenomena in MHD plasmas, although they are frequently approximated to a simpler form.

The validity of assuming the heavy particle properties prescribed is now considered in more detail.

The heavy particles cannot maintain a constant temperature in practice, since they are receiving collisional energy from the electrons, an estimate for the time-scale τ of temperature changes can, however, be obtained as follows.

$$\frac{\partial U_n}{\partial t} \sim L \sim j^2/\sigma \sim \sigma v^2 B^2 \sim 1.5 n_n k_B T/\tau$$

For $T_e = 3000^{\circ}K$, $T = 1500^{\circ}K$, $\sigma = 200$ M m^{-1}, $v = 500$ m sec^{-1} and $B = 1$ T, it follows that $\tau \sim 10^{-2}$ secs. If one considers a single segment of extent, say 5×10^{-2} m, and a flow velocity of 500 m sec^{-1}, then the heavy particles will remain in this section of the duct for 10^{-4} secs, during which time the temperature of the particles will be little affected by the energy transfer.

Similarly, if it is assumed that the $\underline{j} \times \underline{B}$ magnetomotive force slows down the heavy particles according to

$$\frac{\partial}{\partial y}(\rho v^2) \sim -j_x B \sim -\sigma v B^2$$

then

$$\delta v/v \sim -\left[\sigma B^2/2\rho v\right] \delta y$$

which gives, for the previous values and $\rho = 1$ kg m^{-3},

$$\frac{\delta v}{v} \sim 10^{-2}$$

for a single segment. The assumption of constant gas flow velocity leads to constant n_n for a constant area channel.

Prescribing constant n_s is equivalent to assuming that the seed fraction is homogeneously mixed with the buffer gas atoms. If this is not so then ionizational non-uniformities will occur even for an initially uniform current density field. The much reduced Hall potentials in the experiments of Haines and McNab (1968) were

attributed partly to inadequate mixing of the seed material with the buffer gas. If the mixing is successful during the seeding stage, then it is reasonable to consider the seed as homogeneously mixed thereafter, owing to the low seeding ratio and thus the dominance of seed atom-buffer gas collisions. The value of n_s is taken to be constant and equal to $0.001\ n_n$ throughout this thesis.

The assumption of quasi-neutrality requires justification; $n_e \neq n_i$ everywhere, of course, since space charge fields exist in the plasma. It is the charge separation in the axial direction of the segmented electrode generator which results in a net current flow in the transverse direction. Fluctuations in electron density due to instabilities and non-uniformities will also result in charge separation; the fundamental assumption is that the charge difference necessary to produce these fields is negligible compared with either n_e or n_i.

The time required to set up the Hall field will be of order $\epsilon_0/\sigma \sim 10^{-13}$ seconds, and the excess charge will reside in the surface boundary layer of the plasma. The resultant current distributions will then be constrained to satisfy equation (2.7).

The volumetric charge excesses are of more interest. If the non-uniformities within the plasma are small, then a linear perturbation of the Ohms law, together with the field equations, give the fractional perturbation in electric field due to the electron density non-uniformities; this gives

$$E^* \sim n_e^* \ .$$

Poisson's equation for the perturbed state is

$$\nabla . \underline{E}' \sim \frac{2\pi}{\lambda} E' \sim (n_i' - n_e') e/\epsilon_o$$

where λ is the scale-length of the non-uniformities. From which it follows, using the previous values, that

$$10^{-7}\, n_e' < (n_i' - n_e') \text{ for } \lambda > 10^{-3} \text{m}.$$

The assumption of quasi-neutrality is therefore justified.

In equation (2.8) it was assumed that the magnetic Reynolds number is negligible, this can be demonstrated from Ampere's law for the perturbed state

$$\nabla \times \underline{B}' = \mu_o \underline{j}' \quad , \quad j' \sim n_e^* \sigma v B$$

from which $$B^* \sim \frac{\lambda \mu_o \sigma v}{2\pi} . n_e^* \sim 10^{-2} \lambda n_e^*$$

which varies approximately from $10^{-5}\, n_e^*$ to $10^{-3} n_e^*$ as λ varies from 10^{-3} m to 10^{-2} m. Moreover, the time required for the field to relax to the perturbed state is of the order of $\mu_o \sigma \left(\frac{\lambda}{2\pi}\right)^2 \sim 10^{-9}$ sec for $\lambda = 10^{-2}$ m.

The assumptions of constant, prescribed, heavy particle properties, non-divergent current field and irrotational electric field, therefore, permits an adequate description of the physical system for the scale-lengths and time scales of interest.

In this thesis there is assumed to be no variation in plasma properties in the direction of the magnetic field, ie: all variables are functions of x, y and t only. Since $\underline{v} = (0, v, 0)$, as in Figures 1.1, 1.2 and 1.3, the previous assumptions lead to

$$\nabla \cdot \underline{V} = \frac{\partial}{\partial y} V = 0 \qquad (2.9)$$

so that ad hoc 'x' dependent velocity profiles can be considered, and

$$\nabla . (n_e \underline{V}_e) = \nabla . (n_e \underline{V} - \underline{j}/e) = \underline{V} . \nabla n_e$$

using equations (2.7) and (2.9).

2.4 Characteristics of Equations

Equations (2.1)-(2.8) are a coupled set of non-linear partial differential equations. In general a solution to these has to be obtained numerically and this is discussed in Chapter V. The mathematical type of the set can be determined simply, however, and the dependence of the mathematical nature of the equations on various physical approximations can be obtained. It is known that highly plausible physical approximations can lead to a radical change in the equation "type", and thus alter the boundary conditions needed to specify the problem, this fact is mentioned by Smith (1967), for example. The latter point is particularly relevant to the numerical solution of partial differential equations. In equation (2.6), for example, the inclusion of a small thermal conductivity into, say, a dominantly convective problem can lead to extremely large, and numerically unacceptable, gradients in the proximity of the boundaries, owing to the physically necessary boundary conditions imposed.

The mathematical characteristics of the basic equations, under various approximations, will now be discussed. Similar work has recently been reported by Kolb (1971), who analyzed the case discussed in Section 2.4a..

There exists no simple formulation for the radiation transfer term in the energy equation, and for this reason it has been omitted. Lutz (1967) has provided an integral description for the energy transfer term, and in Chapter VI it is considered as an addition to the thermal conduction; in the following work it will not be considered.

(a) Full Set Including Thermal Conductivity

Equation (2.1) can be written

$$n_{et} + v\, n_{ey} = a_1 \tag{2.10}$$

where the subscripts x, y and t represent partial differentiation with respect to these variables.

Using $$\nabla \equiv \nabla n_e \frac{\partial}{\partial n_e} + \nabla T_e \frac{\partial}{\partial T_e}$$

together with the definitions, $p = T_{et}$, $q = T_{ex}$ and $r = T_{ey}$, the energy equation can be replaced by the set

$$a_2 n_{ex} + a_3 n_{ey} + a_4 (q_x + r_y) = a_5 \tag{2.11}$$

with the identities

$$p_x - q_t = 0 \tag{2.12}$$

and

$$p_y - r_t = 0 \tag{2.13}$$

Eliminating $\underline{E}$ between equations (2.2) and (2.8), and with $\underline{j} = (f, g, o)$, these become

$$f_y - g_x + a_6 n_{ex} + a_7 n_{ey} = a_8 \tag{2.14}$$

Finally $\nabla \cdot \underline{j} = 0$ is

$$f_x + g_y = 0 \tag{2.15}$$

Defining a function $\gamma(x, y, t) = 0$, then this represents a characteristic manifold of the first order set of equations (2.10)-(2.15), if (Courant and Hilbert, 1962)

$$\begin{vmatrix} \gamma_t + v\gamma_y & 0 & 0 & 0 & 0 & 0 \\ a_2\gamma_x + a_3\gamma_y & 0 & a_4\gamma_x & a_4\gamma_y & 0 & 0 \\ 0 & \gamma_x & -\gamma_t & 0 & 0 & 0 \\ 0 & \gamma_y & 0 & -\gamma_t & 0 & 0 \\ a_6\gamma_x + a_7\gamma_y & 0 & 0 & 0 & \gamma_y & -\gamma_x \\ 0 & 0 & 0 & 0 & \gamma_x & \gamma_y \end{vmatrix} = 0$$

ie: $$\gamma_t(\gamma_x^2+\gamma_y^2)(\gamma_x^2+\gamma_y^2)(\gamma_t+v\gamma_y)=0$$

which can be classified according to

$$\gamma_t(\gamma_x^2+\gamma_y^2)=0 \qquad \text{Parabolic}$$

$$\gamma_x^2+\gamma_y^2=0 \qquad \text{Elliptic}$$

together with $$\gamma_t+v\gamma_y=0$$

The parabolic characteristics correspond to the solution of the energy equation for the temperature.

The elliptic characteristics correspond to the solutions for $\underline{j}$; a disturbance in $\underline{j}$ within the field affects all other points simultaneously. This is a result of neglecting temporal variations in equations (2.2) and (2.7), the current density essentially adjusts itself instantaneously to any variation in electric field.

The last equation defines the characteristics for the continuity equation, these are the lines $y = vt + c$.

The boundary conditions necessary to specify the above problems consist of the following. For the energy equation, initial values for T_e, and constraints on T_e at all points of the domain boundary. For the field equations taken with the Ohms law, constraints on $\underline{j}$ at all points of the domain boundary; and for the continuity equation, initial values for n_e, and specifications of n_e for all $t>0$ along some single valued curve in the physical domain, $y = f(x)$. The nature of the boundary constraints depends, of course, on the physical system.

(b) Full Set Neglecting Thermal Conductivity

The elimination of $\underline{E}$ between equations (2.2) and (2.8) leads to a term $n_{ex}T_{ey} - n_{ey}T_{ex}$ in the resultant equation. This non-linearity in the differentials was automatically removed by the introduction of the auxiliary variables q and r in the previous case.

The simplest way of removing this non-linearity in the present case is by defining variables $p = n_{et}$, $q = n_{ex}$ and $r = n_{ey}$. The continuity equation becomes

$$p + vr = \dot{n}_e$$

or
$$p_t + vr_t + a_1 T_{et} = a_2 \tag{2.16}$$

on differentiating with respect to time,

with
$$p_x - q_t = 0 \tag{2.17}$$

and
$$p_y - r_t = 0 \tag{2.18}$$

The a's are in general different for each of the cases (a) - (e) considered in this section.

The energy equation may be written explicitly for the temperature, the result is

$$\frac{3}{2} n_e k_B \left[\frac{\partial T_e}{\partial t} + \underline{v}_e \cdot \nabla T_e\right] + \frac{k_B T_e}{n_e e} \underline{j} \cdot \nabla n_e = j^2/\sigma - L - \left[I_p + \frac{3}{2} k_B T_e\right] \dot{n}_e$$

or
$$T_{et} + (v_{ex}) T_{ex} + (v_{ey}) T_{ey} = a_3 \tag{2.19}$$

using equations (2.7) and (2.9) and the definition of the current density.

The Ohms law and field equations become

$$f_y - g_x + a_4 T_{ex} + a_5 T_{ey} = 0 \tag{2.20}$$

and
$$f_x + g_y = 0 \tag{2.21}$$

The characteristic determinant of equations (2.16)-(2.21) is

$$\begin{vmatrix} a_1\gamma_t & \gamma_t & 0 & v\gamma_t & 0 & 0 \\ 0 & \gamma_x & -\gamma_t & 0 & 0 & 0 \\ 0 & \gamma_y & 0 & -\gamma_t & 0 & 0 \\ \gamma_t + \underline{v}_e \cdot \nabla\gamma & 0 & 0 & 0 & 0 & 0 \\ a_4\gamma_x + a_5\gamma_y & 0 & 0 & 0 & \gamma_y & -\gamma_x \\ 0 & 0 & 0 & 0 & \gamma_x & \gamma_y \end{vmatrix} = 0$$

or $$\gamma_t^2 (\gamma_t + \underline{v}_e \cdot \nabla\gamma)(\gamma_t + v\gamma_y)(\gamma_x^2 + \gamma_y^2) = 0$$

which can be classified according to

$$\gamma_x^2 + \gamma_y^2 = 0 \qquad \text{Elliptic}$$

with $$\gamma_t + \underline{v}_e \cdot \nabla\gamma = 0$$

$$\gamma_t + v\,\gamma_y = 0$$

and $$\gamma_t^2 = 0$$

One root of $\gamma_t^2 = 0$ corresponds to the differentiation throughout of the continuity equation, whilst the other is a re-statement of the initial value requirements for n_e, $n_{et} = p$. Both roots arise because of the enlarged set of equations used, and provide no extra physical information.

The omission of thermal conductivity from the energy equation results in a first order equation for T_e. The characteristic surfaces for this equation satisfy $\gamma_t + \underline{v}_e \cdot \nabla\gamma = 0$. These correspond to real surfaces moving along with the electron fluid, in the same way

that the characteristics for the continuity equation correspond to real surfaces moving along with the heavy particles. In steady state the characteristics for the continuity equation and energy equation correspond to the integral curves of $dx = 0$ and $dy/dx = v_{ey}/v_{ex}$ respectively, ie: the flow lines of the system. Some of the characteristics of the energy equation must originate at the cathodes, and terminate at the anodes. In the case when $v = 0$, and excluding electrode leakage, all the characteristics originate at the cathodes and terminate at the anodes. It would therefore seem that the specification of T_e requires similar conditions to those for n_e, with additional conditions, in general, at the cathodes for all $t > 0$.

(c) Full Set with the Assumption of Saha Equilibrium

The assumption of Saha equilibrium becomes a valid approximation when the time scales for ionization-recombination processes are much shorter than those typifying other physical phenomena described by the continuity equation. Equation (2.10) is replaced by $n_e = S(T_e)$ and derivatives involving T_e may be replaced using the relationship

$$\nabla n_e = \partial S/\partial T_e \cdot \nabla T_e = S' \nabla T_e$$

The energy equation may be written

$$\frac{\partial \epsilon_e}{\partial t} + \nabla(\epsilon_e \underline{v}_e) + P_e \nabla \cdot \underline{v}_e = j^2/\sigma - L + \nabla \cdot \left[\frac{K_e}{S'} \nabla n_e \right]$$

in which $\epsilon_e = U_e + I_p n_e$ = thermal + ionization energy. To remove the non-linearity in this equation the following variables are defined, $p = n_{et}$, $q = n_{ex}$ and $r = n_{ey}$.

The energy equation can therefore be replaced by the set

$$q_x + r_y = a_1 \tag{2.22}$$

$$p_x - q_t = 0 \tag{2.23}$$

and

$$p_y - r_t = 0 \tag{2.24}$$

The field equations can be written

$$f_y - g_x = a_2 \tag{2.25}$$

and

$$f_x + g_y = 0 \tag{2.26}$$

The characteristic determinant for equations (2.22)-(2.26) becomes

$$\begin{vmatrix} 0 & \gamma_x & \gamma_y & 0 & 0 \\ \gamma_x & -\gamma_t & 0 & 0 & 0 \\ \gamma_y & 0 & -\gamma_t & 0 & 0 \\ 0 & 0 & 0 & \gamma_y & -\gamma_x \\ 0 & 0 & 0 & \gamma_x & \gamma_y \end{vmatrix} = 0$$

or

$$\gamma_t (\gamma_x^2 + \gamma_y^2)(\gamma_x^2 + \gamma_y^2) = 0$$

which can be classified according to

$$\gamma_t (\gamma_x^2 + \gamma_y^2) = 0 \qquad \text{Parabolic}$$

$$\gamma_x^2 + \gamma_y^2 = 0 \qquad \text{Elliptic}$$

The energy equation is therefore parabolic, requiring initial conditions for n_e, or T_e, and boundary constraints on n_e or T_e, all around the domain.

(d) Full Set with Assumption of Saha Equilibrium and Neglecting Thermal Conductivity

In this case the energy equation can be written

$$n_{et} + a_1 n_{ex} + a_2 n_{ey} = a_3 \tag{2.27}$$

with $a_1 = (v_{ex})\left\{\frac{3}{2}n_e k_B/S' - k_B T_e\right\}\left[\frac{3}{2}n_e k_B/S' + I_p + \frac{3}{2}k_B T_e\right]^{-1}$

and $a_2 = \left[(v_{ey})\left\{\frac{3}{2}n_e k_B/S' - k_B T_e\right\} + v\left\{I_p + 5/2 k_B T_e\right\}\right]\left[\frac{3}{2}n_e k_B/S' + I_p + \frac{3}{2}k_B T_e\right]^{-1}$

The non-linearity in the field equations, as discussed in case (b), is not present when Saha equilibrium is assumed, these equations are therefore

$$f_y - g_x + a_4 n_{ex} + a_5 n_{ey} = 0 \qquad (2.28)$$

and

$$f_x + g_y = 0 \qquad (2.29)$$

The determinant for this set is

$$\begin{vmatrix} \gamma_t + a_1\gamma_x + a_2\gamma_y & 0 & 0 \\ a_4\gamma_x + a_5\gamma_y & \gamma_y & -\gamma_x \\ 0 & \gamma_x & \gamma_y \end{vmatrix} = 0$$

ie: $(\gamma_t + a_1\gamma_x + a_2\gamma_y)(\gamma_x^2 + \gamma_y^2) = 0$

or $\gamma_x^2 + \gamma_y^2 = 0$ Elliptic

and $\gamma_t + a_1\gamma_x + a_2\gamma_y = 0$

The characteristics for the energy equation do not have simple physical representations in this case. In the steady state the characteristics satisfy $dx/dy = a_1/a_2$. For $\underline{j} = 0$ these are the flow lines $x = \text{const}$. For $v = 0$ the characteristics are everywhere parallel to the electron velocity flow vector. The general case is therefore intermediate between these two, and it would seem that the conditions required to specify n_e are the same as those required to specify T_e in case (b).

(e) Neglect of Spatial Gradients in Energy Equation

The energy equation is

$$\frac{\partial \epsilon_e}{\partial t} = j^2/\sigma - L$$

which taken with equations (2.28) and (2.29) gives

$$\begin{vmatrix} \gamma_t & 0 & 0 \\ a_4\gamma_x + a_5\gamma_y & \gamma_y & -\gamma_x \\ 0 & \gamma_x & \gamma_y \end{vmatrix} = 0$$

or $$\gamma_t(\gamma_x^2 + \gamma_y^2) = 0$$

The system is therefore overall parabolic requiring initial conditions for n_e. The above equations do not go over into elliptic type in the steady-state, however, unlike the usual parabolic sets.

In this case one has

$$j^2/\sigma = L = [f^2 + g^2]/\sigma \tag{2.30}$$

together with equations (2.28) and (2.29). Differentiating equation (2.30) with respect to x gives

$$f f_x + g g_x + a_1 n_{ex} = 0 \tag{2.31}$$

The Ohms law and $\nabla \cdot \underline{j} = 0$ are

$$f_y - g_x + a_2 n_{ex} + a_3 n_{ey} = 0 \tag{2.32}$$

and

$$f_x + g_y = 0 \tag{2.33}$$

The determinant for this set is thus

$$\begin{vmatrix} a_1\gamma_x & f\gamma_x & g\gamma_x \\ a_2\gamma_x + a_3\gamma_y & \gamma_y & -\gamma_x \\ 0 & \gamma_x & \gamma_y \end{vmatrix} = 0$$

or $\gamma_x = 0$

with $$\gamma_x^2(a_1+a_2g) - \gamma_x\gamma_y(a_2f - a_3g) + \gamma_y^2(a_1 - a_3f) = 0 \qquad (2.34)$$

The first root is a result of the differentiation of the algebraic relationship (2.30) and is of no interest. The second root corresponds to the equation type of the steady current distribution. In all previous cases this has been elliptic. Taking the total derivative of the characteristic function it follows that

$$m = dy/dx = -\gamma_x/\gamma_y$$

Equation (2.28) becomes

$$m^2(a_1 + a_2g) + m(a_2f - a_3g) + (a_1 - a_3f) = 0$$

which has real, ie: hyperbolic, characteristics in the (x, y) plane if

$$(a_2f - a_3g)^2 > 4(a_1 + a_2g)(a_1 - a_3f)$$

To obtain an idea of when the transition, elliptic to hyperbolic, occurs the coefficients have been computed in the limit of a Coulomb collision dominated plasma with

$$\partial \ln n_e/\partial\xi >> \partial \ln T_e/\partial\xi, \quad \xi = (x, y)$$

This follows from the Saha relationship. The assumption $n_e << n_s$ is also made. This gives

$$a_1 = -(f^2 + g^2)/n_e = -j^2/n_e$$

and $$a_2 = -f\beta/n_e; \quad a_3 = -g\beta/n_e$$

The condition for hyperbolicity is thus

$$\beta > 2$$

which corresponds to the onset of electrothermal waves, as mentioned in Chapter I. A more physical insight can be obtained by considering the linearized versions of equations (2.31)-(2.33). Assuming that the

plasma consists of stationary, linear non-uniformities of the form

$$\chi = \chi_0 + \chi' \exp i(K_x x + K_y y)$$

where χ_0 is constant, then equations (2.25)-(2.27) become

$$f_0 f' + g_0 g' + a_{10} n_e' = 0$$

$$k_y f' - k_x g' + a_{20} n_e' k_x + a_{30} n_e' k_y = 0$$

$$k_x f' + k_y g' = 0$$

Eliminating f', g' and n_e' gives

$$k_x^2(a_{10} + a_{20}g_0) - k_x k_y(a_{20}f_0 - a_{30}g_0) + k_y^2(a_{10} - a_{30}f_0) = 0$$

so that for infinitesimal non-uniformities it follows that $\frac{\delta x}{\delta y} = \frac{K_x}{K_y} = -\frac{dy}{dx}$ for the characteristics, ie: the non-uniformity 'wavefronts' are oriented along the characteristics everywhere in the plasma. Moreover, stationary, linear non-uniformities exist only for $\beta > 2$ in an otherwise gradient-free plasma. This point is taken up again in Chapter III

The hyperbolicity of the latter set of equations was first noted by Oliver et al (1967), and Lengyel (1971) used the method of characteristics to evaluate the current distribution in a segmented generator in the binary-collision dominated regime with constant β . In this limit he also found that the two families of characteristics coincided with the current stream lines and electric field lines respectively.

The importance of the hyperbolicity of the current distribution lies in the possibility of infinite gradients occurring within the plasma. In the hyperbolic problem the solution propagates along the characteristics, and discontinuities across the characteristics are permissible.

The dominant features in the full energy equation (2.6) are the Ohmic heating and elastic collision losses; one can therefore conclude that despite the elliptic nature of the current distribution in the full set of equations, the solutions will demonstrate certain hyperbolic-like characteristics. The gradients in the field at large β becoming large but not infinite due to the presence of gradient terms in the energy equation. Elliptic boundary conditions all round the domain are necessary, but large gradients near the boundaries will occur. The effect of these large gradients on the numerical evaluation of the current distribution will be discussed in Chapter V.

2.5 Summary

The basic equations governing the non-equilibrium plasma have been stated, and the assumptions involved in treating them as a closed set discussed. The assumptions of constant heavy particle temperature, velocity and number density, together with quasi-neutrality and negligible magnetic Reynolds number, have been shown to be reasonable approximations for the time-scales, and scale-lengths pertinent to electrothermal instabilities, segmentation non-uniformities and so forth. The mathematical 'type' of the equations, together with the characteristics and necessary boundary conditions, have been discussed under various physically plausible approximations.

The current distribution was shown to be elliptic except in the case where Ohmic heating balances elastic collision losses everywhere, and Saha equilibrium is assumed. The distribution is then hyperbolic for $\beta > 2$, and the characteristics were shown to coincide with the 'wavefronts' of infinitesimal non-uniformities. Since Ohmic heating and elastic collision losses are, in general, the dominant features of the energy equation, certain hyperbolic-like characteristics are likely to manifest themselves in the complete elliptic solutions, in particular the presence of large but finite gradients in the solution.

CHAPTER III

CHARACTERISTIC TIMES AND LENGTHS OF THE ELECTROTHERMAL INSTABILITY

3.1 Introduction

An important feature of the noble-gas-alkali metal plasma is its susceptibility to the electrothermal instability. The instability has been repeatedly observed in experiments involving magnetized MHD plasmas, and the major characteristics of the instability have been well documented. These characteristics are summarised below.

The electrothermal instability has a threshold as a function of Hall parameter. Below the critical Hall parameter, β_{crit}, which is approximately 2, the plasma is stable and can maintain a uniform state. The instability manifests itself as non-uniformities in electron density and temperature. For β not much greater than β_{crit} these non-uniformities are approximately plane-wave like, ie: one-dimensional, and satisfy

$$\frac{\underline{j} \times \underline{k} \cdot \underline{B}}{\underline{j} \cdot \underline{k} |\underline{B}|} \approx 1$$

where $\underline{k}$ is the wavenumber of the instability.

The non-uniformities, or striations, move relative to the heavy particle fluid with a velocity of the order of 10 m sec^{-1}. At larger values of β the structure becomes more complex and no longer one-dimensional. Finally, the wavelengths for the non-uniformities are observed to be of the order of the duct dimensions.

The linear theory for the infinite plasma (Nedospasov, 1968; Nelson et al, 1969; Nelson, 1969; Hiramoto, 1970; Zampaglione, 1972) has proved successful in describing the experimentally observed wave speed, wave orientation and critical Hall parameter. The linear growth rate for the instability has not been measured to date, but Shipuk et al (1968) noted that striations required approximately 10^{-4} sec to appear in their experiments. The full set of equations (2.1)-(2.8) has been linearized and solved numerically by Nelson and Haines (1969); and the effects of thermal conduction and radiation transfer on the instability growth discussed.

In sections 3.2-3.5 a linear theory of the instability is considered for the infinite plasma, and in section 3.6 the effect of boundaries for the linear problem is discussed. Section 3.7 briefly discusses the non-linear aspects of one-dimensional non-uniformities.

The analyses presented below have been greatly simplified, since it is not the intention to duplicate the theoretical work of the previously mentioned authors; it is nevertheless necessary to present this work for two reasons. Firstly, a numerical simulation of the system requires a knowledge of the behaviour of the perturbed system, in order to decide on the choice of time and space increments necessary for numerical stability; and secondly, an insight into the solutions for the perturbed equations allows a direct comparison with numerical results in the linear phase. This leads both to a check on the numerical results and a greater understanding of the phenomena.

3.2 Linear Perturbation of the Equations

In this section the stability of equations (2.1)-(2.8) to linear perturbations will be investigated. The equations are transformed to the heavy particle frame, and all spatial gradients in the energy equation are neglected; this will be justified later. One-dimensional, small amplitude perturbations in n_e, T_e, $\underline{j}$ and $\underline{E}$ about a uniform state will be considered, and the equations linearized with respect to the perturbations. The uniform state is assumed to be in Saha equilibrium at the electron temperature, the Ohmic heating everywhere balancing the elastic collision losses.

The coordinate system for the one-dimensional problem is shown in figure 3.1; all quantities are written in the form

$$\chi = \chi_0 + \chi' \exp i(\omega t - ky)$$

where χ_0 is the uniform, undisturbed state.

Perturbation of the field equations - The perturbed versions of equations (2.7) and (2.8) are:

$$\underline{k} \cdot \underline{j}' = 0 = \underline{k} \times \underline{E}'$$

or $$E_x' = 0 \quad \text{and} \quad j_y' = 0.$$

Perturbation of the Ohms law - The 'x' component of equation (2.2) for the perturbed electric field and current is

$$j_x'/\sigma_0 - j_{ox}/\sigma_0^2 \cdot \sigma' = E_x' - j_{oy}\beta_0/\sigma_0\left[\beta'/\beta_0 - \sigma'/\sigma_0\right] - \beta_0 j_y'/\sigma_0$$

which gives

$$j_x'/j_0 = \sigma'/\sigma_0 \cdot \sin\alpha + \beta_0 \cos\alpha\left[\sigma'/\sigma_0 - \beta'/\beta_0\right] \qquad (3.1)$$

where $$j_{ox} = j_0 \sin\alpha \;, \quad j_{oy} = j_0 \cos\alpha$$

Perturbation of the Continuity Equation - The perturbed version of equation (2.1) in the heavy particle frame is:

$$\partial n_e/\partial t = i\omega n_e' = a_0 n_e' + a_1 T_e' \tag{3.2}$$

where $a_0 = \partial \dot{n}_e/\partial n_e$, $a_1 = \partial \dot{n}_e/\partial T_e$

Perturbation of the Energy Equation - Neglecting spatial gradients and radiation transfer in equation (2.6) gives, for the perturbed state,

$$a_2 \partial n_e'/\partial t + a_3 \partial T_e'/\partial t = i\omega [a_2 n_e' + a_3 T_e'] = (j^2/\sigma)' - L' \tag{3.3}$$

where $a_2 = 3/2\, K_B T_{e0} + I_p$ and $a_3 = 3/2\, n_{e0} K_B$

Perturbation of the Ohmic Heating -

$$(j^2/\sigma)' = -j_0^2 \sigma'/\sigma_0^2 + 2\, j_0^2/\sigma_0 \cdot j_x'/j_0 \cdot \sin\alpha$$

which from equation (3.1) becomes

$$(j^2/\sigma)' = \sigma' \left[j_0^2 \beta_0/\sigma_0^2 \cdot \sin 2\alpha - j_0^2/\sigma_0^2 \cdot \cos 2\alpha \right] - j_0^2 \beta_0'/\sigma_0 \sin 2\alpha \tag{3.4}$$

which with the definitions

$$j_0^2/\sigma_0^2 \left[\beta_0 \sin 2\alpha - \cos 2\alpha \right] \sigma' = a_4 n_e' + a_5 T_e'$$

and

$$-j_0^2 \beta'/\sigma_0 \cdot \sin 2\alpha = a_6 n_e' + a_7 T_e'$$

becomes

$$(j^2/\sigma)' = [a_4 + a_6] n_e' + [a_5 + a_7] T_e' \tag{3.5}$$

Perturbation of the Elastic Collision Losses -

$$-L' = a_8 n_e' + a_9 T_e' \tag{3.6}$$

where $a_8 = -\partial L_0/\partial n_e$, $a_9 = -\partial L_0/\partial T_e$

The equations (3.1)-(3.6) are combined to give

$$n_e' \left[i\omega a_2 - (a_4 + a_6 + a_8) \right] = \left[(a_5 + a_7 + a_9) - i\omega a_3 \right] T_e' \tag{3.7}$$

and

$$n_e' \left[i\omega - a_0 \right] = a_1 T_e' \tag{3.8}$$

3.3 Electrothermal Growth Rates

The coefficients a_0 to a_9 are all real and $i\omega$ must therefore be real. It follows from this that the waves are stationary in the heavy particle frame. This is a result of neglecting spatial gradients in the energy equation.

Eliminating n_e' and T_e' from equations (3.7) and (3.8), and writing $g = i\omega$ it follows that

$$g^2 - g b_0 - b_1 = 0 \qquad (3.9)$$

where $$b_0 = [(a_5 + a_7 + a_9) + (a_0 a_3 - a_1 a_2)]/a_3$$

and $$b_1 = [a_1(a_4 + a_6 + a_8) - a_0(a_5 + a_7 + a_9)]/a_3$$

Equation (3.9) is the dispersion relation for small amplitude electrothermal waves. This has two roots $g_\pm$, where

$$g_\pm = b_0/2 \pm [b_1 + b_0^2/4]^{1/2}$$

and corresponds to the existence of two modes with growth rates g_+ and g_-.

3.4 Electrothermal Modes

The two modes g_+ and g_- are referred to as the ionization mode and fast-thermal mode respectively (Nelson et al, 1969). The fast-thermal mode is always severely damped, whilst the ionization mode can become unstable under certain conditions. The properties of the latter mode were summarised in section 3.1.

(a) Fast-Thermal Mode

The decay time for this mode, $|g_-^{-1}|$, is plotted as a function of T_e in figure 3.2. Time scales rather than frequency scales are

plotted since these are a more relevant feature for numerical analysis. The wave is always severely damped, its decay time rapidly decreasing with increasing T_e. Owing to its short decay time the wave is little affected by Ohmic heating or collision losses, and the total energy, thermal and ionization, is approximately conserved. The wave can therefore be described by the equations

$$\partial n_e'/\partial t = a_0 n_e' + a_1 T_e' \quad ; \qquad a_1 > 0, \; a_0 < 0$$

and

$$\partial T_e'/\partial t = -\, a_2/a_3 \cdot \partial n_e'/\partial t$$

Physically, a small positive perturbation in T_e leads, through ionization, to an increase in electron density and ionization energy. Since the total energy is approximately conserved, the increase in ionization energy results in a large decrease in thermal energy which stabilizes the electron temperature. The decay time decreases with increasing T_e because of the increasing rates of ionization and recombination at higher temperatures.

The ratio of the fractional fluctuations is given by

$$T_e^*/n_e^* = -\, a_2 n_{eo}/a_3 T_{eo} \sim -T_P/T_{eo}$$

so that

$$|T_e^*| \gg |n_e^*|$$

Moreover,

$$|a_0 n_{eo}/a_1 T_{eo}| \ll 1$$

giving

$$g_- \sim -\, T_P/T_{eo} \cdot [a_1 T_{eo}/n_{eo}] \sim -\left[T_P/T_{eo}\right]^2 \nu_{ro}$$

where ν_{ro} is defined by

$$\dot{n}_{eo} = n_{eo}(\nu_{io} - \nu_{ro})$$

The perturbed energy equation, again excluding source terms but with compressional effects and convection included, takes the form

$$n_{eo} I_p \partial n_e^*/\partial t + 3/2\, n_{eo} k_B T_{eo}\, \partial T_e^*/\partial t = -iK\left[3/2\, T_e^* - n_e^*\right] j_{oy} k_B T_{eo}/e$$

$$\approx -\, i\, \frac{3 k_B T_{eo}}{2e}\, j_{oy} K T_e^*$$

and $3/2 \frac{k_B T_{eo}}{e} j_{oy} K T_e^* / \frac{3}{2} n_{eo} k_B T_{eo} g_- T_e^* \sim 10^{-4}$

for $\lambda = 10^{-2}$m and $T_e = 3000^{\circ}$K. The effects of wave motion are therefore negligible during the decay time of the wave.

(b) Ionization Mode

Growth times for this mode are plotted in figure 3.3 as a function of T_e, and for several magnetic field strengths. The angle between $\underline{j}_0$ and $\underline{K}$ is taken to be $\pi/4$, since this is approximately the angle for maximum growth of an unstable wave. The growth rate decreases at lower temperatures owing to the reduced Ohmic heating, j_0^2/σ_0, necessary to maintain the non-equilibrium ionization; and less importantly the effect of decreasing ionization rates at lower temperatures. The growth rate decreases at higher temperatures as a result of the increased electron collision frequency and correspondingly decreased Hall parameter, figure 1.6. For the range of temperatures and magnetic field strengths considered in figure 3.3 β_{crit} is approximately 1.7, the exact value depending on T_e. The inclusion of thermal conduction and radiation transfer in the energy equation would also modify this value.

From equation (3.8) with $i\omega = g_+$ it follows that if $|g_+| \ll |a_0|$ Saha equilibrium can be assumed. In figure 3.4 the ratio $|g_+/a_0|$ is plotted as a function of T_e for several magnetic field strengths. It is seen that for $T_e \gtrsim 3000^{\circ}$K and $\beta \lesssim 8$, $|g_+/a_0| \lesssim 0.1$, so that Saha equilibrium becomes a valid approximation. In this case equation (3.2) becomes

$$n_e^*/T_e^* \approx -a_1 T_{eo}/a_0 n_{eo} \approx T_p/2T_{eo} \gg 1$$

The angular dependence of the instability arises from equation (3.4) for the perturbed Ohmic heating. In the Coulomb collision dominated regime $\sigma^* \approx 0$ and $\beta^* \approx - n_e^*$, according to $T_e^* << n_e^*$, so that

$$(j^2/\sigma)^* \approx n_e^* \beta_0 \sin 2\alpha$$

which maximises at $\alpha = \pi/4$

Similarly, in the binary collision dominated regime $\sigma^* \approx n_e^*$ and $\beta^* \approx 0$.

$$(j^2/\sigma)^* \approx n_e^* \left[\beta_0 \sin 2\alpha - \cos 2\alpha\right]$$

which maximises at $\alpha = \frac{\pi}{4} + \frac{1}{2}\tan^{-1} 1/\beta_0$, and approaches $\pi/4$ at large β_0 .

The perturbed energy equation (3.3), but with compressional effects and convection included, takes the form

$$n_{e0}(I_p + 3/2\, k_B T_{e0})\, \partial n_e^*/\partial t + \tfrac{3}{2} n_{e0} k_B T_{e0}\, \partial T_e^*/\partial t = (j^2/\sigma)' - L'$$
$$- iK\left[\tfrac{3}{2} T_e^* - n_e^*\right] k_B T_{e0}\, j_{0y}/e$$

or $$n_{e0} I_p\, \partial n_e^*/\partial t \approx (j^2/\sigma)' - L' + i\, k_B T_{e0}\, j_{0y} K n_e^*/e$$

from $T_e^* << n_e^*$. The imaginary part of this equation gives the wave velocity

$$\omega_r/K \approx T_{e0}/T_p \cdot j_0/n_{e0} e \cdot \cos\alpha \sim 10 \text{ m sec}^{-1}$$

for $T_{e0} = 3000^{\circ}$K; and for $\lambda = 10^{-2}$m, ω_r/g_+ varies from approximately 10^{-2} to 10^{-1} as β varies from 9 to 2.6. The effects of wave motion are therefore not important during the growth time of an unstable wave, provided β is not too close to β_{crit}.

The electron thermal conduction becomes an important damping mechanism for the wave when

$$\nabla \cdot (K_{e0} \nabla T_e)' = -k^2 K_{e0} T_e' \sim (j^2/\sigma)'$$

which is satisfied for $\lambda < 10^{-3}$m when $\beta_o > 2$ at $T_e = 3000^oK$. Neglecting all spatial gradients in the energy equation is therefore reasonable for the characteristic growth times and observed wavelengths of the electrothermal instability.

3.5 Simplified Model of Ionization Mode

In order to obtain a simple analytic expression for the growth rate, and critical Hall parameter of the ionization mode, the preceding analysis will be simplified still further. Fluctuations in T_e will be neglected compared with those in n_e, and the two extreme regimes of a Coulomb collision dominated plasma and a binary collision dominated plasma will be discussed.

(a) Coulomb Collision Dominated Plasma

The perturbed energy equation becomes

$$n_{eo} I_p \sigma_o g_+ n_e^*/j_o^2 = (j^2/6)^* - L^*$$

with $$(j^2/6)^* = n_e^* \beta_o \sin 2\alpha$$

and since $$L = 3 n_e k_B (T_e - T) \frac{m_e}{m_s} \nu_{ec} \propto n_e^2$$

$$L^* = 2 n_e^*$$

giving $$g_+ = j_o^2/\sigma_o n_{eo} I_p \cdot (\beta_o \sin 2\alpha - 2)$$

and $$g_{+\,max} = j_o^2/\sigma_o n_{eo} I_p \cdot (\beta_o - 2) \qquad (3.10)$$

Thus, $\beta_{crit} = 2$ in this approximation, and the growth rate is proportional to the zero order Ohmic heating in the plasma. The source of the instability is clear. The presence of small amplitude non-uniformities lead to a perturbed current flow which will interact with the local electric fields, in particular the Hall field, to produce additional dissipation in the plasma, which cannot be wholly transferred to the heavy particles by elastic collisions. This excess energy will be

taken up in ionizing collisions to produce an increased electron density in the peaks of the wave, which will serve to maintain the perturbed currents. The wave will grow until non-linear effects become important.

(b) Binary Collision Dominated Plasma

In this case one has

$$n_{e_0} I_p \sigma_0 g_+ n_e^* / j_0^2 = (j^2/6)^* - L^*$$

with $$(j^2/6)^* = n_e^* (\beta_0 \sin 2\alpha - \cos 2\alpha)$$

and since $$L = 3 n_e K_B (T_e - T) \frac{m_e}{m_n} \nu_{eB} \propto n_e$$

$$L^* = n_e^*$$

giving $$g_+ = j_0^2 / \sigma_0 n_{e_0} I_p \cdot (\beta_0 \sin 2\alpha - \cos 2\alpha - 1)$$

and $$g_{+\,max} = j_0^2 / \sigma_0 n_{e_0} I_p \cdot \left[\sqrt{1+\beta_0^2} - 1 \right] \qquad (3.11)$$

In this approximation $\beta_{crit} = 0$. This result follows from the relative inefficiency of energy transfer through binary collisions, and neglect of the fluctuations in T_e. Moreover, since binary collisions dominate for $T_e < 2500^{\circ}K$, from figure 1.5, finite ionization-recombination rates will have a substantial stabilizing effect on the wave.

3.6 Effect of Boundaries on the Electrothermal Instability

In this section the approximations of section 3.5(a) will be used to determine the effects of finite geometry on the growth of the instability. The geometry of the system is shown in figure 3.5. The plasma is contained between two electrically insulating walls situated at $x = 0$ and $x = H$. The plasma is of infinite extent in the 'y' direction

and a uniform discharge is maintained along its length. Similar studies have been made by Nelson (1969) and Riedmüller (1970). The problem is considered here because of its relevance to numerical simulations of the bounded plasma, and also because it demonstrates the hyperbolic nature of the basic equations in this approximation.

(a) Linear Perturbation of the Equations

The plasma is assumed to be dominated by Coulomb collisions and fluctuations in T_e are neglected compared with those in n_e. From section 3.5(a) the energy equation may be written

$$\partial n_e^*/\partial \tau = (j^2/\sigma)^* - 2 n_e^*$$

where $$\tau = j_o^2/\sigma_o n_{eo} I_p \cdot t$$

and the perturbed Ohmic heating is

$$(j^2/\sigma)' = 2 j_{oy} j_y'/\sigma_o \qquad j_{oy} = j_o = \text{constant}$$

since $j_{ox} = 0$, and $\sigma^* = 0$ in this approximation. Defining a stream function for the perturbed current

$$j_y'/j_o = \partial\psi/\partial x \qquad \text{and} \qquad j_x'/j_o = -\partial\psi/\partial y$$

automatically satisfies $\nabla . \underline{j}' = 0$ and reduces the number of variables to two. This gives

$$(j^2/\sigma)^* = 2\,\partial\psi/\partial x$$

The energy equation therefore becomes

$$\partial n_e^*/\partial \tau = 2\,\partial\psi/\partial x - 2 n_e^* \qquad (3.12)$$

The perturbed Ohms law in component form, may be written

$$E_x' = j_x'/\sigma_o + \beta_o j_y'/\sigma_o + \beta_o \beta^* j_o/\sigma_o$$

and

$$E_y' = j_y'/\sigma_o - \beta_o j_x'/\sigma_o$$

which gives, using $\nabla \times \underline{E}' = 0$ and the definition of ψ ,

$$\nabla^2 \psi = -\beta_0 \partial n_e^* / \partial y \tag{3.13}$$

Equations (3.12) and (3.13) combine to give

$$\frac{\partial}{\partial \tau} \nabla^2 \psi + 2 \nabla^2 \psi + 2\beta_0 \frac{\partial^2 \psi}{\partial x \partial y} = 0 \tag{3.14}$$

with the boundary conditions $\psi(0,y,\tau) = 0 = \psi(H,y,\tau)$, ie: the total current flow down the duct remains constant and $j_x' = 0$ at the walls. Assuming a separable solution of the form

$$\psi(x,y,\tau) = \sum_n \exp(g_n \tau)\, \psi_n(x,y)$$

this gives, when substituted into equation (3.14)

$$\nabla^2 \psi_n + a_n \partial^2 \psi_n / \partial x \partial y = 0 \tag{3.15}$$

where

$$a_n = 2\beta_0 / (g_n + 2) \tag{3.16}$$

If the perturbations possess a single wavelength, $L = \frac{2\pi}{K_y}$, in the 'y' direction, then a solution to equation (3.15) which satisfies the boundary conditions is

$$\psi_n(x,y) = \sin \frac{n\pi x}{H} \left\{ \begin{array}{l} C_1 \sin k_y (y - a_n x/2) \\ C_2 \cos k_y (y - a_n x/2) \end{array} \right\} \tag{3.17}$$

with

$$g_n = \beta_0 \left[1 + \left(\frac{nL}{2H} \right)^2 \right]^{-1/2} - 2 \tag{3.18}$$

The above solution for $\psi_n(x,y)$ corresponds to eddy current flow in the (x, y) plane, the number of closed eddies between the walls being equal to 'n'. Figure 3.6 shows the distribution of n_e^* for an n = 1 mode with $C_2 = 0$, L = H and $\beta_0 = 4.5$, and figure 3.7 the corresponding distributions for ψ . This is approximately plane-wave like. From equation (3.18) it is seen that the effect of finite geometry is to increase $\beta_{0\,crit}$ above the infinite plasma value. This is because the boundary conditions do not allow the 'wave vector' to attain the direction of maximum growth with respect to $\underline{j}_0$.

A detailed description of the wave orientation, and its effect of the stability of a given mode has been given by Nelson (1969), the general conclusions are that the 'wave vector' for a given 'n' mode becomes closer to the direction for maximum growth as β_o is increased. With increasing β_o successively higher 'n' modes become unstable, and the final distribution is a sum of approximate 'plane-waves', each possessing a different orientation with respect to $\underline{j}_0$.

(b) Hyperbolic Nature of the Equations

It was shown in Chapter II that the equations corresponding to the above physical approximations are parabolic in general and hyperbolic in steady-state. This is also true for the linearized equations (3.12) and (3.13). The use of a separable solution leads to a hyperbolic set. The condition that equation (3.15) be hyperbolic is $|a_n| > 2$, which is automatically satisfied by the previous solutions, equations (3.17) and (3.18). In obtaining these solutions, however, the system was assumed to be periodic in the 'y' direction, ie: a length of the duct was chosen arbitrarily, and boundary conditions for specified all around the chosen interval. This procedure would be necessary for an elliptic problem, but requires some justification for the hyperbolic problem. To simplify the discussion further, the case of linear, steady-state non-uniformities is considered, ie: $g_n = 0$. Equation (3.14) may then be written in the form of a wave equation

$$\frac{\partial^2 \psi}{\partial x^2} - \frac{\partial^2 \psi}{\partial t'^2} = 0 \quad , \qquad t' = \frac{y - \beta_o/2 \cdot x}{\sqrt{\beta_o^2/4 - 1}}$$

The characteristics for this equation are

$$y_+ = \left[\beta_0/2 + \sqrt{\beta_0^2/4 - 1} \right] x + c_+$$

and

$$y_- = \left[\beta_0/2 - \sqrt{\beta_0^2/4 - 1} \right] x + c_-$$

A solution to the hyperbolic problem is uniquely determined in a region bounded by the element of the boundary along which ψ is specified, and the characteristics which pass through the extremities of the element, Ames (1969).

In figure 3.8 a few of the characteristics are drawn in the physical (x,y) plane. The characteristics are straight lines in this case, in the non-linear problem they would form two families of curves. It can be seen that specification of ψ on AE leads to a unique solution of ψ within ABE. Specification of ψ along AG, however, would lead to a determination of ψ outside the physical domain and would also specify the solution along CI. a section of the physical boundary. Since this is not plausible, boundary conditions need only be applied along AF, of length L, to determine the solution within ACF. Similarly, specification of ψ along HC will determine ψ within HCA. The solution is therefore restricted to an area AFHC, and Fourier analysis in the 'y' direction is permitted over an interval L. In the previous section only one Fourier mode, k_y, was considered. The length L can be determined from geometry, and

$$L = H \left[\beta_0^2 - 4 \right]^{1/2} \tag{3.19}$$

corresponding to $\vartheta_n = 0$ and $n = 1$ in equation (3.18).

As mentioned in Chapter II, possible discontinuities in the field gradients can occur across the characteristics; whilst this is permissible in an analytic Fourier series, in which the boundaries are approached in opposite senses, it is not always permissible numerically. This is because numerically the condition of periodicity is satisfied by equating east-west mesh boundaries. Provided these boundaries do not coincide with the characteristics, however, this procedure is valid.

3.7 Non-Linear Effects of the Electrothermal Instability

In the linear theory of the instability the average plasma properties remain constant at the unperturbed values. If second order effects are considered this is no longer true, and the averaged plasma parameters are affected by the presence of non-uniformities. In this section the effect of one-dimensional non-uniformities on the effective conductivity and effective Hall parameter for the infinite plasma will be briefly discussed. The results presented below are similar to those obtained by Rosa (1962), who considered a plasma comprising alternate layers of conductivity σ_1 and σ_2 and Hall parameter β_1 and β_2, but in a somewhat different form.

All plasma parameters are taken to be functions of 'x' only, and represented as $\chi(x) = \chi_0 + \chi'(x)$ where χ_0 is the space average of χ. The field equations give $j'_x = 0$ and $E'_y = 0$. The components of Ohms law are written in the following way:

$$j_y = \sigma \mathcal{E}_y + \beta j_x \tag{3.20}$$

and $$\left[\frac{1+\beta^2}{\sigma}\right] j_x = \mathcal{E}_x - \beta \mathcal{E}_y \tag{3.21}$$

Taking the 'x' average of equations (3.20) and (3.21) gives, neglecting the ∇p_e contribution to current flow,

$$j_{oy} = \sigma_o \mathcal{E}_{oy} + \beta_o j_{ox} \tag{3.22}$$

and $$\left[\frac{1+\beta^2}{\sigma}\right]_o j_{ox} = \mathcal{E}_{ox} - \beta_o \mathcal{E}_{oy} \tag{3.23}$$

putting $a_o = \sigma_o\left[\frac{1+\beta^2}{\sigma}\right]_o - \left[1+\beta_o^2\right] \geqslant 0$ from Schwarz's inequality.

Solving equations (3.22) and (3.23) for $\underline{\mathcal{E}}_o$ gives

$$j_{oy} - \beta_o j_{ox} = \sigma_o \mathcal{E}_{oy} \tag{3.24}$$

and $$j_{ox}(1+a_o) + \beta_o j_{oy} = \sigma_o \mathcal{E}_{ox} \tag{3.25}$$

(a) Effective Conductivity

The average Ohmic heating is computed from equations (3.24) and (3.25), the result is:

$$(j^2/\sigma)_o = j_{ox}\mathcal{E}_{ox} + j_{oy}\mathcal{E}_{oy}$$
$$= j_o^2/\sigma_o\left[1 + a_o\cos^2\alpha\right]; \quad j_{ox} = j_o\cos\alpha$$

The effective conductivity can therefore be written

$$\frac{\sigma_{eff}}{\sigma_o} = \frac{j_o^2/\sigma_o}{(j^2/\sigma)_o} = \frac{j_o}{\sigma_o \mathcal{E}_{o\parallel}} = \left[1 + a_o\cos^2\alpha\right]^{-1} \leqslant 1 \tag{3.26}$$

(b) Effective Hall Parameter

The components of the averaged electric field parallel and perpendicular to $\underline{j}_0$ are

$$\mathcal{E}_{o\parallel} = \mathcal{E}_{ox}\cos\alpha + \mathcal{E}_{oy}\sin\alpha$$

and $$\mathcal{E}_{o\perp} = \mathcal{E}_{ox}\sin\alpha - \mathcal{E}_{oy}\cos\alpha$$

Substituting these values in equations (3.24) and (3.25) gives

$$\beta_{eff} = \frac{\mathcal{E}_{o\perp}}{\mathcal{E}_{o\parallel}} = \frac{\beta_o + a_o\sin\alpha\cos\alpha}{1 + a_o\cos^2\alpha} \tag{3.27}$$

For the highest growth rate waves-$\alpha = \pi/4$, in this coordinate system, so that

$$\frac{\sigma_{eff}}{\sigma_0} = \left[1 + a_0/2\right]^{-1} \ll 1$$

and

$$\beta_{eff} = \left[\beta_0 - a_0/2\right]\left[1 + a_0/2\right]^{-1} \ll \beta_0$$

3.8 Summary

The linearized equations of the electrothermal system were found to possess two modes, the fast-thermal mode and the ionization mode. The fast-thermal mode is always severely damped, whilst the ionization mode is unstable for β greater than about two. The orientation of the wave vector for maximum growth was found to satisfy

$$\frac{\underline{j} \times \underline{k} \cdot \underline{B}}{\underline{j} \cdot \underline{k} \, |\underline{B}|} \approx 1$$

The assumption of Saha equilibrium was shown to be a reasonable approximation for the description of the ionization mode at large T_e. Simple analytic expressions for the velocity of the ionization mode and its growth rate were obtained.

The effect of finite geometry was found to have a stabilizing influence on waves of a given periodicity; and the 'periodicity' assumption for the hyperbolic problem justified under certain conditions.

Finally, the effective conductivity and Hall parameter were found to be decreased, in second order, owing to the presence of non-uniformities. It is shown in Chapters VI and VII that σ_{eff} and β_{eff} are considerably modified by large amplitude non-uniformities in the plasma parameters.

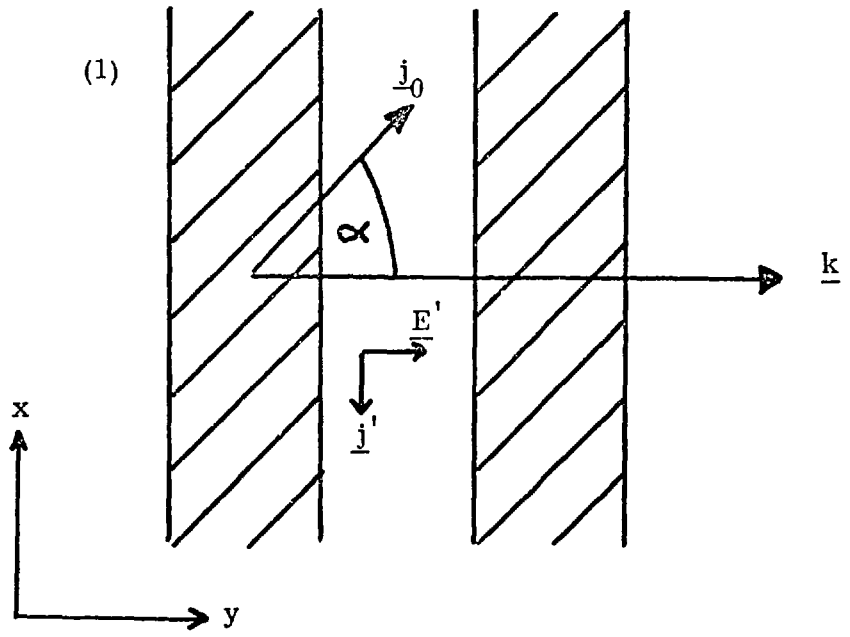

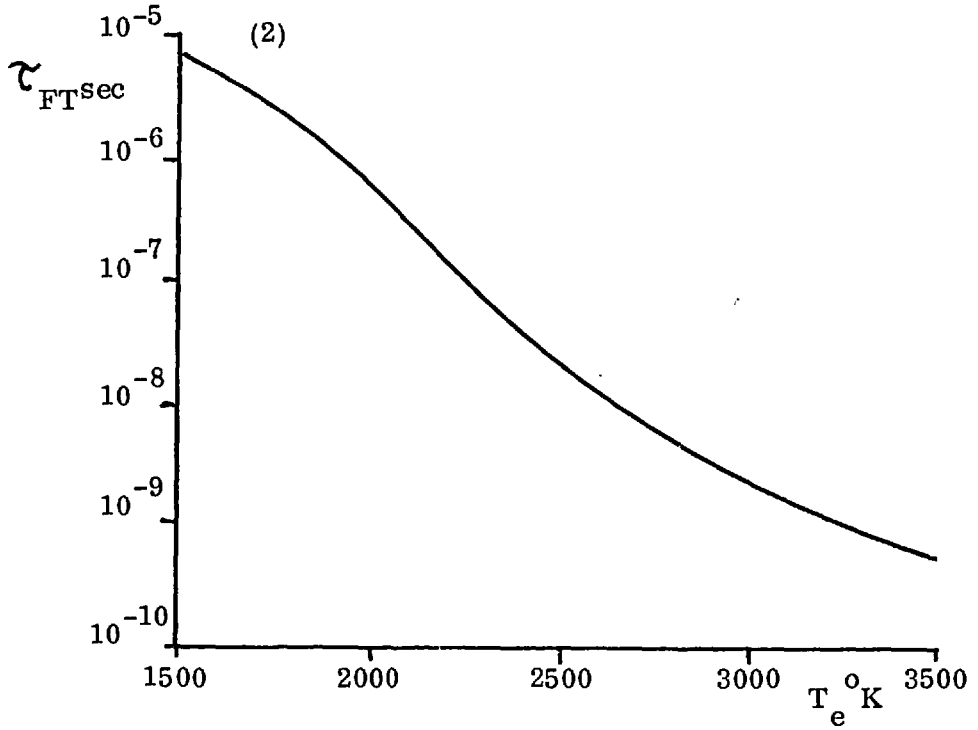

(1) Figure 3.1: Coordinate system for one-dimensional electrothermal wave theory.

(2) Figure 3.2: Decay time for the fast-thermal mode $\tau_{FT} = |g_-^{-1}|$ against T_e.

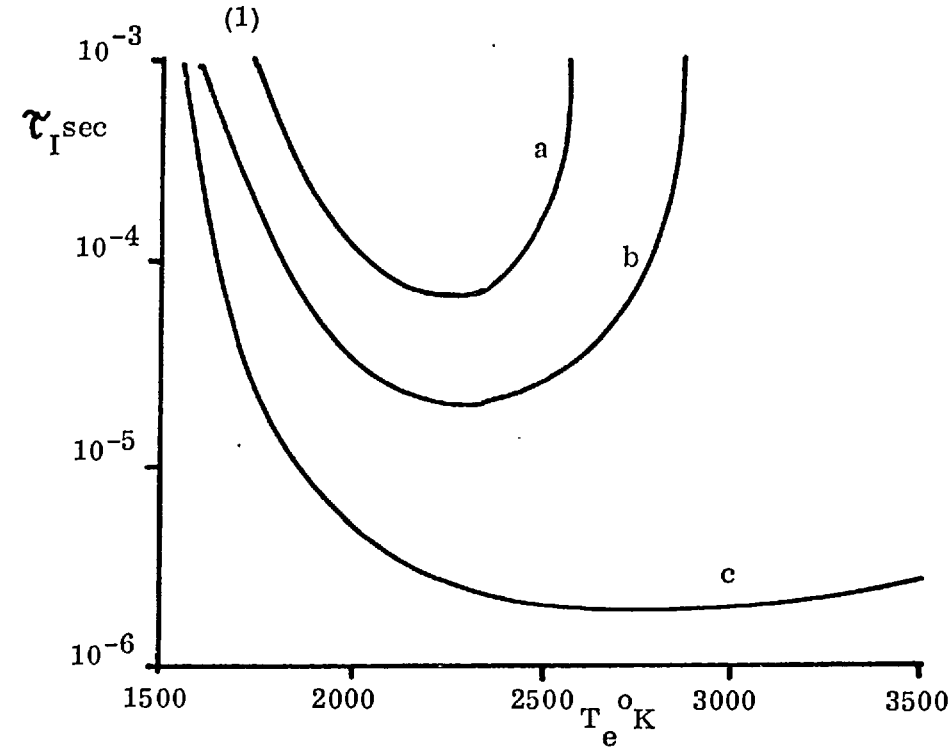

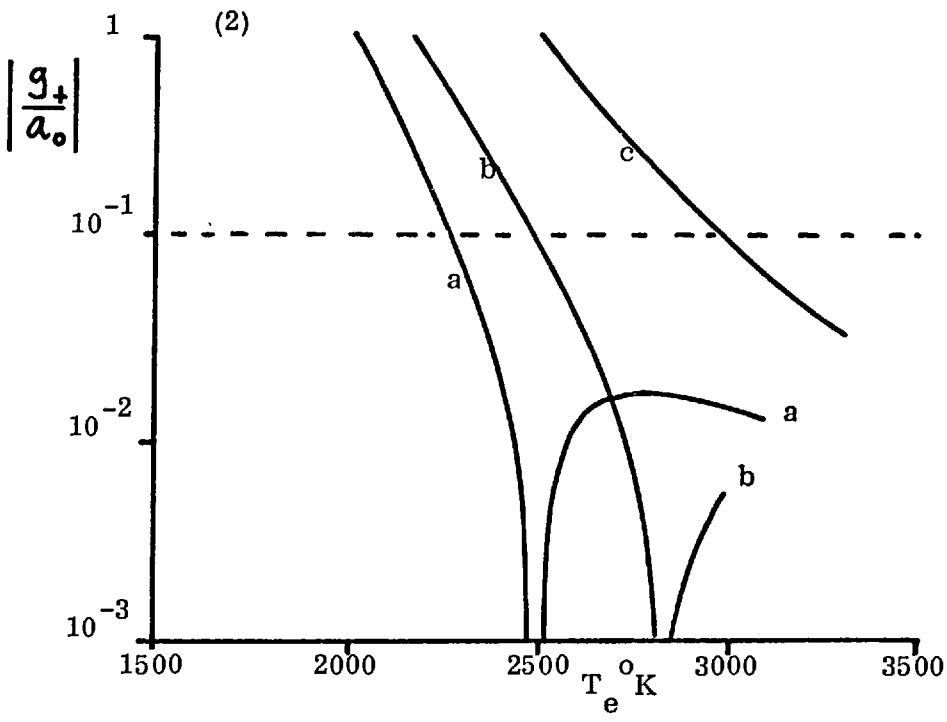

(1) Figure 3.3: Ionization mode growth time $\tau_I = |g_+^{-1}|$ against T_e for (a) B = 0.5 T; (b) B = 1 T; (c) B = 6 T.

(2) Figure 3.4: $|g_+/a_0|$ against T_e for (a) B = 0.5 T; (b) B = 1 T; (c) B = 6 T.

(1)

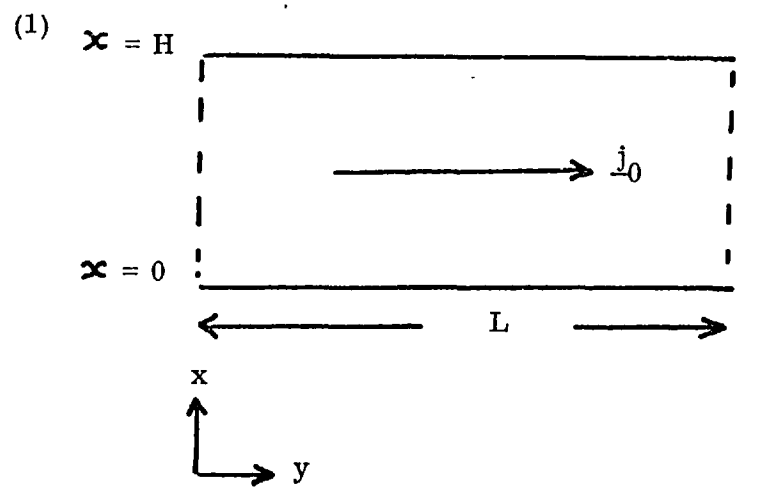

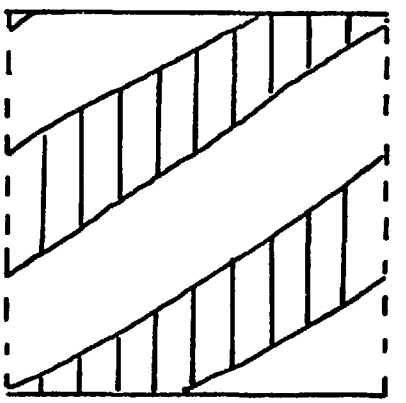

(2)

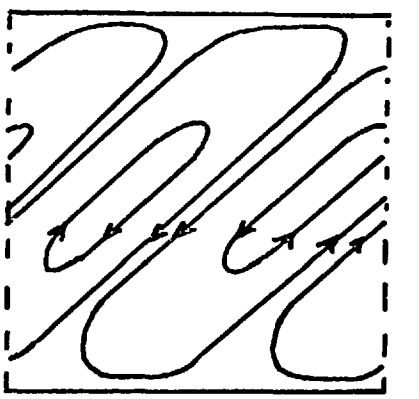

(3)

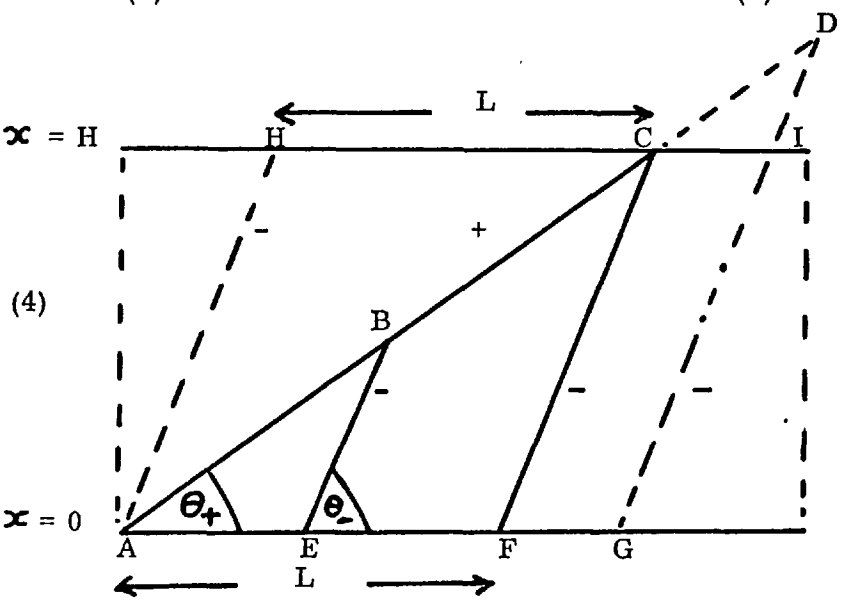

(1) Figure 3.5: Geometry for boundary analysis.

(2) Figure 3.6: n_e^* for $n = 1$, $C_2 = 0$, $L = H$, $\beta = 4.5$. $n_e^* > 0$ shaded.

(3) Figure 3.7: ψ for above values.

(4) Figure 3.8: Characteristics + and - in (x,y) plane.

CHAPTER IV

DYNAMIC STABILIZATION OF THE ELECTROTHERMAL INSTABILITY

4.1 Introduction

In this Chapter the possibility of stabilizing the electrothermal instability by applying an oscillation to the steady current in an MHD generator is examined. A linear plane-wave analysis is used.

In Chapter III it was shown that the growth rate of the instability is dependent on the orientation of the wave vector with respect to the steady state current density flowing in the duct. The angle between $\underline{j}_0$ and $\underline{k}$ being α. It was found that the growth rate for the instability maximises for an α of the order of $\pi/4$ and $5\pi/4$, and that the disturbance remains in the unstable regime over a range of angles $\pm\Delta\alpha$ about these values. $\Delta\alpha$ depending upon plasma properties and Hall parameter. It is this directional property of the instability which makes it amenable to dynamic stabilization.

The electric fields considered will induce an oscillatory time dependence in α, the oscillatory part having an amplitude of oscillation, η, sufficient to remove the current vector from the zone of instability for any given $\underline{k}$ during part of the cycle. In this way it is hoped that net stability results for all $\underline{k}$. It is assumed therefore that

$$\alpha(t) = \alpha_0 + \eta \sin \Omega t \qquad (4.1)$$

where α_0, the angle determined by the steady part of the total current, is taken to be $\pi/4$.

4.2 The Stabilizing Fields

In order to achieve the variation in α given by equation (4.1) the current density must vary in time, ie:

$$\underline{j}(t) = \underline{j}_0 + \underline{j}'(t)$$

where $\underline{j}_0$ is the steady state current density in absence of dynamic stabilization. It is convenient to oscillate $\underline{j}$ while maintaining its magnitude constant at $|\underline{j}_0|$, so that the Ohmic heating within the duct will remain unaltered during the oscillation. This means that the ambient plasma parameters will remain constant also, since in the non-equilibrium plasma they depend solely on the Ohmic heating, and the analysis of the instability is greatly simplified. One has therefore

$$j_x = |\underline{j}_0| \sin\alpha(t) \qquad (4.2a)$$

$$j_y = |\underline{j}_0| \cos\alpha(t) \qquad (4.2b)$$

with $\underline{K} = |\underline{K}|\hat{y}$

From which it follows that

$$|\underline{j}'(t)| = 2\,|\underline{j}_0| \sin\left[\eta/2 \sin\Omega t\right]$$

which vanishes when averaged over time. The directional property of $\underline{j}'(t)$ is given by the scalar product

$$\underline{j}'(t) \cdot \underline{j}_0 = |\underline{j}_0|\,|\underline{j}'(t)| \cos\left[\pi/2 + \eta/2 \cdot \sin\Omega t\right]$$

The electric fields required to affect the above current modulation are found from the zero order Ohms law. In the frame of reference of the heavy particles the two components of the Ohms law, equation (2.2), may be written

$$j_x = \frac{\sigma_o}{1+\beta_o^2}\left[E_x - \beta_o E_y\right] \tag{4.3a}$$

$$j_y = \frac{\sigma_o}{1+\beta_o^2}\left[E_y + \beta_o E_x\right] \tag{4.3b}$$

where $\underline{E}$ is the Lorentz electric field and σ_o, β_o the zero order electrical conductivity and Hall parameter respectively. $\underline{E}$ is now considered to comprise a stationary part $\underline{E}_0$ and an applied oscillating part $\underline{E}_A(t)$.

From equations (4.2) and (4.3) it follows that

$$|\underline{j}_o| \sin\alpha(t) = \frac{\sigma_o}{1+\beta_o^2}\left[\left\{E_{ox}+E_{Ax}(t)\right\} - \beta_o\left\{E_{oy}+E_{Ay}(t)\right\}\right]$$

and

$$|\underline{j}_o| \cos\alpha(t) = \frac{\sigma_o}{1+\beta_o^2}\left[\left\{E_{oy}+E_{Ay}(t)\right\} + \beta_o\left\{E_{ox}+E_{Ax}(t)\right\}\right]$$

The components of the applied oscillating field, perpendicular and parallel to $\underline{j}_0$, as obtained from the above expressions may be written in the following form

$$E_{A\perp}(t) = -|\underline{j}_o|/\sigma_o \cdot \left[\beta_o - \sqrt{1+\beta_o^2}\,\cos(\eta \sin\Omega t + \delta_1)\right]$$

$$E_{A\parallel}(t) = -|\underline{j}_o|/\sigma_o \cdot \left[1 + \sqrt{1+\beta_o^2}\,\sin(\eta \sin\Omega t + \delta_1)\right]$$

where $\delta_1 = \tan^{-1}\left[-1/\beta_o\right]$

These components can be written in Fourier series form, the coefficients in the series being Bessel functions of argument η and of order equal to that of their associated Fourier component. For η in the range of interest these coefficients rapidly decrease with increasing order.

4.3 Stability Analysis

The equations used for this analysis are:

(i) Saha equilibrium, equation (1.4). The assumption of Saha equilibrium has been discussed in Chapter III. The inclusion of finite ionization-recombination rates has a stabilizing effect on the wave; the limiting values of Ω for stability obtained here may therefore be considered maximum estimates.

(ii) Electron energy equation, equation (2.6) with $\underline{v} = 0$. It is assumed that radiation transfer and thermal conduction are negligible, ie: only waves satisfying $\lambda \gg 10^{-3}$m are considered. The inclusion of these effects would have a stabilizing effect on the wave.

(iii) The Ohms law and field equations, equations (2.2), (2.7) and (2.8) with $\underline{v} = 0$.

The above set of equations is linearized and the first order energy equation, together with the Ohms law and field equations give

$$P\,\partial n_e^*/\partial t + B'\cos\alpha(t)\,\partial n_e^*/\partial y - \tfrac{3}{2}B'\cos\alpha(t)\,\partial T_e^*/\partial y$$

$$+ n_e^*\left[Q - R\sin^2\alpha(t) - L\beta_0\sin\alpha(t)\cos\alpha(t)\right]$$

$$+ A\,\partial T_e^*/\partial t + T_e^*\left[S + J\sin^2\alpha(t)\right] = 0 \qquad (4.4)$$

It has been assumed that electrothermal waves are propagating in the y direction so that

$$\partial/\partial x = 0 = \partial/\partial z$$

The coefficients in equation (4.4) are given by:

$$P = n_{eo} k_B T_{eo} \left[3/2 + T_p/T_{eo} \right]$$

$$Q = \frac{j_o^2}{\sigma_o} \left[2 - \frac{\nu_{eco}}{\nu_{eo}} \left\{ 1 - 1/2 \ln \Lambda_o \right\} \right] + 3 n_{eo} k_B (T_{eo} - T) \frac{m_e}{m_s} \left[1 - 1/2 \ln \Lambda_o \right] \nu_{eco}$$

$$R = 2 j_o^2 / \sigma_o \left[1 - \frac{\nu_{eco}}{\nu_{eo}} \left\{ 1 - 1/2 \ln \Lambda_o \right\} \right]$$

$$S = -\frac{j_o^2}{\sigma_o} \left[\frac{3 \nu_{eco}}{2 \nu_{eo}} \left\{ 1/\ln \Lambda_o - 1 \right\} + \frac{\nu_{eBo}}{\nu_{eo}} \left\{ \phi + 1/2 \right\} \right] + 3 n_{eo} k_B (T_{eo} - T)$$

$$\cdot \left[\frac{3 m_e}{2 m_s} \nu_{eco} \left\{ 1/\ln \Lambda_o - 1 \right\} + \frac{m_e}{m_n} \nu_{eBo} (\phi + 1/2) \right]$$

$$+ 3 n_{eo} k_B T_{eo} \left[\frac{m_e}{m_s} \nu_{eco} + \frac{m_e}{m_n} \nu_{eBo} \right]$$

$$B' = j_o k_B T_{eo} / e$$

$$A = 3/2 \, n_{eo} k_B T_{eo}$$

$$L = 2 j_o^2 / \sigma_o$$

$$J = 2 j_o^2 / \sigma_o \left[\frac{\nu_{eco}}{\nu_{eo}} \left\{ 3/2 \ln \Lambda_o - 2 - \phi \right\} + (\phi + 1/2) \right]$$

$$\phi = \left[1 - 10^3 / 1.1 T_{eo} \right]^{-1}$$

The first order Saha equation is

$$a_0 T_e^* + b_0 n_e^* = 0 \tag{4.5}$$

with $a_0 = 3/2 + T_p/T_{eo}$

and $b_0 = [n_{eo} - 2n_s]/[n_s - n_{eo}]$

Assuming modified plane wave solutions

$$\begin{bmatrix} n_e^*(t) \\ T_e^*(t) \end{bmatrix} = \begin{bmatrix} n_e^*(o) \\ T_e^*(o) \end{bmatrix} \cdot \xi(t) \cos(\omega t - Ky)$$

where $\xi(t)$ is the characteristic growth function for the disturbance and ω is a function of time. Substituting into equation (4.4) one forms the condition for non-trivial solutions with equation (4.5), namely that the determinant formed from the coefficients of $n_e^*(0)$, $T_e^*(0)$ in equations (4.4) and (4.5) should vanish. This yields

$$\begin{aligned} &\cos(\omega t - Ky)\left[a_0 P\, \partial\xi/\partial t + a_0 Q\, \xi - a_0 R\, \xi \sin^2\alpha \right. \\ &\left. - a_0 L \beta_0 \xi \sin 2\alpha/2 - b_0 A\, \partial\xi/\partial t - b_0 (S + J\sin^2\alpha)\xi \right] \\ &+ \sin(\omega t - Ky)\left[a_0 B' K \xi \cos\alpha - a_0 P \xi\, \partial(\omega t)/\partial t \right. \\ &\left. + b_0 A \xi\, \partial(\omega t)/\partial t + 3/2\, b_0 B' K \xi \cos\alpha \right] = 0 \end{aligned}$$

The coefficients of $\sin(\omega t - ky)$ and $\cos(\omega t - ky)$ must vanish. This yields two differential equations, one for $\xi(t)$, and the other for V_p, the phase velocity, where

$$V_p(t) = \omega(t)/K$$

The initial condition for the solution of $V_p(t)$ is that at $t = 0$ V_p must remain finite.

$$V_p(t) = \frac{a_0 + 3/2\, b_0}{a_0 P - b_0 A} \cdot B' \cdot \left[J_0(\eta) \cos\alpha_0 + 2 \sum_{\substack{n=-\infty \\ \neq 0}}^{\infty} \frac{J_n(\eta)}{n\Omega t} \sin\left(\frac{n\Omega t}{2}\right) \cos\left\{\alpha_0 + \frac{n\Omega t}{2}\right\} \right]$$

where the J_n's are Bessel functions of the first kind. The solution for the growth function may be written

$$\log \xi(t) = \left[a_1 - a_2 \cos(2\alpha_0 + \phi_0) J_0(2\eta)\right] t - \frac{2a_2}{\Omega} \sum_{\substack{n=-\infty \\ \neq 0}}^{\infty} \frac{J_n(2\eta)}{n} \sin\left(\frac{n\Omega t}{2}\right) \cos\left(2\alpha_0 + \phi_0 + \frac{n\Omega t}{2}\right)$$

where

$$\phi_0 = \tan^{-1}\left[\frac{a_0 L \beta_0}{a_0 R + b_0 J}\right]$$

$$a_1 = \frac{2b_0 S + a_0 R + b_0 J - 2a_0 Q}{2(a_0 P - b_0 A)}$$

$$a_2 = \frac{\sqrt{(a_0 L \beta_0)^2 + (a_0 R + b_0 J)^2}}{2(a_0 P - b_0 A)}$$

4.4 Discussion of Results

From the expression for $\log \xi(t)$ it is noted that stability results if

$$a_1 - a_2 \cos(2\alpha_0 + \phi_0) J_0(2\eta) < 0$$

This is a necessary condition for stability, but as a result of the oscillating term in $\log \xi(t)$, may not be a sufficient condition. The oscillating term will modify the instantaneous growth rate of the disturbance, and

consequently the amplitude of the disturbance is modified. The smaller Ω the larger the effect of this term.

At the plasma parameters of interest

$$a_1 \, , \quad \cos(2\alpha_0 + \phi_0) < 0 \quad ; \quad a_2 > 0$$

leading to the stability criterion

$$\frac{a_1}{a_2} \sec(2\alpha_0 + \phi_0) \gg J_0(2\eta) \tag{4.6}$$

The stability criterion in absence of dynamic stabilization is

$$\frac{a_1}{a_2} \sec(2\alpha_0 + \phi_0) \gg 1$$

leading to an α_0 for maximum growth rate, and a critical Hall parameter below which the waves are stable. Since $J_0(2\eta) < 1$ for $\eta > 0$ the oscillation of the steady state current increases the critical Hall parameter, leaving the direction for maximum growth unchanged.

$\beta_{0\,\mathrm{crit}}$ as a function of η is shown in figure 4.1. The gas parameters used are $T = 1500^{\circ}K$; $n_n = 10^{25} m^{-3}$; $n_s = 10^{22} m^{-3}$; $T_{e0} = 2500^{\circ}K$. The seed considered is cesium and the neutral gas is argon. Computer plots show that the stabilization is little affected by the value of T_{e0} in the range $2000\text{-}3000^{\circ}K$. A significant feature of this curve is the initial large rise in η and the subsequent decrease in slope. This means that if useful dynamic stabilization is to be achieved, large amplitude fluctuations in the current density are required.

The oscillating part of $\log \xi(t)$ has period $2\pi/\Omega$ and the amplitudes of its terms are inversely proportional to Ω. Since the terms appear in the argument of the exponential representing $\xi(t)$ it is preferable that they be as small as possible and therefore Ω as large as possible.

To illustrate how the growth function varies with time and Ω, $\xi(t)$ is plotted as a function of time for several cases where the stability condition, equation (4.6) is satisfied.

In figure 4.2 $\beta_0 = 2$ and the η used corresponds to $\beta_{0\,crit} = 2.2$. For case (a) the maximum amplitude of the oscillating part of $\log\xi(t)$ is approximately 10^{-3}, and $\xi(t)$ is approximately a decaying exponential. The $\Omega = 2\pi.10^4 sec^{-1}$ case lies too close to (a) to warrant plotting.

In figure 4.3 $\beta_0 = 8$ and the η used corresponds to $\beta_{0\,crit} = 8.8$. If one attempts to stabilize this case using an applied frequency $= 2\pi.\ 10^3 sec^{-1}$ the initial fluctuation in $\xi(t)$ is so large, due to the oscillating part of $\log\xi(t)$, that within a very short time the growth function is completely outside the linear regime and the analysis fails. Therefore, the larger the Hall parameter, the larger will be the minimum Ω for linear stability. However, a condition on the magnitude of Ω is imposed by the skin effect.

For small skin effect Ω must satisfy

$$\Omega << 1/\ell^2\mu_0\sigma_0$$

where ℓ is some characteristic dimension of the duct. Assuming $\sigma = 10^2 M\ m^{-1}$ and $\ell = 1$ m it follows that

$$\Omega << 2\pi \cdot 10^3 \ sec^{-1}$$

Skin effects therefore present a problem at high β_0 ; however, this difficulty could be removed if the oscillatory electric fields were applied through probes placed in the body of the plasma with a smaller separation than the duct dimension. Since $\Omega_{max} \propto \ell^{-2}$ useful values of Ω might then be permissible.

For any device using this method of dynamic stabilization to operate as a generator, it is of course necessary that the power supplied to produce the oscillating electric fields should not be greater than the power supplied to the load. Consider the segmented Faraday generator shown in figure 4.4; only one segment circuit is shown and R_1, R_2 represent the resistances of the source providing fields E_{s1}, E_{s2} respectively. From Ohms law it follows that

$$E_x = E_{s1} - j_x\left[1/\sigma_1 + 1/\sigma_L\right] + vB \qquad (4.7a)$$

and

$$E_y = E_{s2} - j_y/\sigma_2 \qquad (4.7b)$$

where $\sigma_1 = H/LWR_1$, $\sigma_2 = \ell/HWR_2$

Using equation (4.3) to eliminate E_x and E_y, and multiplying equation (4.7a) by j_x, and equation (4.7b) by j_y, equations are obtained for the power supplied per unit volume of the generator by the sources, P_{s1}, P_{s2}. When averaged over time these become

$$\langle P_{S1}\rangle = \frac{j_0^2}{2\sigma_0}\left[1 + J_0(2\eta)\right]\left[1 + \sigma_0/\sigma_L + \sigma_0/\sigma_1\right] - vBj_0J_0(\eta)$$

and

$$\langle P_{S2}\rangle = \frac{j_0^2}{2\sigma_0}\left[1 - J_0(2\eta)\right]\left[1 + \sigma_0/\sigma_2\right]$$

Subtracting the sum of these from the average power dissipated in the load, $j_0^2/2\sigma_L\left[1 + J_0(2\eta)\right]$, one obtains the time averaged net power output,

$$P_N = j_0vBJ_0(\eta) - \frac{j_0^2}{2}\left[2/\sigma_0 + 1/\sigma_1 + 1/\sigma_2 + J_0(2\eta)\{1/\sigma_1 - 1/\sigma_2\}\right]$$

Previously it has been assumed that $|\underline{j}|$ remains equal to $|\underline{j}_0|$ after applying the oscillating fields, this may not be necessary in practice.

The current density will depend on the applied field, if $|\underline{j}|$, denoted previously by $\underline{j}_0$ can be altered (by altering the fields), then its most desirable value will be that which maximises P_N. Assuming σ_1 and σ_2 are constant and ignoring the dependence of j_0 on σ_0 one obtains for the maximum value of P_N

$$P_N = \tfrac{1}{2}\sigma_0 v^2 B^2 J_0^2(\eta)\left[2 + \sigma_0\{1/\sigma_1 + 1/\sigma_2\} + J_0(2\eta)\sigma_0\{1/\sigma_1 - 1/\sigma_2\}\right]^{-1}$$

with the optimum value of $\underline{j}$ given by

$$|\underline{j}| = 2P_N / vBJ_0(\eta)$$

4.5 Summary

The analysis presented here shows that the critical Hall parameter for the electrothermal instability in an MHD generator can be increased by applying oscillatory electric fields to the plasma, in such a way that the generator current density oscillates in direction. The extent of the increase depends on the amplitude of the oscillation; and the stabilizing effect will only be present if the frequency of the oscillations is sufficiently large. If this frequency is too low, then although the linear theory will give stable solutions in normally unstable situations, ie: solutions which tend to zero as t tends to infinity, there will be present large scale oscillations in the amplitude of the electron density fluctuations at smaller values of t. These large scale oscillations take the fluctuations out of the linear regime and the analysis breaks down.

The form of the applied oscillatory fields considered is rather complicated. The reason, paradoxically, was to simplify the analysis in that these fields arrange for the magnitude of the generated current, $|\underline{j}|$ to be constant in time. It follows that dynamic stabilization appears in the equations of the instability simply as an oscillation in α, the angle between $\underline{j}$ and $\underline{k}$.

In a practical situation simpler fields may have to be applied, with $|\underline{j}|$ not constant; however it seems likely that the stabilizing effect of the oscillating direction of $\underline{j}$ will still be present.

(1)

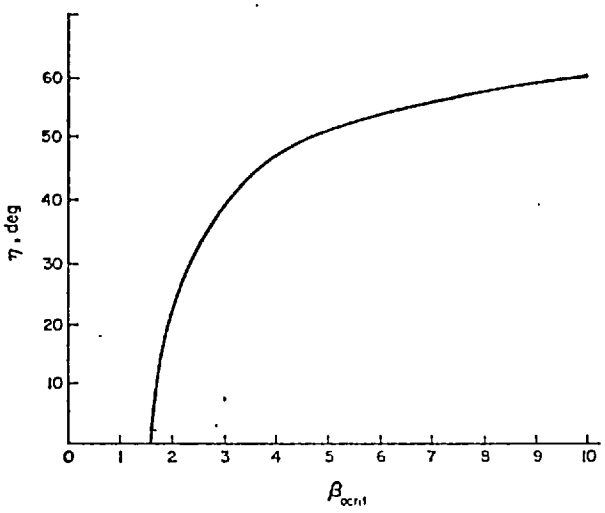

(2)

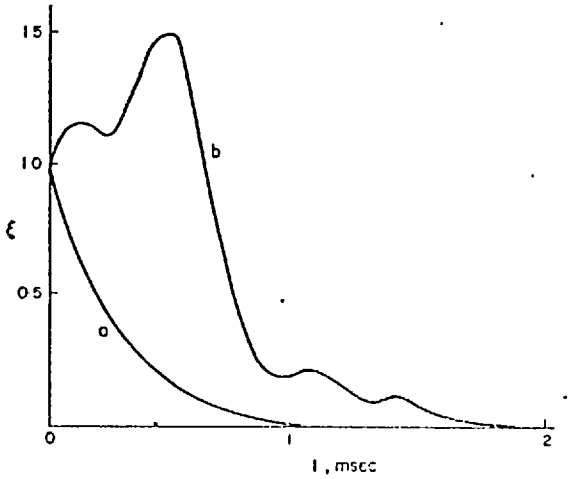

(1) Figure 4.1: β_{crit} against oscillation amplitude η . Ω is assumed to be sufficiently large for the equality in equation 4.6 to yield linear plane waves.

(2) Figure 4.2: ξ against time. (a) $\Omega = 2\pi.10^{6}\text{sec}^{-1}$; (b) $\Omega = 2\pi.10^{3}\text{sec}^{-1}$. $\beta_0 = 2.0$.

(1)

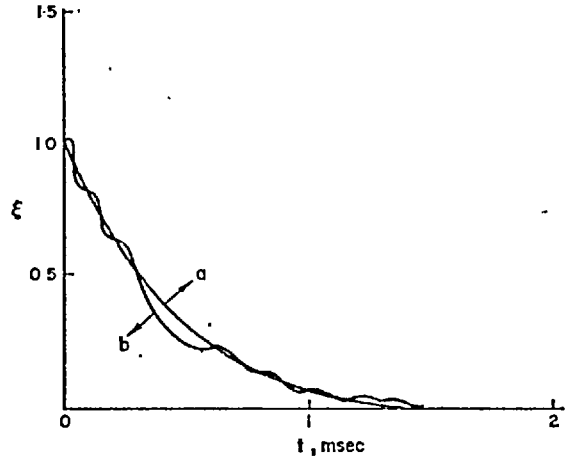

(2)

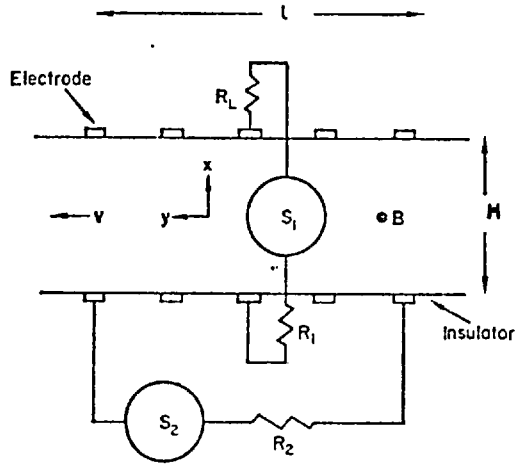

(1) Figure 4.3: ξ against time. (a) $\Omega = 2\pi.10^6 \text{sec}^{-1}$; (b) $\Omega = 2\pi.10^4 \text{sec}^{-1}$. $\beta_0 = 8.0$.

(2) Figure 4.4: (x, y) section of a segmented electrode duct with stabilizing sources S_1 and S_2.

CHAPTER V

NUMERICAL SOLUTION OF THE ELECTROTHERMAL EQUATIONS

5.1 Introduction

The strong non-linearity of the equations describing the electron temperature and density of non-equilibrium partially ionized plasmas, necessitate the use of numerical methods for the solution of these equations. Furthermore, the complicated boundary conditions imposed on the electric and current fields in experimental configurations, requires a numerical approach if realistic comparisons of experimental results with available theoretical models are to be made.

Several authors have reported the results of such numerical calculations, (Lengyel, 1969, 1971; Kim, 1969; Oliver et al, 1967; Argyropoulos et al, 1967, 1969). With the exception of the latter, which was time independent, the calculations were restricted to solutions for the current flow in uniform plasmas, or to the determination of temperature, density and current fields in non-equilibrium plasmas, at low values of the Hall parameter. Numerical simulations of the electrothermal instability, in simple geometries, have recently been performed and these are mentioned in Chapter VI.

In this Chapter a time-dependent numerical model of the electron fluid, according to equations (2.1)-(2.8) will be presented. In sections 5.2 and 5.3 an analysis of the characteristic time scales for the system is used to determine stability criteria for the explicit treatment of the time dependent equations; and in sections 5.4 - 5.7 the treatment of convective terms, external circuit effects and the solution of the Ohms law are considered, together with the boundary conditions necessary to specify the problem.

Finally, some results of the computations are given which demonstrate the difficulties involved in the numerical simulation of this problem; these difficulties include the extremely small time-step for stability of the explicit time-dependent scheme when following the fast-thermal mode; the occurrence of large gradients at the boundaries due to Hall effect, and finally, the presence of slight mesh uncoupling, as discussed by Roberts et al (1970) for example, as a result of the second order accurate treatment of convective terms. These problems are overcome in Chapters VI and VII.

5.2 Analysis of Time-Scales

For an explicit calculation to be stable and accurate, restrictions on the size of the time-step must be enforced; these are of the form

$$\Delta t < |\tau| \tag{5.1}$$

where τ characterizes the time-scale of a physical process to be simulated. Physically, if the evolution of a process is to be followed, then the interval of time chosen, Δt, must be less than that required for the process to evolve.

In equations (2.1)-(2.8) there are a large number of interacting physical processes to be considered; these processes, together with the wave phenomena associated with them, have to be resolved by any explicit numerical scheme. In the following work the characteristic length scale is taken to be Δ , the mesh step.

(a) Continuity Equation

$$\partial n_e/\partial t = -\underline{v}\cdot\nabla n_e + n_e(\nu_i-\nu_r) = \sum_m n_e/\tau_{m,n_e}$$

This defines the following time scales

$$|\tau_{n_e}| = \frac{\Delta}{v}\ ,\quad |\tau_{i,n_e}| = \nu_i^{-1},\quad |\tau_{r,n_e}| = \nu_r^{-1} \qquad (5.2)$$

corresponding to convection, ionization and recombination. The functional forms for ν_i and ν_r are given in Chapter II.

(b) Energy Equation

$$\partial u_e/\partial t = -\nabla\cdot(u_e\underline{v}_e) + j^2/\sigma - L - I_p n_e(\nu_i-\nu_r) - P_e\nabla\cdot\underline{v}_e + \nabla\cdot(K_e\nabla T_e)$$
$$= \sum_m u_e/\tau_{m,u_e}$$

This defines the following time scales:

Ohmic heating

$$|\tau_{H,u_e}| = 1.5\, n_e k_B T_e \sigma / j^2$$

Collisional cooling

$$|\tau_{c,u_e}| = T_e\left[2(T_e-T)\sum_s \frac{m_e}{m_s}\nu_{es}\right]^{-1}$$

Ionization term

$$|\tau_{i,u_e}| = 1.5\, T_e/T_p \cdot \tau_{i,n_e}$$

Recombination term

$$|\tau_{r,u_e}| = 1.5\, T_e/T_p \cdot \tau_{r,n_e}$$

Compression and Convection

These take the form

$$|\tau_{u_e}| = \Delta/|\underline{v}_e|$$

Thermal Conduction

$$|\tau_{T,u_e}| = 1.5\, n_e K_B \Delta^2 / K_e$$

The characteristic time-scales for the ionization-recombination processes in the energy equation are approximately $T_e/T_p \sim 10^{-1}$ shorter than those for the continuity equation.

(c) Wave Processes

The fast-thermal mode and the ionization mode were discussed in Chapter III. It was shown that, in general, the imaginary parts of the complex frequency for both waves greatly exceeded the real parts. Accordingly, only the growth and decay scales will be considered. From Chapter III,

$$|\tau_{FT}| \sim \left(\frac{T_e}{T_p}\right)^2 \tau_{r,n_e} \qquad \text{Fast-thermal mode}$$

and

$$|\tau_I| \sim \frac{T_p}{T_e} \frac{\tau_{H,u_e}}{|\beta - 2|} \qquad \text{Ionization mode}$$

In order to satisfy equation (5.1), Δt must be chosen such that

$$\Delta t < |\tau|_{min}$$

where $|\tau|_{min}$ is the shortest time-scale defined in (a)-(c) above. In the case of a system perturbed from some uniform equilibrium, one has $|\tau_{H,u_e}| \approx |\tau_{c,u_e}|$ and $|\tau_{i,u_e}| \approx |\tau_{r,u_e}|$. Plots of τ_{H,u_e}, τ_{r,u_e}, τ_I and τ_{FT} as functions of T_e are plotted in figure 5.1 for this case. For $T_e > 2500^{\circ}K$ it is seen that

$$|\tau_{FT}| << |\tau_{r,u_e}| << |\tau_{H,u_e}| << |\tau_I|$$

The smallness of $|\tau_{FT}|$ compared with the ionization-recombination time scales in the energy equation is a result of the strong dependence of τ_{i,u_e}, τ_{r,u_e} on n_e and T_e.

5.3 Time Differencing

Equations (2.1) and (2.6) can be written

$$\partial \underline{u}/\partial t = \underline{f}$$

where $\underline{u} = \begin{bmatrix} n_e \\ u_e \end{bmatrix}$ and $\underline{f} = \begin{bmatrix} f_1 \\ f_2 \end{bmatrix}$

$\underline{f}$ represents both local algebraic terms and spatial gradient terms. The integration scheme for the time dependent equations is of the form (Lilley, 1965),

$$\underline{f}^{(n+1/2)} = \left[\partial \underline{u}/\partial t\right]^{(n+1/2)} = \left[\underline{u}^{(n+1)} - \underline{u}^{(n)}\right]/\Delta t + O(\Delta t^2)$$

where $$\underline{f}^{(n+1/2)} = \frac{1}{2}\left[3\underline{f}^{(n)} - \underline{f}^{(n-1)}\right] + O(\Delta t^2)$$

where 'n' represents the time level. This method is rapid, since updated quantities are obtained directly from those previously found, it is second order accurate, and unlike the leap-frog scheme, it does not suffer from time-splitting instabilities. Calculations are initiated with a second-order Runge-Kutta method, as discussed by Young (1968) for example, which is also used to revise the value of Δt when necessary.

In the following sub-sections the stability of the above scheme to both local terms and flux terms will be considered. The formal procedure for testing the stability of a finite-difference scheme is to linearize the basic equations, rewrite them in finite-difference form, and then Fourier analyze the set. This procedure is itself a numerical exercise for reasonably complex systems, and has been avoided here by the use of a rather more heuristic approach in which the stability of the scheme to local terms, and flux terms, is considered separately.

(a) Stability to Local Terms

Consider the simple equation

$$\partial u/\partial t = u/\tau \,, \qquad \tau = \text{const} > 0$$

According to the above scheme

$$u_d^{(n+2)} - u_d^{(n+1)} = p\left[3u_d^{(n+1)} - u_d^{(n)}\right], \quad p = \Delta t/2\tau$$

which has the solution

$$u_d^{(n)} = A_+ a_+^n + A_- a_-^n$$

where $$2a_{\pm} = 1+3p \pm \left[(1+3p)^2 - 4p\right]^{1/2}$$

and $a_- < 1$ for all $p > 0$. The difference solution which approximates the solution of the differential equation is a_+. The condition

$$\Delta t < 0.48\,\tau \tag{5.3}$$

is necessary if a_+ is to be presented as a series in positive powers of $\Delta t/\tau$, this gives,

$$a_+ = \exp(\Delta t/\tau) - 5/12\,(\Delta t/\tau)^3 + O\left[(\Delta t/\tau)^4\right]$$

from which $$u_d^{(n)}/u^{(n)} \approx 1 - 5/12 \cdot n\,(\Delta t/\tau)^3 \exp(-\Delta t/\tau)$$

for $\frac{5}{12} n \left(\frac{\Delta t}{\tau}\right)^3 \exp\left(-\frac{\Delta t}{\tau}\right) < 1$. The above scheme approximates the exact solution to second order accuracy in $\Delta t/\tau$. Since $u_d^{(1)}$ is found from a Runge-Kutta method, $A_- << A_+$, and in any event $a_-^n \to 0$ as n becomes large. The overall accuracy can be increased by reducing Δt and increasing n for a given $n\Delta t$. For an exponentially decreasing solution the stability condition is slightly less restrictive than that given by equation (5.3).

(b) Stability to Flux Terms

Consider the simple convection equation

$$\partial u/\partial t = -v\,\partial u/\partial x \qquad v = \text{const}$$

Since each Fourier mode of the solution has a real frequency, the solution is bounded in time. Defining the amplification factor, g, as

$$g u_d^{(n)} = u_d^{(n+1)}$$

the condition for a bound (stable) difference solution is,

$$|g| \leq 1$$

Using $[\partial u/\partial x]^{(n)} = [u_{j+1}^{(n)} - u_{j-1}^{(n)}]/2\Delta$ and $u_j^{(n)} \propto \exp i(jk\Delta)$ the difference scheme gives,

$$g^2 - g\left[1 - 3i\alpha^2 \sin\theta\right] - i\alpha^2 \sin\theta = 0$$

in which $\theta = k\Delta$ and $\alpha^2 = v\Delta t/2\Delta$. This has two roots; for $\alpha^2 \leq 0.5$ $|g_-| < 1$ and

$$|g_+| = 1 + \frac{1}{4}\left(\frac{v\Delta t}{\Delta}\right)^4 \sin^4\theta + \cdots > 1$$

The scheme therefore possesses a small instability in fourth order, which maximises for waves of length 4Δ, ie: the ~~shortest~~ $2\lambda_{min}$ waves on the mesh. The instability can be removed quite simply, however, if after every time-step new values of the variables are defined according to

$$u_{dj}^{(n+1)*} = u_{dj}^{(n+1)} + \eta^2\left[u_{dj+1}^{(n)} + u_{dj-1}^{(n)} - 2u_{dj}^{(n)}\right]$$

The amplification factor then becomes

$$|g_+| = 1 + \frac{1}{4}\left(\frac{v\Delta t}{\Delta}\right)^4 \left[\sin^4\theta - \frac{\epsilon}{2}\sin^2\theta/2\right] + \cdots$$

where $\eta^2 = \frac{\epsilon}{32}\left(\frac{v\Delta t}{\Delta}\right)^4$. The scheme is therefore stabilized in fourth order for $\epsilon \geq 5$. The ratio of artificial "diffusion" to the spatial truncation error is of the order of $\left(\frac{v\Delta t}{\Delta}\right)^3/k\Delta \ll 1$, in general, so that the accuracy is little affected.

The instability has not been observed in this work, and the use of stabilization not required. This is probably due to the large time-scale for convection; $\Delta/|v_e|$ greatly exceeds the electrothermal time-scales,

and so $|\underline{v}_e| \Delta t/\Delta$ is correspondingly small. The local terms, Ohmic heating and so forth, generally dominate the system, except where gradients become large.

5.4 Treatment of Convective Terms

If source terms and diffusion terms are omitted from the equations of electron continuity and energy they take the form

$$\partial n_e/\partial t = -\nabla.(n_e \underline{v}_e) \tag{5.4}$$

and

$$\partial u_e/\partial t = -\nabla.(u_e \underline{v}_e) \tag{5.5}$$

If electron motion is occurring within a closed volume, and $\underline{v}_{e\perp} = 0$ at the boundaries, then the total number of electrons and their energy are conserved. Finite-difference approximations to the divergence terms are available which also conserve these quantities. One of the more commonly used conservative methods for the equations of fluid motion is the Lax-Wendroff scheme, as discussed by Roberts et al (1970), Richtmyer and Morton (1967), Ames (1969) for example. An alternative conservative scheme devised by Arakawa (1966) has been used for this work.

The flux terms in equations (5.4) and (5.5) may be written in Jacobian form for two-dimensional motion, this follows from $\nabla.\underline{v} = 0$ and $\nabla.\underline{j} = 0$.

$$\partial n_e/\partial t = J(n_e, \phi)$$

and

$$\partial u_e/\partial t = J(u_e, \phi) - 3k_B/2e \cdot J(T_e, \psi)$$

where $v_x = -\partial\phi/\partial y$, $v_y = \partial\phi/\partial x$, $j_x = -\partial\psi/\partial y$

and

$$j_y = \partial\psi/\partial x$$

The simplest integral constrai nts on the Jacobian terms are (Arakawa, 1966):

$$\int_S J(p,q)\,dx\,dy = 0, \quad \int_S pJ(p,q)\,dx\,dy = 0, \quad \int_S qJ(p,q)\,dx\,dy = 0$$

where p and q are any arguments and the integration is over the domain in the plane of motion, along the boundary of which either p or q is constant. The first of the above constraints ensures that the total number of electrons and their energy are conserved when n_e and U_e satisfy equations (5.4) and (5.5). The other constraints do not demonstrate simple physical conservation laws in this application; nevertheless, a difference scheme which exhibits these mathematical constraints seems preferable to one that does not. The nine-point difference scheme suggested by Arakawa satisfies the above integral constraints, and is therefore conservative. Numerical tests of the method, and comparisons with other methods are given by Arakawa (1970).

5.5 Solution of the Ohms Law

The Ohms law, together with the two field equations, can be combined to give a single second order equation in ψ, the current density stream function. From Ohms law

$$\underline{E} = -\underline{V}\times\underline{B} - \nabla P_e/n_e e + \underline{j}/\sigma + \underline{j}\times\underline{B}/\sigma$$

the equation for ψ is derived from $\nabla\times\underline{E}\left(\partial\psi/\partial x, \partial\psi/\partial y, n_e, T_e\right) = 0$, in which $\frac{\partial}{\partial z} = 0$, $\nabla\cdot\underline{V} = 0$, $\underline{j}_z = 0$ and $\underline{B}$ = constant, this gives

$$\nabla^2\psi + P\,\partial\psi/\partial x + Q\,\partial\psi/\partial y = R \qquad (5.6)$$

in which $$P = \sigma\left[\partial/\partial x\,(1/6) - \partial/\partial y\,(\beta/6)\right]$$

$$Q = \sigma\left[\partial/\partial y\,(1/6) + \partial/\partial x\,(\beta/6)\right]$$

and $$R = k_B \sigma / n_e e\, J(T_e, n_e)$$

Equation (5.6) is an elliptic equation in ψ . A second order accurate, finite difference approximation to this equation at the point (i, j) can be written

$$\psi_{i+1,j}\left[1+P_{ij}\,\Delta/2\right]+\psi_{i-1,j}\left[1-P_{ij}\,\Delta/2\right]+\psi_{i,j+1}\left[1+Q_{ij}\,\Delta/2\right]$$
$$+\,\psi_{i,j-1}\left[1-Q_{ij}\,\Delta/2\right]-4\psi_{ij} = R_{ij}\,\Delta^2 \qquad (5.7)$$

Equation (5.7) is one of the set of linear algebraic equations for the unknowns ψ_{ij} ; the set is solved iteratively at each time-step using the method of successive-over-relaxation (SOR) or successive-under-relaxation (SUR) (see Ames, 1969, for example).

The iteration procedure can be expressed as

$$\psi_{ij}^{(p+1)} = \psi_{ij}^{(p)} + \omega \mathcal{R}_{ij} \qquad (5.8)$$

in which p is the iteration level, ω is a relaxation parameter which lies in the range $1 < \omega < 2$ for SOR, and $0 < \omega < 1$ for SUR; and $\mathcal{R}_{ij}$, the residue, is defined as

$$\mathcal{R}_{ij} = \frac{1}{4}\left[\psi_{i+1,j}^{(p)}\,(1+P_{ij}\,\Delta/2) + \psi_{i-1,j}^{(p+1)}\,(1-P_{ij}\,\Delta/2)\right.$$
$$\left.+\,\psi_{i,j+1}^{(p)}\,(1+Q_{ij}\,\Delta/2) + \psi_{i,j-1}^{(p+1)}\,(1-Q_{ij}\,\Delta/2) - \Delta^2 R_{ij}\right] - \psi_{ij}^{(p)}$$

The relaxation parameter is chosen to optimise the convergence rate. The stability of equation (5.8) can be investigated using the methods applied in section 5.3(b), and a value of ω for optimum convergence obtained. In practice, the optimum value of ω is found by trial; at

the beginning of each run ω_{opt} is found by testing several values of ω, each successively differing by 0.1. For large β the value of ω_{opt} may change several times during a run, and always decreases as the calculation proceeds.

The iterations are stopped when a convergent solution is reached which satisfies $|\psi_{i,j}^{(p+1)} - \psi_{i,j}^{(p)}| \leq \epsilon$ for all $\psi_{i,j}$. A convergence criterion based on fractional convergence has little value here, because the quantity of physical interest is the current density, defined as

$$j_{x\,i,j} = -[\psi_{i,j+1} - \psi_{i,j-1}]/2\Delta \quad , \quad j_{y\,i,j} = [\psi_{i+1,j} - \psi_{i-1,j}]/2\Delta$$

and the fractional error in Ohmic heating due to finite convergence error is $\delta(j^2)/j^2 \sim 2\epsilon/|j|\Delta$. The value of ϵ is therefore chosen to match the conditions of a particular simulation. For $\langle T_e \rangle \sim 3000^{\circ}K$, $\langle j \rangle \sim 10^5 A\ m^{-2}$ and $\Delta = 2 \times 10^{-3} m$, ϵ is chosen to be 0.01 and $\delta(j^2)/j^2 \sim 10^{-4}$. Similarly, for smaller values of $\langle j \rangle$, ϵ is chosen to be correspondingly smaller.

5.6 Inclusion of Circuit Effects

Unlike the previous numerical studies cited in section 5.1, the total current flow is not taken to be constant. The implications of this are discussed in Chapter VI. For each iteration of equation (5.7) over the mesh, an evaluation of the voltage drop across the plasma between electrodes is made. This is done by integrating the Ohms law numerically between successive electrode pairs, using the Simpson's rule method to give

$$\Delta\phi' = B\int_0^H v\,dx + \int_0^H \frac{1}{n_e e}\frac{\partial P_e}{\partial x}\,dx - \int_0^H (j_x + \beta j_y)/6 \cdot dx$$

The total current flow through a given electrode pair is therefore $(\Delta\phi'+V_s)/R_L$, where V_s is any external source of voltage, and R_L the load resistance. The value of I obtained leads to new boundary conditions for ψ at the next iteration. The final convergent solution for ψ is therefore consistent with the external conditions of the problem.

5.7 Boundary Conditions

A single electrode pair configuration is shown in figure 5.2. The boundary conditions for the electrical quantites are

(i) $\underline{E}_{\parallel} = 0$ on electrodes

(ii) $\underline{j}_{\perp} = 0$ on insulators

(iii) $$V_s+\Delta\phi' = R_L \iint_{electrode} j_x \, dz\,dy$$

For the insulating walls at $x = 0$ and $x = H$, $j_x = -\frac{\partial\psi}{\partial y} = 0$, ie: $\psi =$ constant. The total current flow through an electrode pair is given by

$$I = \iint_{electrode} j_x \, dz\,dy = -\iint \partial\psi/\partial y \, dz\,dy = -W(\psi_o-\psi_1)$$

ie: $$\psi_1 = \psi_o + I/W$$

where W is the extent of the duct in the 'z' direction. In the segmented electrode ducts considered in this Chapter and in Chapter VII, it is assumed that the ends of the duct, and the external circuits of each electrode pair, are electrically separate, ie: there can be no net current flow in the 'y' direction. This condition is satisfied by equating the values of ψ along AB, CD to those along EF, GH respectively. The evaluation of I at each iteration for ψ therefore leads to an adjustment of ψ_1 , which alters the boundary data for ψ .

The condition that $\underline{E}_{||} = 0$ at the electrodes leads to

$$\partial\psi/\partial x = \frac{\sigma}{n_e e}\,\partial P_e/\partial y - \beta\,\partial\psi/\partial y \qquad (5.9)$$

from the Ohms law with $E_y = 0$. In terms of compass point notation, figure 5.3, the second order accurate, finite-difference approximation of this condition is

$$\psi_N - \psi_S = \left(\frac{\sigma}{n_e e}\right)_c (P_{eE} - P_{eW}) - \beta_c (\psi_E - \psi_W) \qquad (5.10)$$

This equation therefore specifies values of ψ which lie outside the physical domain, ψ_S for the south boundary electrodes, ψ_N for the north. These values are eliminated using equation (5.7), and the resultant equations for ψ_c on each electrode, determined in terms of the three nearest neighbour points which lie inside the physical domain. When the resultant set of equations for ψ is solved using the relaxation method at each point, it is found that severe convergence problems are encountered at the electrodes; this difficulty has been overcome by solving the internal, non-boundary points using SOR or SUR, and from these values at each iteration, determining the electrode values by inverting the matrix for the unknowns.

The current density at each boundary point, and hence the Ohmic heating, can be found to second order accuracy by elimination of the external values between the boundary conditions and equation (5.7).

The coefficients P, Q and R, as defined by equation (5.6), are evaluated to second order accuracy everywhere. At the south boundary for example,

$$\partial/\partial x\,(1/\sigma)_c = \left[4/\sigma_N - 3/\sigma_c - 1/\sigma_{FN}\right]/2\Delta$$

(a) Open System

In the case when the boundaries AE, DH of figure 5.2 are open, ie: AE represents the system inlet, and DH the outlet, the additional conditions $\psi = \psi_1$ along AE, and $\psi = \psi_0$ along DH are imposed. This is equivalent to defining upstream and downstream "infinities" which limit the region of current flow. The solution for ψ is therefore specified by boundary conditions at all points around the domain, in accordance with the ellipticity of the problem.

The boundary conditions for the time dependent equations are more difficult. The reason for this is two-fold. Firstly, the conditions at the boundaries require a detailed knowledge of the plasma-boundary interactions, which is not yet available; and secondly, the discreteness of the mesh automatically requires conditions to be applied which are not always necessary physically.

In the continuity equation, the second order treatment of the flux term requires conditions on n_e to be specified along hypothetical (external) mesh columns, west of AE and east of DH. The first conditions are required physically, since these determine the state of the electron fluid entering the inlet, initial conditions only do not specify the problem since the physical domain is finite, and the characteristics are not mapped on to this plane for all $t > 0$ by specifying $n_e(t = 0, 0 \leqslant x \leqslant H, 0 \leqslant y \leqslant L)$. The conditions at the outlet are necessary due to the discreteness of the mesh. The values of n_e at the external column of points are put equal to those along DH, in this way there can be no false growth in electron density behind the boundary, since free convection is permitted.

If thermal conduction is omitted from the energy equation, it possesses real characteristics. The conditions for T_e at the inlet and outlet are chosen in the same way as those for the continuity equation. Additional conditions are needed at the electrodes, however, and the above 'free convection' treatment for the convective terms is used. It would seem preferable to define physical conditions at the cathode and use 'free convection' at the anode; the conditions at the cathode are complex, however, and the former treatment would seem the better alternative.

(b) Periodic System

In this case the segment ADEH in figure 5.2 is considered to be one of an infinite number of identical segments between $-\infty < y < \infty$. The boundary conditions required along AD and EH are the same as for case (a). The boundary conditions along AE and DH are $n_e(y = 0) = n_e(y = L)$, $T_e(y = 0) = T_e(y = L)$ and $\underline{j}(y = 0) = \underline{j}(y = L)$, and it is no longer necessary to introduce external mesh columns behind AE and DH. The specification of ψ along AD and EH, together with the assumption of periodicity, leads to a unique solution for ψ. Similarly, initial conditions for T_e and n_e, together with the previously mentioned boundary conditions along AD and EH, specify the solution for n_e and T_e for all time. Such periodic conditions are observed experimentally (Dodel, 1970), when sufficiently large numbers of identical electrode segments are used.

To illustrate the above concepts some early results of segmented electrode duct simulations are discussed below. These preliminary calculations are intended to give an indication of the usefulness of the above methods to the simulation of this problem. Thermal conduction and radiation transport are omitted from the energy equation.

5.8 Some Results for Segmented Electrodes

Two numerical experiments will be discussed; firstly, a single electrode pair system with (a) applied electric fields and (b) equivalent $\underline{V} \times \underline{B}$ fields; and secondly a multiple electrode system operating under the influence of $\underline{V} \times \underline{B}$ fields. The heavy particle temperature is $2000^{\circ}K$, and all load resistances are 1 Ohm. For $t \leqslant 0$ the heavy particle temperature and electron temperature are equal, and at $t = 0$ the external circuits are closed and the electrons allowed to heat.

The results for zero magnetic field are shown in figures 5.4-5.7. The heavy particle velocity is 1500 m/sec and the duct cross-section (5 x 5) cm^2, a 15 x 35 mesh is employed.

Plots of the ratio of effective plasma resistance to initial value, R_p', as a function of time are shown in figure 5.4. These plots are for the first 10 μ secs of operation for four electric field strengths. The characteristic features of the curves are the initial rise in R_p' and subsequent approach to a steady state of non-equilibrium electrical conduction. The larger the applied field, the greater the initial rise in R_p'.

This is due to the increased binary collision frequency reducing the conductivity in times of the order of the electron heating time, the ionization effects taking place more slowly. The maximum is reached when the electron density increases sufficiently to compensate for the increased collision frequency. The characteristic time for the rise in R_p' is 0.05-3 μ secs, while the characteristic time for the fall in R_p' is 1.5-20 μ secs.

Figures 5.5 and 5.6 show the distribution of electron temperature and number density at the final steady state along the centre axis of the duct, and along electrode boundaries for one field strength. The steady state is reached in 40-60 μ sec. These distributions are not symmetric with respect to the electrode centre because of convection. Due to the slow recombination after the electrode region, the increase in electron density persists downstream. Convection is less dominant in the electron temperature distribution, due to rapid cooling by elastic collisions after the electrode region. However, the energy released by recombination keeps the temperature above the initial value in the downstream section. These curves demonstrate the importance of convection on the distributions. From figure 5.7 it is seen that the regions of highest conductivity exist near the insulator walls downstream. This results in a downstream asymmetry of the discharge, together with a slight current concentration on the downstream electrode corner points, resulting in an elevated temperature there.

Results for one electrode pair with finite magnetic field are shown in figures 5.8 and 5.9. Duct and flow parameters are identical to the previous case, the $\underline{V} \times \underline{B}$ fields correspond to the three lowest applied electric fields. The initial Hall parameters for the three cases are 0.7, 1.4 and 2.7, and the corresponding initial values of $R_p(B = 0)/R_p(b = 0)$ are 1.2, 1.7 and 3.0 respectively. The increasing values resulting from the increase of effective current path due to Hall effect. The general features of the discharge are the diagonal current flow in the duct, together with large current concentration on the upstream edge of the internal anode and the downstream edge of the cathode. The electron temperature in the duct centre is less than in the corresponding B = 0 case, while the electrode edges have temperatures much greater than the average values. Figure 5.8 shows the evolution of R_p' for the first 10μ sec of operation. These curves differ from the B = 0 case in that R_p drops below the initial value at earlier times. The maxima are reduced and decrease with increasing Hall parameter. The reduced heating in the bulk of the plasma, and the rapid ionization at the electrode edges result in the average scalar conductivity being greater at early times for the finite $\underline{B}$ case. The heating leads also to a reduction in Hall parameter which reduces the effective current path in the plasma, and decreases R_p'. Both of these effects reduce R_p' at early times and they become more effective at larger Hall parameter.

No calculations with finite B reached a steady state. Fluctuations in R_p', the Hall voltage and the direction of current flow appeared at 35, 10 and 2μ secs for the three cases. These fluctuations are caused by numerically induced non-uniformities and vanish for $\underline{v} = 0$. The non-

uniformities are of small amplitude and have been smoothed out in figures 5.5-5.9. The transient conductivity profiles for the lowest field case are shown in figure 5.9. Calculations assuming a parabolic viscous profile show a reduced R_p', compared with plane profile cases for equal induced voltages. This is due to the decreased relaxation length for ionization near electrode surfaces. Fluctuations eventually occur for this case also.

Results for five electrode pairs with magnetic field are shown in figures 5.10-5.13. The gas velocity is 2000 m/sec, and a (31 x 77) mesh is used. The induced field is 400 V/m and the initial Hall parameter 1.7. The gas transit time across the insulator sections between electrode pairs is 3μ sec, and the insulator to electrode length ratio is one-third. Plots of total current output and corresponding Hall voltage for the first 2μ sec of operation are shown in figure 5.10. The Hall voltage is defined here as the potential difference between the beginning of the inlet section and the end of the outlet section. The abrupt change in dI/dt which occurs at 1.1μ sec is accompanied by a similar change in the rate of fall of Hall voltage. After this there is a tendency for current in the duct centre to flow increasingly in the downstream direction. There is evidence of electrode current leakage occurring near this time which may be connected with these changes.

The current distribution in the duct at 2.2μ sec is shown in figure 5.11. At this time the plasma in the centre of the duct has a conductivity lower than the initial value (25 Mhos/m), while the conductivity in the shorting regions between cathodes is approximately 50 Mhos/m,

figure 5.13. This is initially due to convection downstream from electrode edges. Maximum current densities are of the order of 4×10^4 A/m^2 and occur at the electrode edges and along shorted insulator sections. In the duct centre the current density is approximately 4×10^3 A/m^2. On the electrode edges the Hall parameter is approximately 1.0, and in the duct centre it is approximately 1.4.

Temperature profiles along the cathode boundary at t = 2.21 μsec are shown in figure 5.12. The temperature has its maximum values at the electrode edges, the density maxima occurring slightly downstream on the insulators. The temperature maxima increase downstream because initially the Ohmic heating on the cathode edges increases in this direction (the density and Ohmic heating increase upstream at the anode boundary). At 2.21 μ sec, when the calculation was terminated, the electron density had not reached equilibrium with the temperature distribution.

5.9 Difficulties with the Numerical Model

(a) Effect of Fast-Thermal Mode

In section 5.2 it was seen that the shortest time-scale of the system is the fast-thermal mode decay time, and therefore $\Delta t < |\tau_{FT}|$ if stable solutions are to be obtained. If one wishes to follow the growth of large amplitude electron density non-uniformities, this condition is restrictive at low T_e and prohibitive at large T_e. This fact is clear from figure 5.1, and the results of section 5.8, which were restricted to low values of β and low non-equilibrium ionization. Even for this case, however, the Hall effect leads to intense heating at the electrode

edges, and values of T_e at these points far exceed the average values. At these points a "fractional step" method is used, in which T_e is explicitly solved according to

$$\partial n_e/\partial t = \dot{n}_e + \text{constant terms}$$

$$\partial U_e/\partial t = -I_p \dot{n}_e + \text{constant terms}$$

using a time-step $\delta t = \Delta t/N$, where $N (> 1)$ is determined by the excess heating, and the constant terms are re-evaluated at each Δt.

(b) Mesh Uncoupling

A further problem encountered is that of mesh uncoupling. This arises from the second order accurate treatment of the $J(\chi, \phi)$ terms. The uncoupling manifests itself as stable, small amplitude waves of length 2Δ, superimposed on the distributions of T_e and n_e, and is only present if the heavy particles have non-zero velocity. The $J(\chi, \psi)$ terms do not appear to produce this effect, and the reasons for this are the smallness of these terms, and the use of a nine-point scheme for the two-dimensional flow; the nine-point scheme is largely redundant for the $J(\chi, \phi)$ terms since these are essentially one-dimensional, ie: representing $V\frac{\partial \chi}{\partial y}$.

The uncoupling can be prevented by applying sufficiently large artificial diffusion, although this will also reduce physical non-uniformities. A more logical approach for this problem is to use a first order method for the terms which arise due to heavy particle convection, ie:

$$\left[\partial \chi/\partial t\right]_j^{(n)} = -\frac{V}{\Delta}\left[\chi_j^{(n)} - \chi_{j-1}^{(n)}\right] \qquad (5.11)$$

and the solution to this equation satisfies

$$\left[\partial\chi/\partial t\right]_j^{(n)} + v\left[\partial\chi/\partial y\right]_j^{(n)} = \frac{v\Delta}{2}\left[\frac{\partial^2\chi}{\partial y^2}\right]_j^{(n)} + O(\Delta^2)$$

The leading term in the truncation error is therefore diffusive rather than dispersive, unlike second order methods, and the large error, short wave modes are heavily damped. This approach is permissible owing to the dominance of local terms, and the decreased accuracy in the $v\partial\chi/\partial y$ terms should not affect the overall accuracy to a great extent. This assumption is found to be valid in Chapter VI, and in Chapters VI and VII the above approach is used when the heavy particle velocity is non-zero.

Another form of mesh uncoupling occurs in the solution of the stream function, ψ. As described in section 5.7, the boundary condition for ψ at the electrodes, as given by equation (5.9), is second order accurate. This treatment leads to a short wave mode occurring near the high gradient electrode edges for $\beta \gtrsim 1.5$. The similarity between equations (5.10) and (5.11), when the ∇p_e term is omitted from equation (5.10), is seen by replacing $x \to t$ and $\beta \to v$, and the cause of the uncoupling is the same in both cases. Because of this uncoupling, a first order treatment of the condition $E_y = 0$ on electrodes is used in Chapter VII, and the two schemes compared numerically. The form of the first order treatment for equation (5.9) is

$$\psi_c = \left[\psi_N + \beta_c \psi_E - 1/2\,(\sigma/n_e e)_c (p_{e_E} - p_{e_W})\right]/(1+\beta_c) \qquad (5.12)$$

on the anode (south boundary), and

$$\psi_c = \left[\psi_s + \beta_c \psi_w + \tfrac{1}{2}\left(\sigma/\eta_e e\right)_c \left(P_{e_E} - P_{e_W}\right)\right] / (1+\beta_c)$$

on the cathode (north boundary).

5.10 Summary

A calculation of the characteristic time scales for the electro-thermal system showed that the shortest time scale is the decay time of the fast-thermal mode. An explicit numerical model of the system was presented which is stable provided restrictions on the size of the time step are enforced. The possibility of a fourth order instability in the treatment of convection terms was found, but not realised in practice.

Some numerical results were presented which demonstrated some of the phenomena present in MHD systems, and the difficulties involved in simulating this problem. These problems include the extremely small time-step required to satisfy $\Delta t < |\tau_{FT}|$, the existence of localized regions of high temperature and the occurrence of mesh uncoupling.

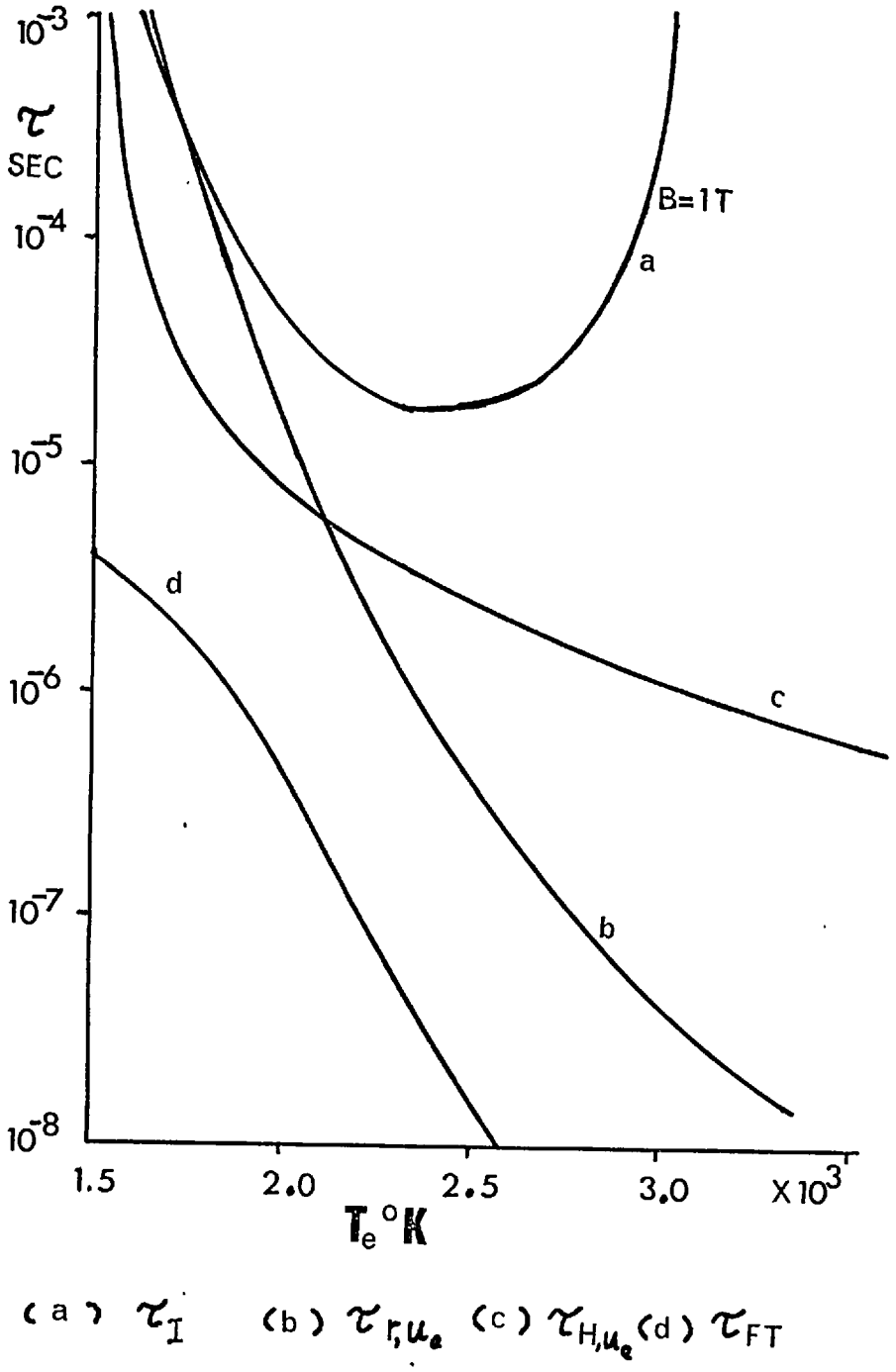

Figure 5.1: Characteristic time scales. (a) ionization mode; (b) ionization time scale in the energy equation; (c) Ohmic heating time scale in the energy equation; (d) fast-thermal mode.

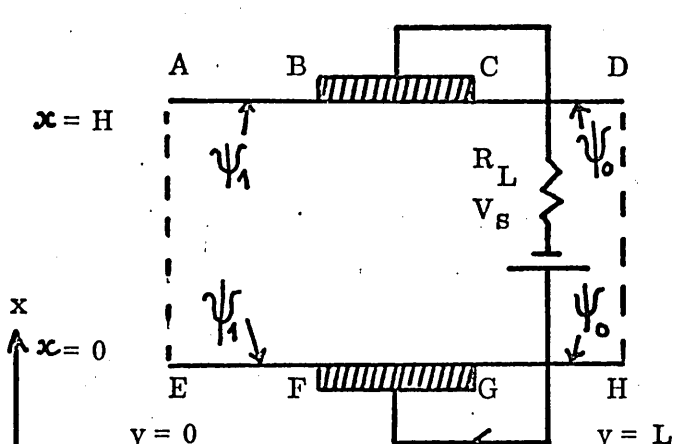

(1)

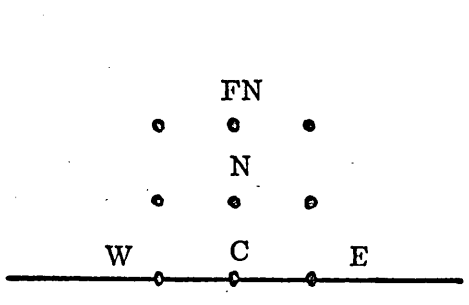

(2)

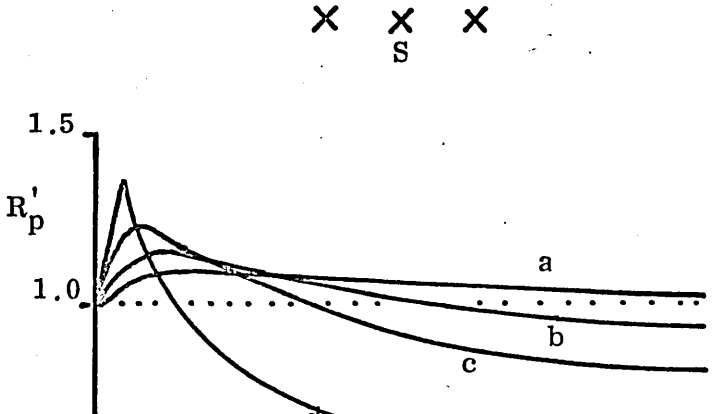

(3)

(1) Figure 5.2: Single electrode pair configuration

(2) Figure 5.3: Grid system on south boundary

(3) Figure 5.4: R_p' against time for applied fields a, b, c, d = 120, 240, 480, 960 V m^{-1}.

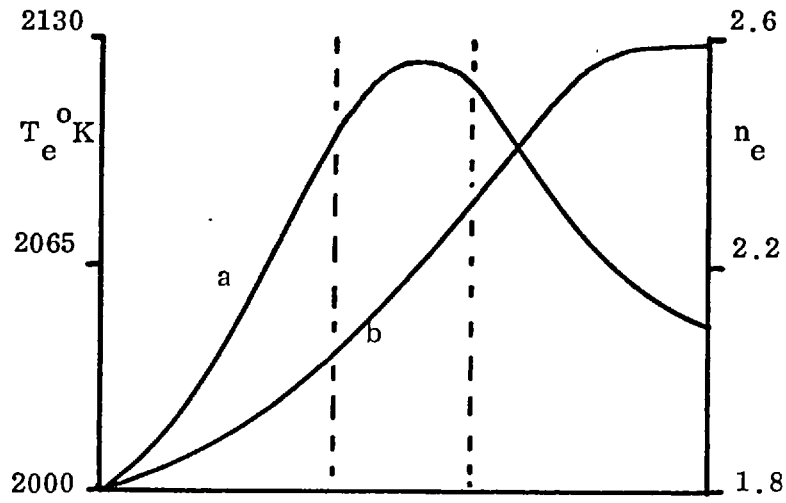

(1)

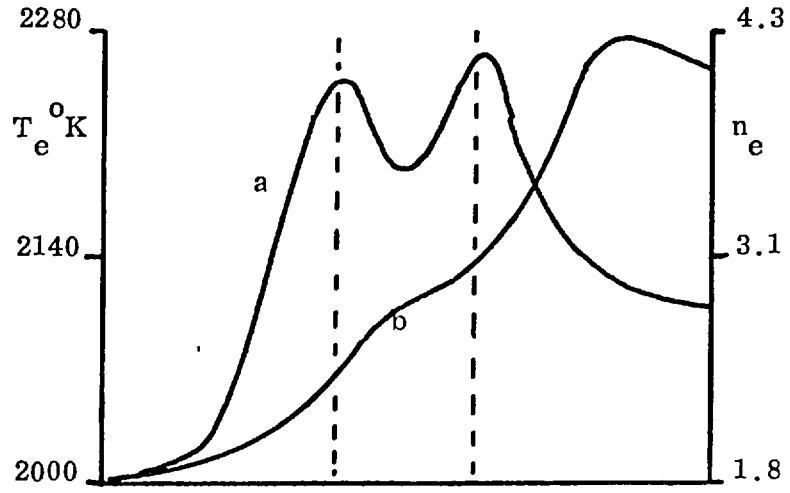

(2)

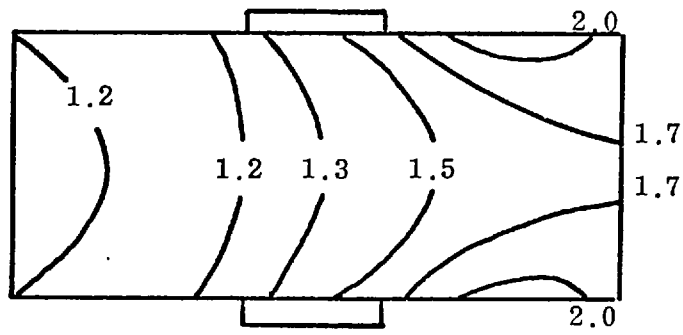

(3)

(1) Figure 5.5: (a) T_e and (b) n_e (x 10^{-19} m^{-3}) along duct centre in steady state for applied field 240 Vm^{-1}

(2) Figure 5.6: as above but along electrode boundary

(3) Figure 5.7: σ / σ_{min} profiles for above case

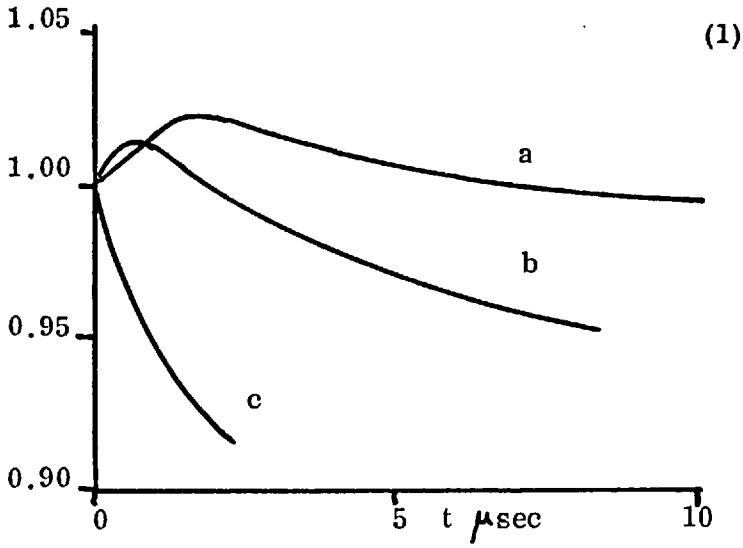

(1)

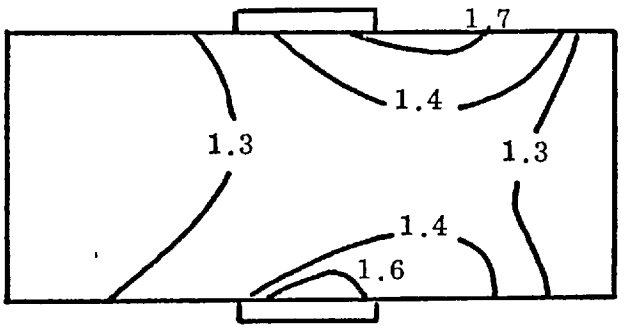

(2)

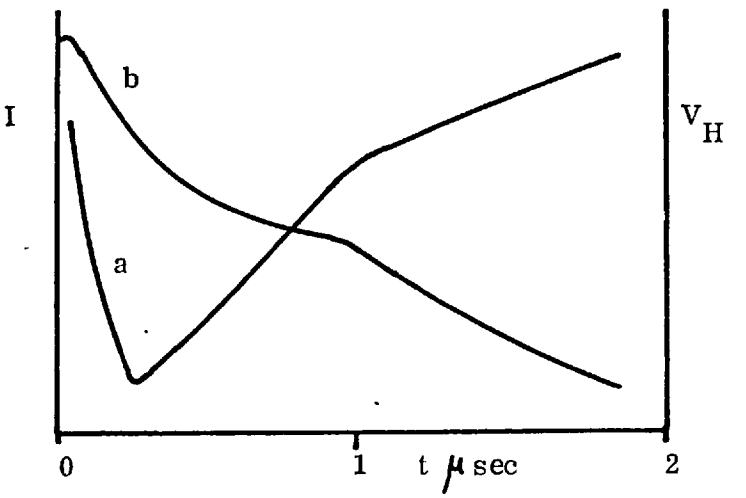

(3)

(1) Figure 5.8: R'_p against time for $\underline{v} \times \underline{B}$ fields a, b, c = 120, 240, 480 V m^{-1}

(2) Figure 5.9: σ/σ_{min} profiles for $\underline{v} \times \underline{B}$ = 120 V m^{-1} at t = 30 μsec

(3) Figure 5.10: (a) total output current, and (b) Hall voltage in arbitrary units against time for 5 electrode pair case

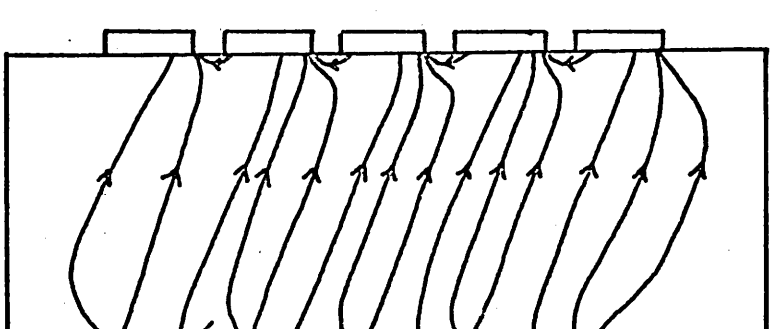

(1)

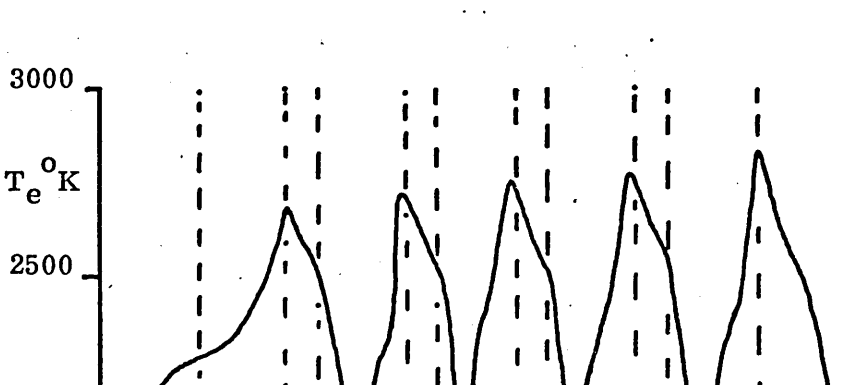

(2)

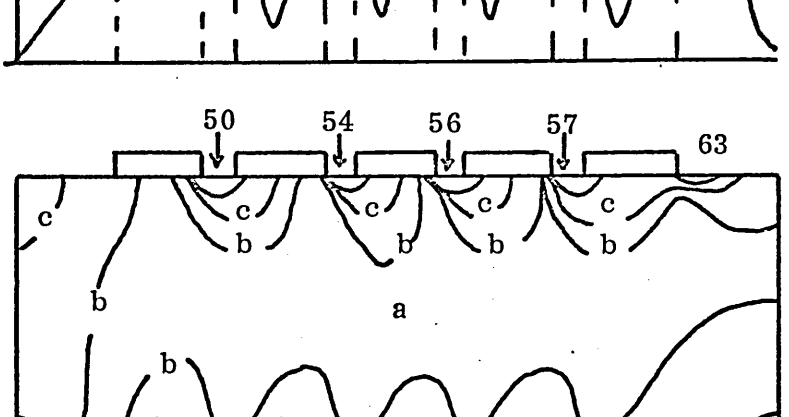

(3)

(1) Figure 5.11: Sample of current distribution at t = 2.2 μsec. This conveys information on current direction only.

(2) Figure 5.12: T_e along cathode boundary at t = 2.2 μsec.

(3) Figure 5.13: σ profiles at t = 2.2 μsec; a, b, c = 22, 23, 24 M m^{-1}.

CHAPTER VI

NUMERICAL SIMULATION OF ELECTROTHERMAL WAVES

6.1 Introduction

In this Chapter the growth of electrothermal waves to their non-linear amplitudes is discussed using a modified version of the previously described numerical model. Two cases of simpler geometry are considered; the formation of instabilities in an infinitely long discharge contained by insulator walls, as shown in figure 3.5, and an infinitely long discharge contained by continuous electrode walls, as shown in figure 1.1. These configurations correspond approximately to those used in experimental investigations of the instability (Riedmüller, 1970; Gilpin et al, 1969; Evans et al, 1970; Kerrebrock et al, 1968; Shipuk et al, 1968), as opposed to the segmented electrode configurations used in simulated power generation experiments.

Numerical methods are necessary for the solution of this problem, since no non-linear theory of the wave, which includes boundary effects, exists yet. The method of solution is as follows. A uniform plasma is considered in which $T_e = 3000^oK$, $T = 1500^oK$ and $n_e = S(T_e)$ everywhere. The uniform current density required to maintain this non-equilibrium state is driven by external voltage sources, and satisfies $j^2/\sigma = L(n_e, T_e)$ within the plasma. At $t = 0$ a small amplitude perturbation is introduced into the uniform distributions and forms the initial conditions for the problem. The evolution of the plasma is thereafter simulated numerically.

Similar work has been reported by Lengyel (1970), and Velikhov et al (1969, 1971). The work presented here is more complete, in that basic equations contain more of the physics involved in wave growth and motion, boundary conditions are treated in a more realistic manner, and circuit-plasma interactions are permitted. Moreover, simulations are in general allowed to evolve to their stationary states, and the dependence of these states on thermal conduction and radiation transfer discussed.

In section 6.2 an approximation is considered which removes the fast-thermal mode from the system, and its validity discussed. Since the initial perturbations applied to the system are very small, the linear growth rates for electrothermal instabilities can be obtained from the simulations, and these are plotted in section 6.3. The remaining sections are concerned with the non-linear aspects of wave formation, circuit-plasma interactions, and wave motion.

6.2 Removal of Fast-Thermal Mode from System

In the experimental studies of electrothermal instabilities and simulated power generation, heavy particle temperatures and electron temperatures are typically in the ranges 1500-2000^{o}K and 2500-3000^{o}K respectively. It can be seen from figure 5.1 that $|\tau_{FT}| \sim 10^{-9}$sec for $T_e = 3000^{o}$K. It was demonstrated in Chapter III that the growth time for the electrothermal instability is of the order of 10^{-5}sec. The large difference between these time scales, at large T_e, means that the fast-thermal mode must be eliminated from the system if the growth of instabilities is to be followed. The fast-thermal mode is eliminated from the system if Saha equilibrium is assumed, and the validity of this assumption is demonstrated below for the linear solutions.

The solution to the linearized equations (3.1)-(3.8) can be written

$$n_e'(t) = \frac{n_e'(0)}{g_- - g_+}\left[(g_- - a_0)\exp(g_+ t) + (a_0 - g_+)\exp(g_- t)\right]$$

$$T_e'(t) = n_e'(0)\left[\frac{a_4 + a_6 + a_8 - a_0 a_2}{a_3(g_+ - g_-)}\right]\left[\exp(g_+ t) - \exp(g_- t)\right]$$

or $$n_e'(t)/n_e'(0) = \alpha_1 \exp(g_+ t) + \alpha_2 \exp(g_- t)$$

and $$T_e'(t)/n_e'(0) = \alpha_3\left[\exp(g_+ t) - \exp(g_- t)\right]$$

in which $T_e'(0) = 0$

The corresponding solutions when $n_e = S(T_e)$ are

$$n_e'(t)/n_e'(0) = \alpha_1' \exp(g_+' t)$$

and $$T_e'(t)/n_e'(0) = \alpha_3' \exp(g_+' t)$$

These solutions are in agreement, for $t \gg |g_-^{-1}|$, when

$$c_1 = |g_+/g_-| \ll 1, \quad c_2 = |(g_+ - g_+')/g_+| \ll 1$$

$$c_3 = |(\alpha_1 - \alpha_1')/\alpha_1| \ll 1, \quad c_4 = |(\alpha_3 - \alpha_3')/\alpha_3| \ll 1$$

and $$|g_+/a_0| \ll 1$$

The latter inequality is the requirement that ionization recombination rates greatly exceed the instability growth rate. This was shown to be the case in Chapter III, figure 3.4, for $T_e = 3000^{\circ}K$ and $\beta \lesssim 8$, ($B \lesssim 6T$).

Figures 6.1-6.4 show C_1, C_2, C_3 and C_4 as functions of T_e for several magnetic field strengths. It is seen that each of these quantities is less than 0.1 for $T_e = 3000^{\circ}K$ and $\beta \lesssim 8 (B \lesssim 6T)$. Saha equilibrium is therefore assumed to lead to realistic solutions of the equations under the above conditions.

The energy equation is solved in the form

$$\frac{\partial}{\partial t}\left[I_p+\tfrac{3}{2}K_B T_e\right]n_e = \frac{\partial \epsilon_e}{\partial t} = -\nabla.(\epsilon_e \underline{v}_e) - P_e \nabla.\underline{v}_e + j^2/\sigma - L + \nabla.(K_e \nabla T_e) - \dot{Q}_R \qquad (6.1)$$

and the continuity equation becomes

$$F(\epsilon_e, T_e) = \epsilon_e^2 + \epsilon_e g(T_e) f(T_e) - n_s g^2(T_e) f(T_e) = 0 \qquad (6.2)$$

where $g(T_e) = I_p + \frac{3}{2}K_B T_e$ and $f(T_e) = \left[\frac{2\pi m_e k_B T_e}{h^2}\right]^{3/2} \exp\left(-\frac{T_p}{T_e}\right)$. The electron energy is therefore solved from equation (6.1) which is used to evaluate T_e from equation (6.2), using a Newton-Raphson iterative method of the form

$$T_e^{(p+1)} = T_e^{(p)} - F^{(p)} / \left[\partial F^{(p)}/\partial T_e\right]$$

The electron density is obtained from the convergent solution of T_e, $T_e^{(n+1)}$, using

$$\epsilon_e^{(n+1)} = n_e^{(n+1)}\left[I_p + 3/2 \cdot K_B T_e^{(n+1)}\right]$$

The limiting time-scale for the equations now becomes the electrothermal instability growth time, which is the required result.

6.3 Growth Rates for Insulator Walls and Electrode Walls

The boundary conditions for both types of wall were discussed in Chapter V. The system is assumed to be periodic in the 'y' direction with periodicity L. The initial perturbation in temperature is usually taken to be

$$T_e^* = 10^{-4} \sin\left[2\pi y/L\right]$$

which defines values for n_e^* from the Saha relation. The distribution of ψ corresponding to the new values of n_e and T_e is evaluated, the distributions for ψ, n_e, T_e forming the initial conditions. Unless stated otherwise, K_e and $\dot{Q}_R$ are assumed to be zero, and the heavy particles are

stationary in sections 6.3-6.7. Apart from section 6.5 the load resistance is taken to be much greater than the plasma resistance per unit volume of duct, ie: $\frac{\sigma_L}{\sigma_P} << 1$, and the effect of wave growth in the duct has little effect on the magnitude of the total current flow. Expressions for σ_L and σ_P are given in section 6.5.

By varying L, maintaining H constant at 5 cm, the effect of geometry on β_{crit} can be investigated; and keeping L/H constant and varying $\underline{B}$, the growth rates of the waves as a function of β can be investigated.

Figure 6.5 shows the critical Hall parameter for onset of the waves as a function of L/H. As L/H $\rightarrow$ 0, β_{crit} tends to the infinite plasma value obtained in Chapter III. The continuous electrode system (a), clearly possesses the higher stability threshold. This is because of the different orientation of the average current density at the walls for each case. For the continuous electrode walls the 'wave vector' for each approximate plane-wave lies further from the region of instability, $\underline{j} \times \underline{k}.\underline{B} \approx \underline{j}.\underline{k}\,|\underline{B}|$, than the corresponding insulator walls case.

Figures 6.6 and 6.7 show the linear growth rates for (a) continuous electrodes and (b) insulator walls as functions of β_o. Growth rates for L/H = 0, 1 and 2 are shown.

These results demonstrate that the time scale for linear growth is of the order of 10^{-5} secs, that the critical Hall parameter is approximately 2, and that the effect of finite geometry is to stabilize the waves, both by decreasing the growth rate and increasing β_{crit}.

Some of these results were obtained in Chapter III using a linear theory, and the graphs plotted here are in excellent agreement with the theoretical results on boundary effects given by Nelson (1969). Whilst these results are therefore not new, they are rapidly obtained numerically and provide a good check on the simulation. In the following sections the non-linear behaviour of the waves at longer times is examined.

6.4 Insulator Walls

The following quantities are defined

$$n_e' = n_e - \langle n_e \rangle$$

$$n_e^* = n_e/\langle n_e \rangle - 1$$

$$\langle |n_e^*| \rangle = \langle |n_e - \langle n_e \rangle| \rangle / \langle n_e \rangle$$

where $\langle\ \rangle$ is an average over the mesh. n_e^* is a measure of the local non-uniformity, and $\langle |n_e^*| \rangle$ is a measure of the average non-uniformity. In sections 6.4-6.7 L = H = 5 cm, v = 0, and unless stated otherwise, a (13 x 13) mesh has been used.

It is found that an initial small amplitude perturbation applied to a uniform unstable plasma leads, in general, to a steady state which is independent of the structure of the perturbation; and that this final non-uniform state has average properties which are appreciably different from the initial state.

(a) Temporal Behaviour of Averaged Parameters

Figure 6.8 shows the temporal development of the electrothermal fluctuations for an initial uniform β , β_0 , of 3.2. The first part of this curve depends on the structure of the initial perturbation, and the time

required to excite the most unstable, n = 1, mode of the system; after the initial conditions have been 'phase-mixed', the growth shows an exponential form, the slope of this line providing a linear growth rate for the waves. The exponential behaviour ceases once $\langle |n_e^*| \rangle$ exceeds approximately 0.1, and the average fluctuation then saturates at approximately 0.3.

Figure 6.9 shows the development of the fractional effective conductivity and Hall parameter, together with the average electron density. For $\beta_0 < \beta_{crit}$, $\sigma_{eff} = \langle \sigma \rangle$ and $\beta_{eff} = \langle \beta \rangle$ owing to the simplicity of the configuration ; it is seen that for β_0 only 50% greater than β_{crit} these quantities are significantly reduced due to the electrothermally induced non-uniformities. These plots have three distinct regions, viz: (i) an initial plateau; (ii) a breakdown region and (iii) a saturation region.

(i) The initial plateau corresponds to the uniform initial state of linear perturbation theory.

(ii) The beginning of the breakdown region occurs at the time for which second order effects begin to be important, ie: when the overall behaviour of the plasma is affected by the non-uniformities. The induced current loops within the non-uniformities become a significant fraction of the total current flow, and the excess dissipation results in an increase in the ionization, leading to an increased average electron density. The magnitude of the increase in $\langle n_e \rangle$ depends on the external circuitry and its interaction with the plasma, since energy is supplied to the plasma

externally. The breakdown begins when $\langle|n_e^*|\rangle$ is approximately 0.05, which would indicate that non-linear behaviour in the peaks and troughs of the wave affect the system quite strongly.

(iii) The saturation region represents the steady state of the system. Higher order contributions to the Ohmic heating tend to increase the heating everywhere in the plasma. In the peaks of the wave, the increased density leads to a more efficient transfer of energy to the heavy particles through elastic collisions. Together with the reduced Hall parameter in the wave peaks, these losses eventually balance the dissipation and growth stops. In the wave troughs the collisional stabilization becomes less efficient, but the higher order contributions to the heating, which are increased by the increased Hall parameter, ensure that the heating is not suppressed too far below the average heating. A balanced system will therefore eventually be reached.

The higher order contributions to the elastic collision losses, together with a reduced Hall parameter, are therefore mainly responsible for stability in the peaks; and the higher order contributions to the Ohmic heating, together with an increased Hall parameter, are mainly responsible for stability in the troughs.

Figure 6.10 shows $\beta_{eff}/\langle\beta\rangle$ as a function of time for different initial values of the Hall parameter β_o . The time at which breakdown occurs can be considered a rough measure of the non-linear growth time, this is approximately 10^{-4} secs for $\beta_o = 3.2$, and is of the order of ten times the linear growth rate in general. Radiation transfer has been included in the energy equation for $\beta_o > 4$, and the reasons for this discussed in section 6.4(b).

(b) Steady State Structure and Wave Velocity

Figures 6.11-6.13 show the saturated global parameters of the system as a function of the initial Hall parameter. As mentioned above, a radiation term has been included in the energy equation for $\beta_0 > 4$. The saturated average Hall parameter and conductivity differ in each case by less than 5% from their initial values, and have therefore not been plotted. These graphs demonstrate that increasing the Hall parameter increases the effect of the instability on the system. In figure 6.11 by decreasing $\sigma_{eff}/\langle\sigma\rangle$ and $\beta_{eff}/\langle\beta\rangle$; in figure 6.12 by increasing the degree of non-uniformity, although $\langle|n_e^*|\rangle$ is tending to saturate with increasing β_0 ; and in figure 6.13 by increasing the internal dissipation in the plasma and thus the average electron density. For $\beta_0 \approx 2\beta_{crit}$ the average fluctuation is approximately 40%, and $\beta_{eff}/\langle\beta\rangle$ and $\sigma_{eff}/\langle\sigma\rangle$ are approximately 50% of their ideal uniform plasma values. In all cases the effective Hall parameter saturates at approximately 2, ie: $\beta_{eff} \approx \beta_{crit}$.

The general features of the electron density distribution in the steady state for $\beta_0 = 4$ are shown in figure 6.14. The hatched regions and blank regions represent $n_e^* > 0$ and $n_e^* < 0$ respectively. It is shown like this because the experiments usually provide photographs of the plasma, and these pick out the broad features of the distributions. It is seen that the wave retains its approximate plane-wave structure in the non-linear state for $\beta_0 \approx 2\beta_{crit}$. The angle between the wavefront and the average current flow decreases with increasing β_0. For $\beta_0 = 2.5$

and 4.0, this angle is 34^{o} and 27^{o} respectively. This behaviour can be attributed to higher electrothermal modes appearing in the solution. According to a simplified analysis by Riedmüller (1970), the inclination of the 'wavefront' to the average current flow for the n^{th} mode is given approximately by

$$\tan\gamma = \left[\sqrt{1+(nL/2H)^2} + nL/2H \right]^{-1}$$

For n = 1 $\gamma = 32^{o}$, and for n = 2 $\gamma = 22^{o}$ with L = H. According to equation (3.18) only one mode is present for $\beta_o = 2.5$ and three for $\beta_o = 4$, the ratio of the growth rates being 6.3 : 3.4 : 1. It would therefore seem likely that the solution for $\beta_o = 4$ comprises a signficant admixture of n = 2 mode.

By continuing the calculation after the steady state has been reached, it is possible to measure the velocity of the non-uniformities in the 'laboratory' frame, which is also the heavy particle frame for these v = 0 calculations. It is found that the waves move with a velocity of approximately 30 m sec^{-1} in the direction of the average current flow, which is along the duct in this case. In these calculations compressional effects dominate convection effects in the energy equation, and the wave motion is mainly due to the compression of the electrons as they stream through the waves. If the heavy particles are moving, it is found that the non-uniformities maintain the above velocity in the heavy particle frame. With v = 200 m sec^{-1}, and using the first order method for the convection term discussed in Chapter V, the saturated parameters differ at most by 5% from the v = 0 case. The artificial diffusion introduced into the solutions by the difference scheme does not, therefore, qualitatively alter the solutions.

Figure 6.15 shows the eddy current flow set up in the non-uniformities. The total current flow is the sum of a uniform average flow and these eddy currents, the increased length of the flow lines resulting in decreased σ_{eff} and β_{eff}. The eddy currents stream through the regions of high electron density, and take return paths through the regions of low density. In the $n_e^* > 0$ regions $\langle \underline{j} \rangle . \underline{j}' > 0$, and in the $n_e^* < 0$ regions $\langle \underline{j} \rangle . \underline{j}' < 0$, where $\underline{j} = \langle \underline{j} \rangle + \underline{j}'$. The local Ohmic heating is therefore

$$j^2/\sigma \propto \langle \underline{j} \rangle^2 + 2\langle \underline{j} \rangle . \underline{j}' + \underline{j}'^2$$

ie: the wave produces excess heating in second order everywhere, and in first order provides additional heating in the wave peaks, and reduced heating in the troughs. The averaged square current density may be written

$$\langle \underline{j}^2 \rangle = \langle \underline{j} \rangle^2 + \langle \underline{j}'^2 \rangle$$

and provided $\langle \underline{j} \rangle$ remains approximately constant, $\sigma_L/\sigma_P \ll 1$, the second term leads to an increase in $\langle n_e \rangle$. This can be easily shown in the limits σ = constant, $\langle \underline{j} \rangle$ = constant. In Chapter I, section 1.5(c), it was shown that $\langle \sigma \rangle / \sigma_{eff} = 1 + \frac{1}{2}\langle \beta \rangle^2 \times \langle n_e^{*2} \rangle$ for one-dimensional non-uniformities, and from equation (3.26)

$$\langle j^2/\sigma \rangle = \frac{\langle \underline{j} \rangle^2}{\langle \sigma \rangle} . \frac{\langle \sigma \rangle}{\sigma_{eff}} = \frac{\langle \underline{j} \rangle^2}{\langle \sigma \rangle} \left[1 + \tfrac{1}{2} \langle \beta \rangle^2 \langle n_e^{*2} \rangle \right]$$

If the final steady state satisfies $j^2/\sigma \approx L$ at each point, then $\langle j^2/\sigma \rangle \approx \langle L \rangle \approx \alpha \langle n_e^2 \rangle = \alpha \langle n_e \rangle^2 \left[1 + \langle n_e^{*2} \rangle \right]$ in the Coulomb dominated regime, where $\alpha = \alpha(T_e)$ is taken to be constant because of the relationship $T_e^* \ll n_e^*$. From the constancy of $\langle \underline{j} \rangle$ and σ this gives

$$\alpha = \langle \underline{j} \rangle^2 / \langle \sigma \rangle n_e^2(t=0)$$

and $$\langle n_e \rangle^2 / n_e^2(t=0) \approx \frac{1 + 1/2 \cdot \langle \beta \rangle^2 \langle n_e^{*2} \rangle}{1 + \langle n_e^{*2} \rangle} > 1 \qquad (6.3)$$

in the unstable regime.

The current pattern in figure 6.15 is predominantly n = 1 mode, and this is in accord with the expectation that the most unstable mode should dominate the system.

It is found that for $\beta_0 > 4$ the solutions for the averaged parameters do not saturate on a (13 x 13) mesh; oscillations occur in the solutions and ω, the relaxation parameter for the solution of ψ, rapidly decreases. For example, for $\beta_0 = 5$ the oscillations begin at $t = 3 \times 10^{-4}$ secs, whilst the initial breakdown region, attributable to the non-linear growth of an n = 1 mode, occurs at $t = 0.3 \times 10^{-4}$ sec. From equation (3.18) it is seen that the linear growth rates of the n = 1 mode and n = 4 mode are in the ratio 10 : 1; if one assumes that the non-linear growth rates also maintain this ratio, then the beginning of the oscillations can be attributed to the non-linear growth of the n = 4 mode. It was shown in Chapter III that the linear solutions for the perturbed current flow are proportional to $\sin(\frac{n\pi x}{H})$, and therefore define a wavelength

$$\lambda_x = 2H/n$$

For a (13 x 13) mesh $H = 12\Delta$, and with n = 4 this gives

$$\lambda_x = 6\Delta$$

This mode is therefore close to the limit of resolution, and it would seem likely that the errors involved in the evaluation of the perturbed heating in this mode could account for the non-physical behaviour.

In order to provide better resolution for the higher modes and thus simulate mode-mode interactions, a $\beta_o = 6 \approx 3\beta_{crit}$ calculation was performed on a (29 x 29) mesh with k_e, $\dot{Q}_R = 0$. Owing to the machine time involved this run was terminated before complete saturation was obtained. The density distribution and total current flow are shown in figures 6.16 and 6.17 at $t = 1.5 \times 10^{-4}$ sec, by which time the n = 3 mode should have fully developed. It is seen that the current flow is approaching a state of large amplitude turbulence, and that this is reflected in the density distribution. The striations are 'wavy' and are breaking up near the boundaries; the non-uniformities still possess a well defined orientation, and this is because the n = 1 mode dominates the system, although n = 2, n = 3 modes are perturbing it to a large extent.

It is evident that the use of such large meshes cannot yield a large amount of physical data owing to the time limitation, because of this a method of stabilizing the $\lambda_x \approx 4\Delta$ waves is discussed in section 6.6.

6.5 Effect of External Circuits on the Steady State

In this section the behaviour of the instability as a function of the ratio of plasma to load resistance for the $\beta_o = 3.2$ case is discussed. The load and plasma conductivities are defined as

$$\sigma_L = \ell / R_L HW \quad , \quad \sigma_p = \ell / R_p HW$$

where R_p is the resistance of the discharge, of length ℓ, and R_L is the total load resistance in the external circuit which maintains the discharge.

As $\sigma_L/\sigma_p \to 1$ the stability of the plasma can be expected to have a substantial effect on the total current flow, which in turn will modify the behaviour of the instability. This behaviour is also of practical importance because the condition of optimum power in an external load is $\sigma_L \approx \sigma_p$.

In order to maintain the same degree of non-equilibrium ionization at t = 0, ie: the same current density, the external voltage has to be decreased with decreasing R_L to satisfy $V_s = I(R_p + R_L)$.

Figure 6.18 shows $\langle\beta\rangle$, $\sigma_{eff}/\langle\sigma\rangle$, $\beta_{eff}/\langle\beta\rangle$, β_{eff} and $\langle|n_e^*|\rangle$ for the steady states of the $\beta_0 = 3.2$ case as a function of $\sigma_L/\sigma_p(t = 0)$. The effect of the wave increases with increasing $\sigma_L/\sigma_p(t = 0)$, $\langle|n_e^*|\rangle$ increasing from 0.33 to 0.37 over the range, and $\beta_{eff}/\langle\beta\rangle$ decreasing by approximately 10%. The effective Hall parameter remains approximately constant at 1.9. Circuit-plasma interactions do not, therefore, have a large effect on the wave for $\sigma_L/\sigma_p \ll 1$.

The reduction in σ_{eff} due to circuit-plasma interactions is shown in figure 6.19; this is again approximately 10% over the range. An interesting feature is the reduction in $\langle n_e\rangle$ with increasing σ_L/σ_p, the dotted line in this figure represents $n_e(t = 0)$. The temporal development of $\langle n_e\rangle$ for three values of $\sigma_L/\sigma_p(t = 0)$ is shown in figure 6.20.

If $\langle \underline{j} \rangle$ is allowed to vary with time, equation (6.3) becomes

$$\frac{\langle n_e\rangle^2}{n_e^2(t=0)} \approx \frac{\langle \underline{j}\rangle^2}{\langle \underline{j}\rangle^2_{t=0}} \left[\frac{1 + 1/2\langle\beta\rangle^2\langle n_e^{*2}\rangle}{1+\langle n_e^{*2}\rangle}\right] \propto \frac{I^2}{I_0^2}$$

where I and I_o are the total current flows in the steady state and at $t = 0$; and

$$\frac{I}{I_o} = \frac{1 + R_{p_o}/R_L}{1 + R_p/R_L} \quad , \quad R_p > R_{p_o}$$

The increased plasma resistance due to instabilities therefore results in a reduction in current, which becomes more marked with decreasing R_L, and suppresses the growth in $\langle n_e \rangle$. When $R_p > R_L$ the total power dissipated in the plasma must decrease with increasing R_p, and the average density is therefore constrained to decrease below its $t = 0$ value.

6.6 Inclusion of Thermal Conductivity and Radiation Damping

The necessity for providing a short wave damping in order to eliminate the higher electrothermal modes at large β_o was mentioned in section 6.4. If this is not done the mesh step must be decreased in order to resolve these modes.

The inclusion of electron thermal conductivity in the energy equation is found to have an insignificant effect on the stability. This is in accord with the results of Chapter III, in which it was shown that thermal conduction only produces a significant stabilizing effect for waves of length less than 1 mm.

A method of taking into account the electron inelastic collision losses was suggested by Lengyel (1970). In this method, each element of the plasma is considered to be emitting line radiation as though it were a black body radiating at the local electron temperature. The radiation has a bandwidth $\delta\lambda'$, which is the width of the cesium resonance doublet

comprising the 8.97×10^{-7}m and 8.55×10^{-7}m lines. Seed radiation from this doublet represents the chief source of inelastic collision losses for the electrons.

Each mesh cell, centred on a mesh point, receives radiant energy through its surface from each of its four nearest neighbours, and emits radiation to these cells. The ratio of loss area to total volume of each mesh cell is $4/\Delta$, and the net power emitted per unit volume of a given mesh cell centred on the point (i,j) is

$$\dot{Q}_{R\,ij} = \frac{4}{\Delta} \cdot 2\pi h c^2 \frac{\delta\lambda'}{\lambda^5} \left[\exp(-h\nu/k_B T_{e\,ij}) - \langle \exp(-h\nu/k_B T_e) \rangle_{ij} \right]$$

where the average is over the four nearest neighbours to (i,j). This expression can be written in differential form using the approximation

$$(\nabla^2 \alpha)_{ij} = \frac{4}{\Delta^2} \left[\langle \alpha \rangle_{ij} - \alpha_{ij} \right] + O(\Delta^2)$$

The result is

$$\dot{Q}_R \approx -\nabla \cdot (K_T \nabla T_e)$$

where

$$K_T = \frac{2\pi h^2 c^3 \delta\lambda'}{\lambda^6 k_B T_e^2} \cdot \Delta \cdot \exp\left(-\frac{h\nu}{k_B T_e}\right)$$

The radiation term, in this approximation, therefore has the form of a heat conduction, and the total effective 'thermal conductivity' is $k' = k_e + k_T$. Values of k_T/Δ and $(1 + \beta^2)k_e$ are plotted as functions of T_e in figure 6.21. For $T_e = 3000^{\circ}$K, $\beta_0 = 0$ and $\Delta = 4.2 \times 10^{-3}$m, one has $k_T/k_e = 74$. Nelson and Haines (1969) linearized the radiation term devised by Lutz (1967) and found the length dependence to be $\lambda^{-\frac{1}{2}}$ rather than the λ^{-2} dependence inherent in the above approximation. The diffusion term is solved in the form, for one dimension,

$$\left[\nabla \cdot (k'\nabla T_e)\right]_j^{(n)} = \left[T_{e\,j+1}(k'_{j+1} + k'_j) - T_{e\,j}(k'_{j+1} + 2k'_j + k'_{j-1}) + T_{e\,j-1}(k'_j + k'_{j-1}) \right]^{(n)} / 2\Delta^2$$

and its stability can be discussed using the methods of Chapter V, section 5.3(a), with

$$\tau \sim -\Delta^2 . \frac{n_e k_B}{4k'} . \left[\frac{T_p}{T_e}\right]^2$$

for the shortest waves on the mesh. The stability criterion is $\Delta t < |\tau|$.

The boundary conditions chosen for this term arrange that the mesh cells situated around boundary points do not transmit energy to the exterior. For an open system these extra conditions must be applied all around the domain, for a periodic system extra conditions along the horizontal boundaries only are necessary. The ellipticity of the current distribution is unaffected by the inclusion of the conduction term.

A comparison of the solutions with and without the 'conductivity' term is given in figure 6.22 for an initial β of 10.0 and on a (13 x 13) mesh. It is seen that the 'conductivity' produces a marked smoothing without producing a large corruption of the averaged values.

The final distributions for this case are shown in figures 6.23 and 6.24. The resolution of modes with $n > 1$ is apparent. It can be shown that the radiation 'conduction' defined above becomes an important damping mechanism for waves of length less than 1 cm for $\beta_o > 2$, $T_e = 3000^{o}K$ and the mesh step used here.

6.7 Growth of Waves in Continuous Electrode Geometry

The only difference between this case and the insulator walls case is that the current is constrained to flow between electrodes situated at $x = 0$ and $x = H$. The initiation of the simulation and other conditions are the same.

Saturation of the averaged parameters has not been obtained in these calculations. Figures 6.25 and 6.26 show the behaviour of $\langle |n_e^*| \rangle$, $\sigma_{eff}/\langle\sigma\rangle$, $\beta_{eff}/\langle\beta\rangle$ and $\langle n_e \rangle$ as a function of time for $\beta_o = 3.2$. In this geometry a lowering of β_{eff} leads to a reduction in the internal impedance of the plasma. This is due physically to the non-uniformities providing a low impedance path between the electrodes; the current lines tend to avoid the low conductivity regions, ie: the wave troughs, and stream through the high conductivity regions to the cathode. The oscillatory behaviour can be attributed to circuit effects. At $t = 1.5 \times 10^{-4}$ sec $\langle n_e \rangle$, $\sigma_{eff}/\langle\sigma\rangle$ and $\beta_{eff}/\langle\beta\rangle$ reach their first minimum, these quantites then increase, presumably in an attempt to saturate as in the insulator walls case; the increase in β_{eff} leads to an increase in the internal impedance and thus, for $\sigma_L < \sigma_p$, the power input from the external source.

This additional heating leads to an increase in $\langle n_e \rangle$, which alters the conditions for wave growth and feeds energy into the wave. The wave grows further in order to compensate for the changed values, and so on until presumably a stationary state is achieved with $\langle n_e \rangle$ substantially different from $n_e(t = 0)$.

Figure 6.27 show the behaviour of $\langle n_e \rangle$ with increasing $\sigma_L/\sigma_p(t = 0)$. For $\sigma_L/\sigma_p(t = 0) = 2$ the decreased impedance, resulting from a decreased β_{eff}, leads to an increase in input power and therefore $\langle n_e \rangle$ rises.

The temporal development of the density and current distributions are shown in the remaining figures. The quantity τ is defined as

$$\tau = \left[j_0^2 / \sigma_0 n_{e0} I_p \right] t$$

The additional structure observed in the density distribution at large τ is difficult to interpret. It may be that because the large amplitude non-uniformities cannot achieve stability, they are themselves unstable to electrothermal instabilities which can grow within them.

6.8 Conclusions and Comparison with Experiment

The majority of experimental studies on electrothermal waves use configurations similar to those simulated in this Chapter. The results obtained here are in good qualitative agreement with these studies. In particular, the following salient features of the simulations correspond to the physical processes observed experimentally:

(i) Saturation of β_{eff} at approximately 2 for $2 < \beta_0 < 10$ (Shipuk et al, 1968; Evans et al, 1970) and reduction of σ_{eff} with increasing β_0, (Shipuk et al, 1968).

(ii) The orientation of the steady structure is such that increasing β_0 tends to align the 'wavefront' in the duct centre with the average current flow (Riedmüller, 1970).

(iii) The structure has a velocity, in the heavy particle frame, of approximately 30 m sec^{-1} in the direction of the average current flow (Evans et al, 1970; Shipuk et al, 1968).

(iv) For $2 < \beta_0 < 4$ the structure is approximately plane-wave like, for larger values of β_0 the structure is more complex, the 'wavefronts' become 'wavy' and the structure breaks up near the walls (Riedmüller, 1970; Shipuk et al, 1968).

(v) The density profiles have the same general form and show the same behaviour with increasing β_0 as the results given by Riedmüller (1968), in particular the occurrence of density maxima near the boundaries.

(vi) Fluctuations in the centre of the channel duct, defined as $(n_{emax} - n_{emin})/(n_{emax} + n_{emin})$, range from 50% for $\beta_0 = 2.5$, to 80% for $\beta_0 = 10$, in qualitative agreement with the results of Shipuk et al (1968) and Riedmüller (1968).

The results presented in this Chapter, and their similarity to experimental results, indicate that the numerical approach to this non-linear problem is capable of simulating a large amount of the essential physics in partially ionized magnetized plasmas.

An obstacle to the long term integration of the equations at large β_0 is the occurrence of physical, short wavelength, unstable modes; these modes can be damped by the inclusion of an approximate form of radiation transport which allows the use of reasonably coarse meshes.

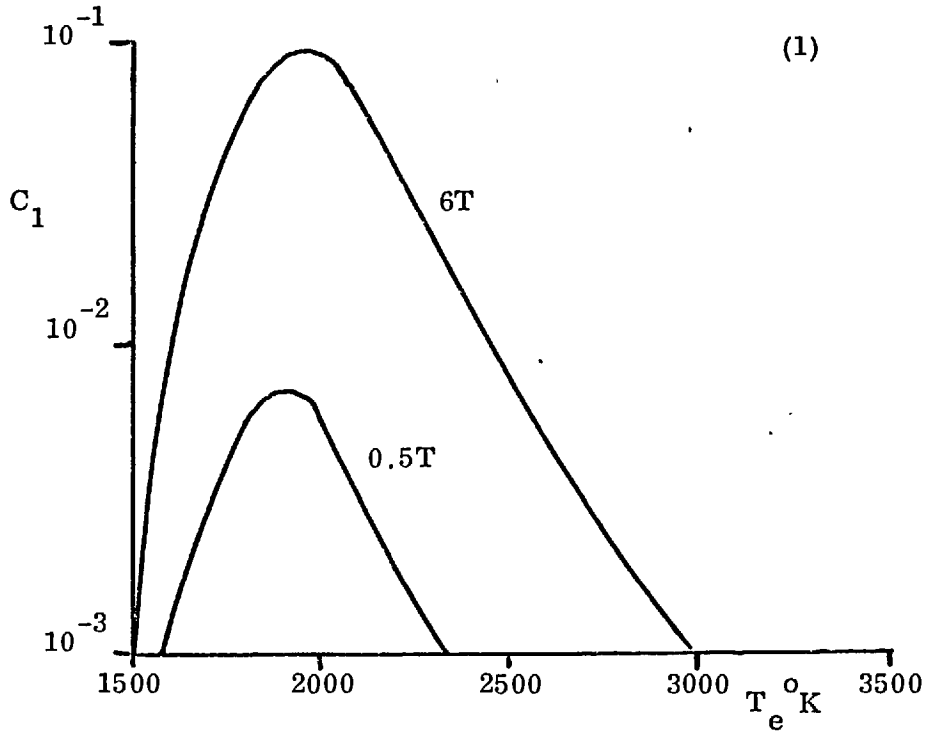

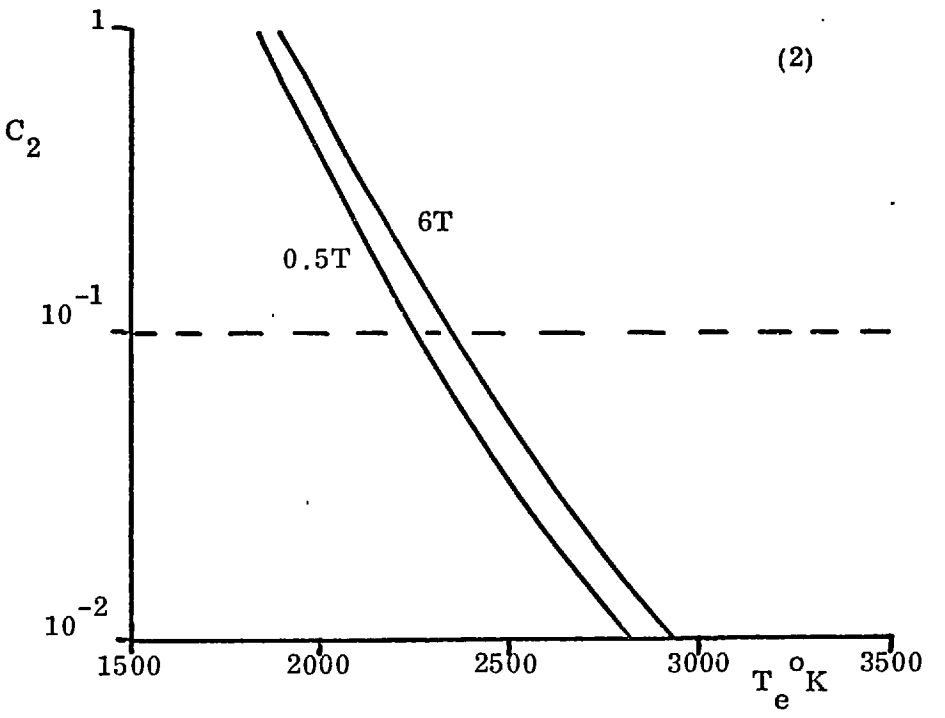

(1) Figure 6.1: C_1 against T_e for B = 6T and 0.5T

(2) Figure 6.2: C_2 against T_e for B = 6T and 0.5T

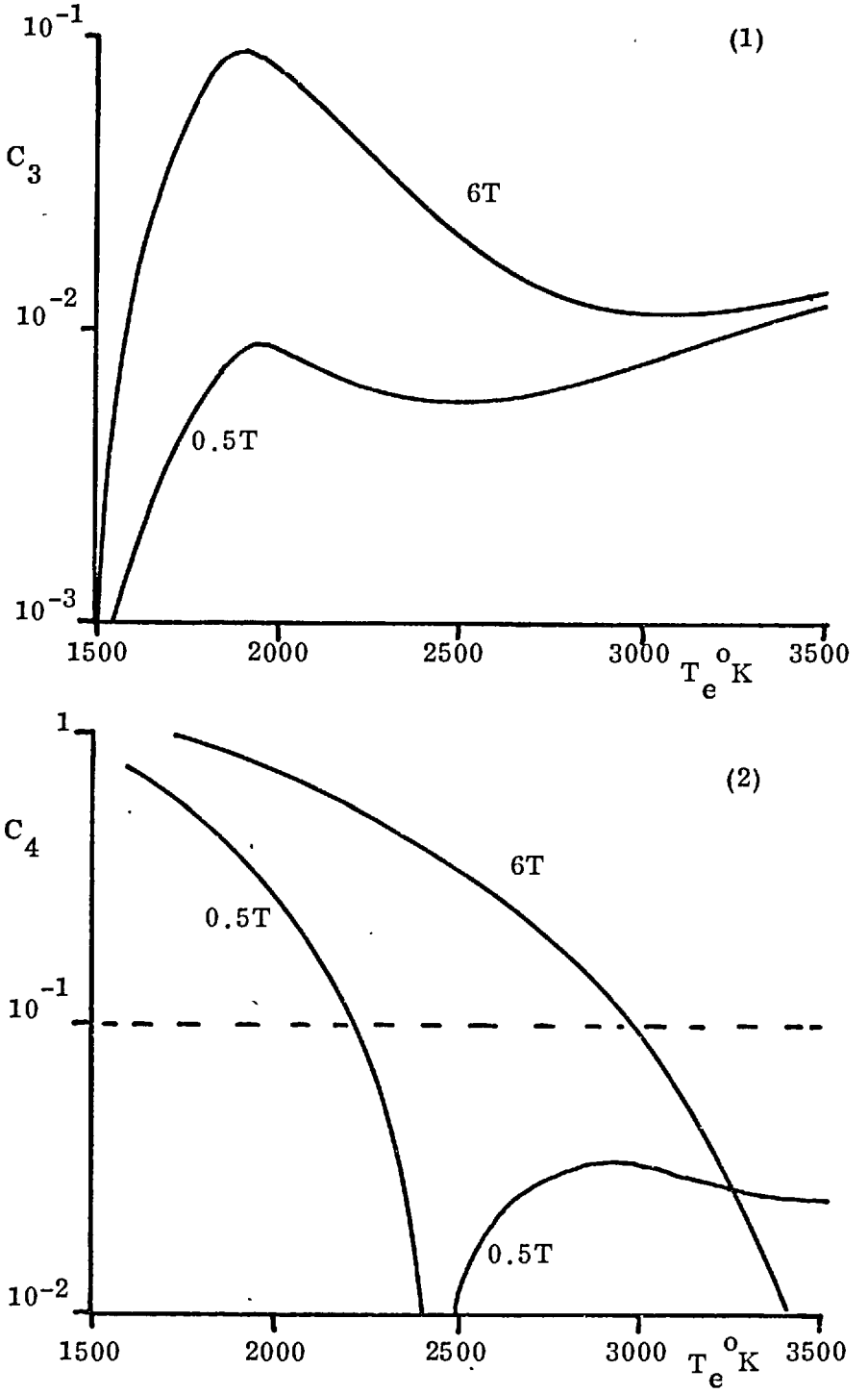

(1) Figure 6.3: C_3 against T_e for B = 6T and 0.5T

(2) Figure 6.4: C_4 against T_e for B = 6T and 0.5T

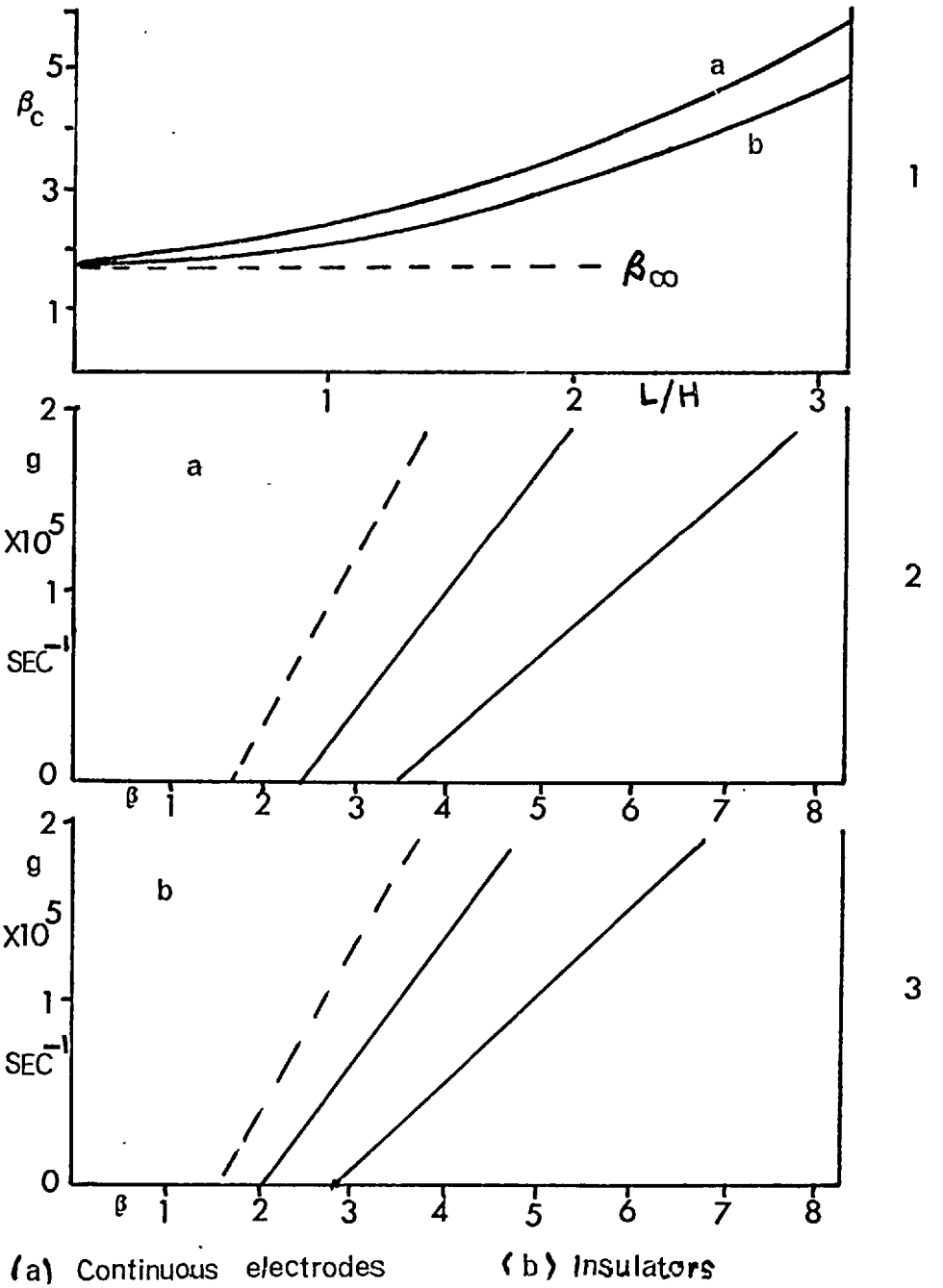

(1) Figure 6.5: β_{crit} against L/H for (a) electrode boundaries; (b) insulator boundaries.

(2) Figure 6.6: Linear growth rates for electrode boundaries. The lines from left to right are for L/H = 0, 1, 2 respectively.

(3) Figure 6.7: Linear growth rates for insulator boundaries. The lines are for L/H = 0, 1, 2 as above.

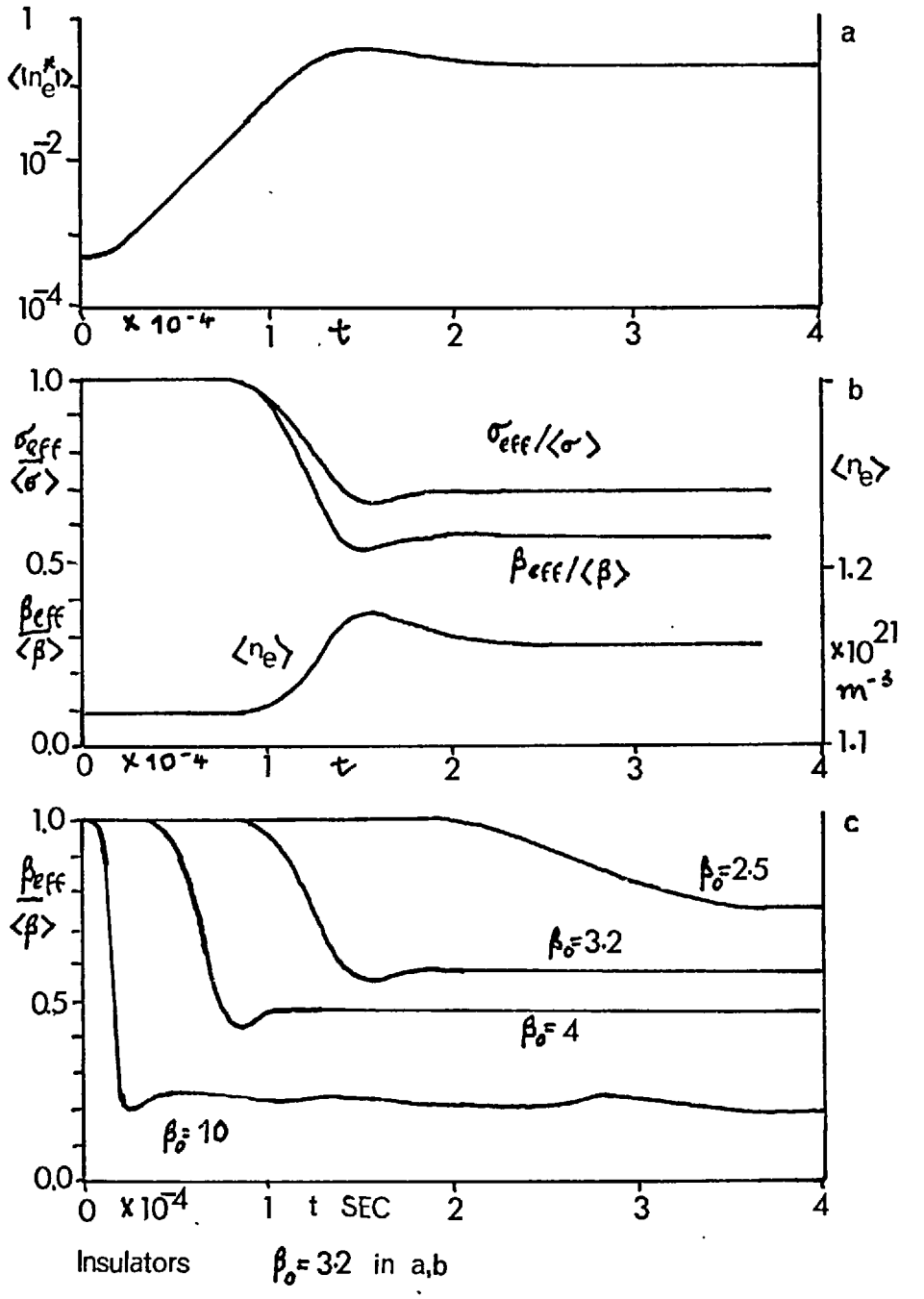

(a) Figure 6.8: Average non-uniformity against time

(b) Figure 6.9: Averaged parameters against time

(c) Figure 6.10: $\beta_{eff}/\langle\beta\rangle$ against time for several β_o

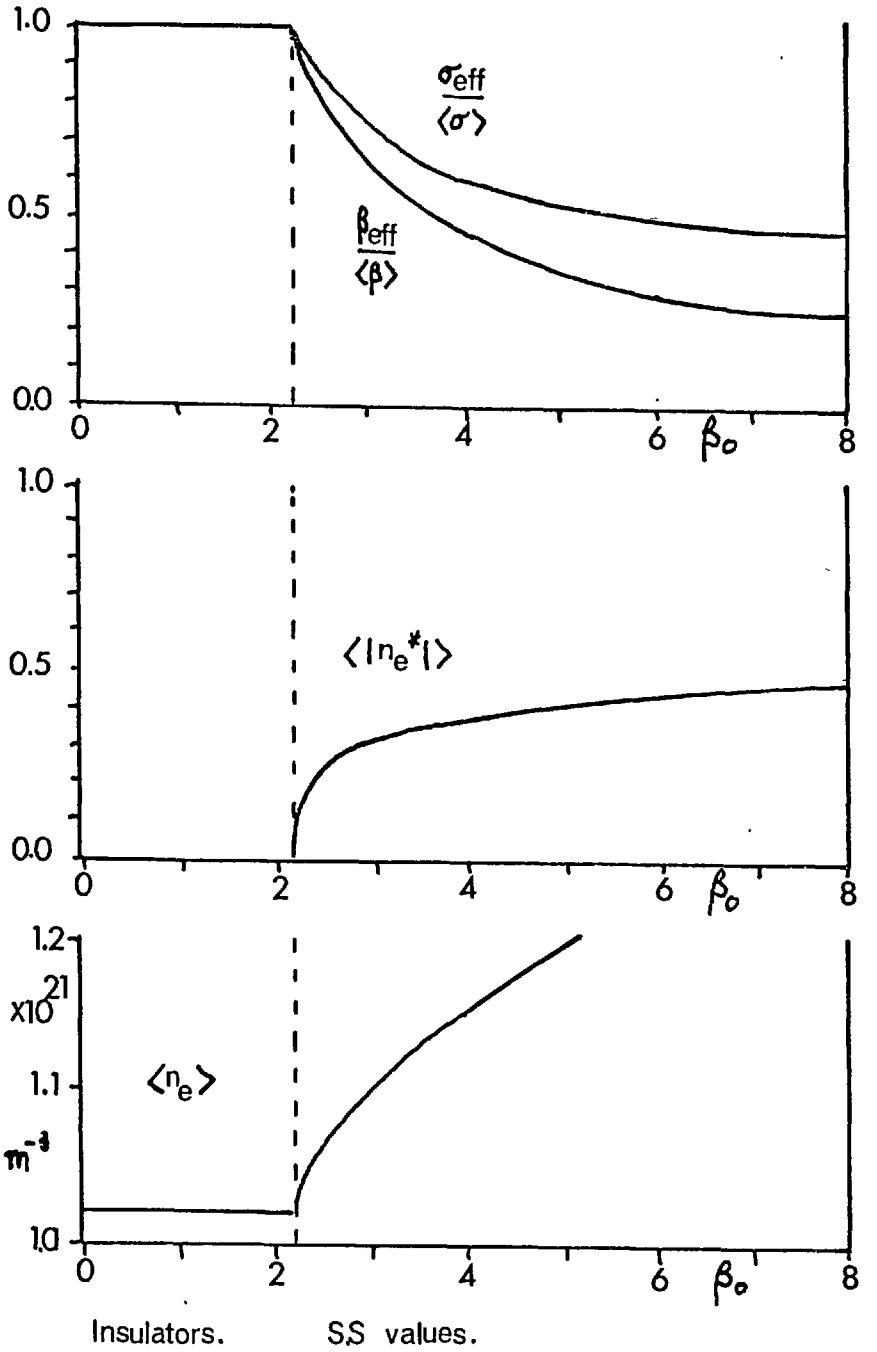

(1) Figure 6.11: $\sigma_{eff}/\langle\sigma\rangle$, $\beta_{eff}/\langle\beta\rangle$ against β_o

(2) Figure 6.12: $\langle|n_e^*|\rangle$ against β_o

(3) Figure 6.13: $\langle n_e\rangle$ against β_o

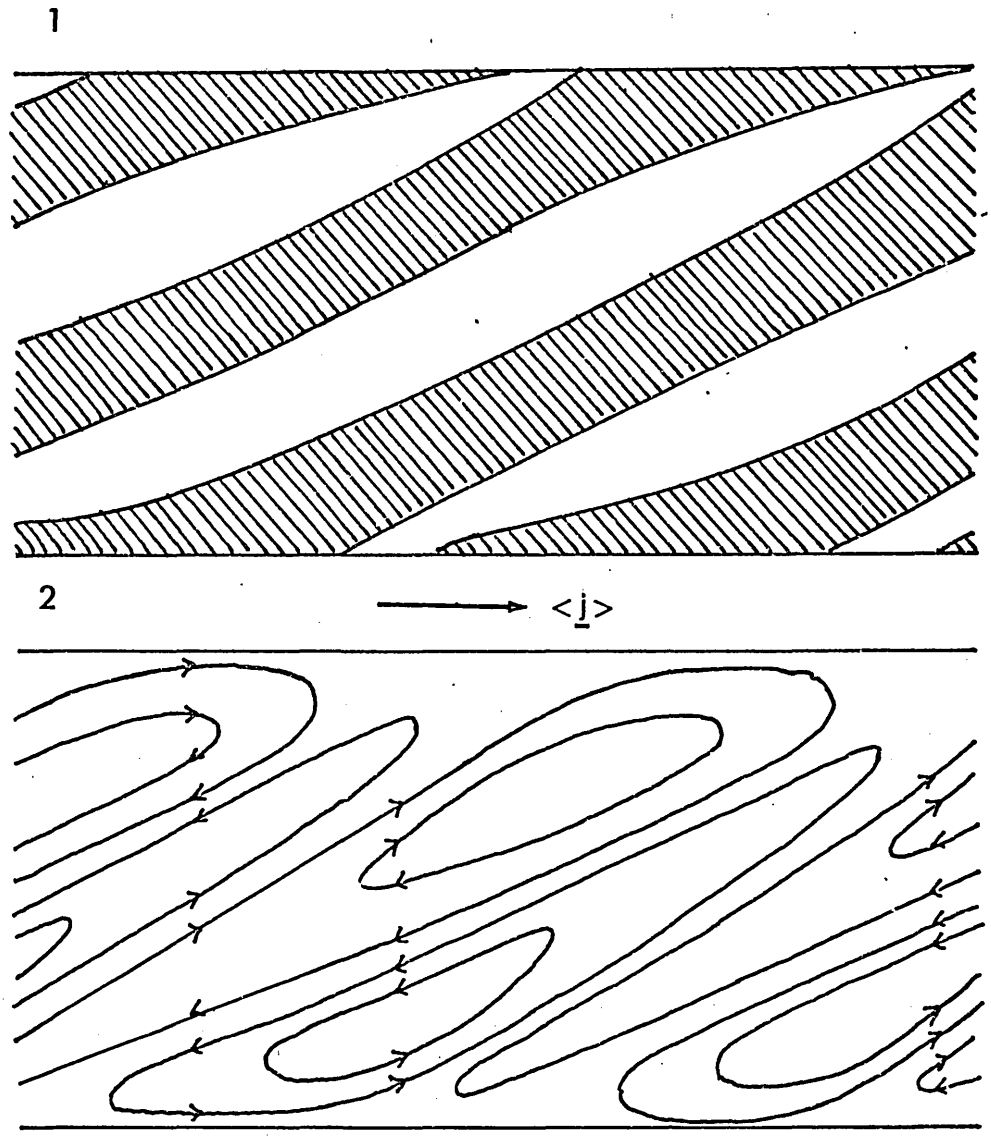

(1) n_e^*. (2) Eddy current flow in wave. $\beta = 4$ at $t=0$

(1) Figure 6.14: Distribution of n_e, shaded regions represent $n_e^* > 0$

(2) Figure 6.15: Current distribution corresponding to $\underline{j} - \langle \underline{j} \rangle$

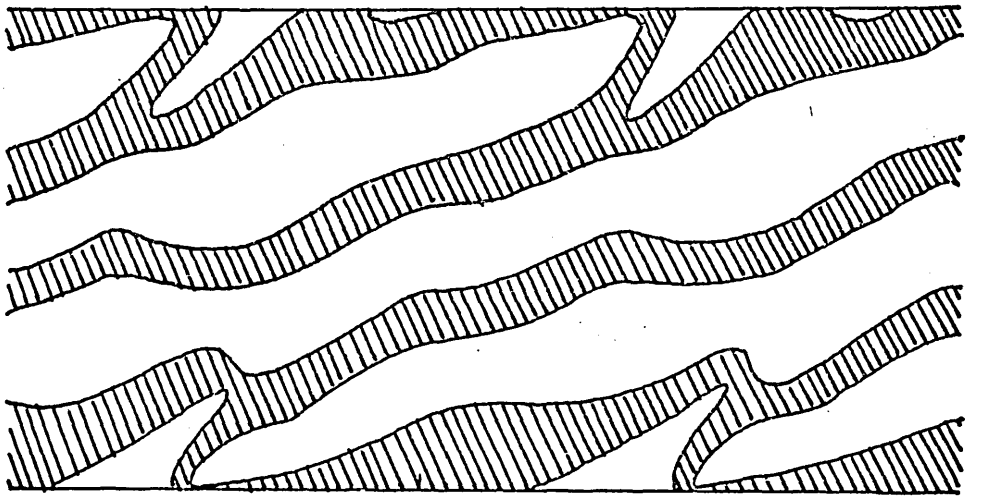

a

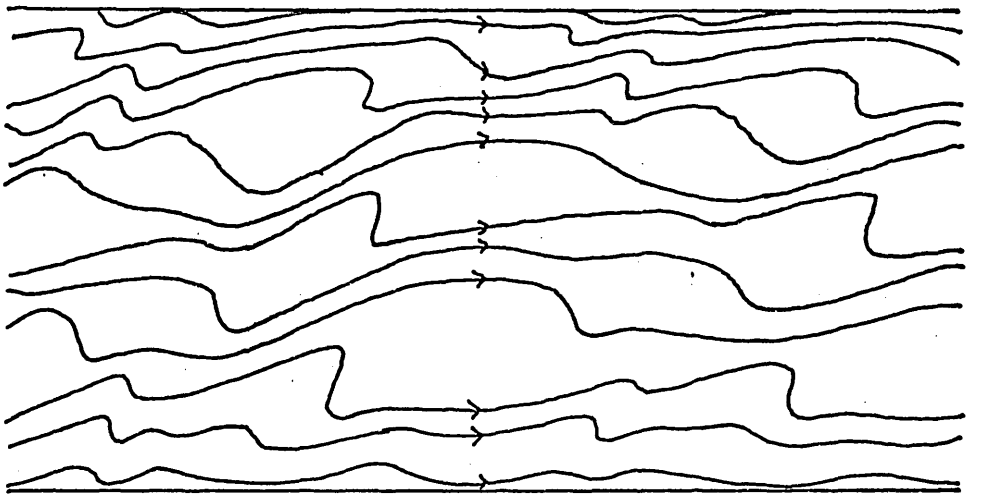

b

$t = 1.5 \times 10^{-4}$ SEC

Insulators. (a) n_e^*, (b) ψ. $\beta = 6$ at $t = 0$

(a) Figure 6.16: Density distribution for $\beta_o \approx 3\,\beta_{crit}$

(b) Figure 6.17: Current stream function ψ for above case

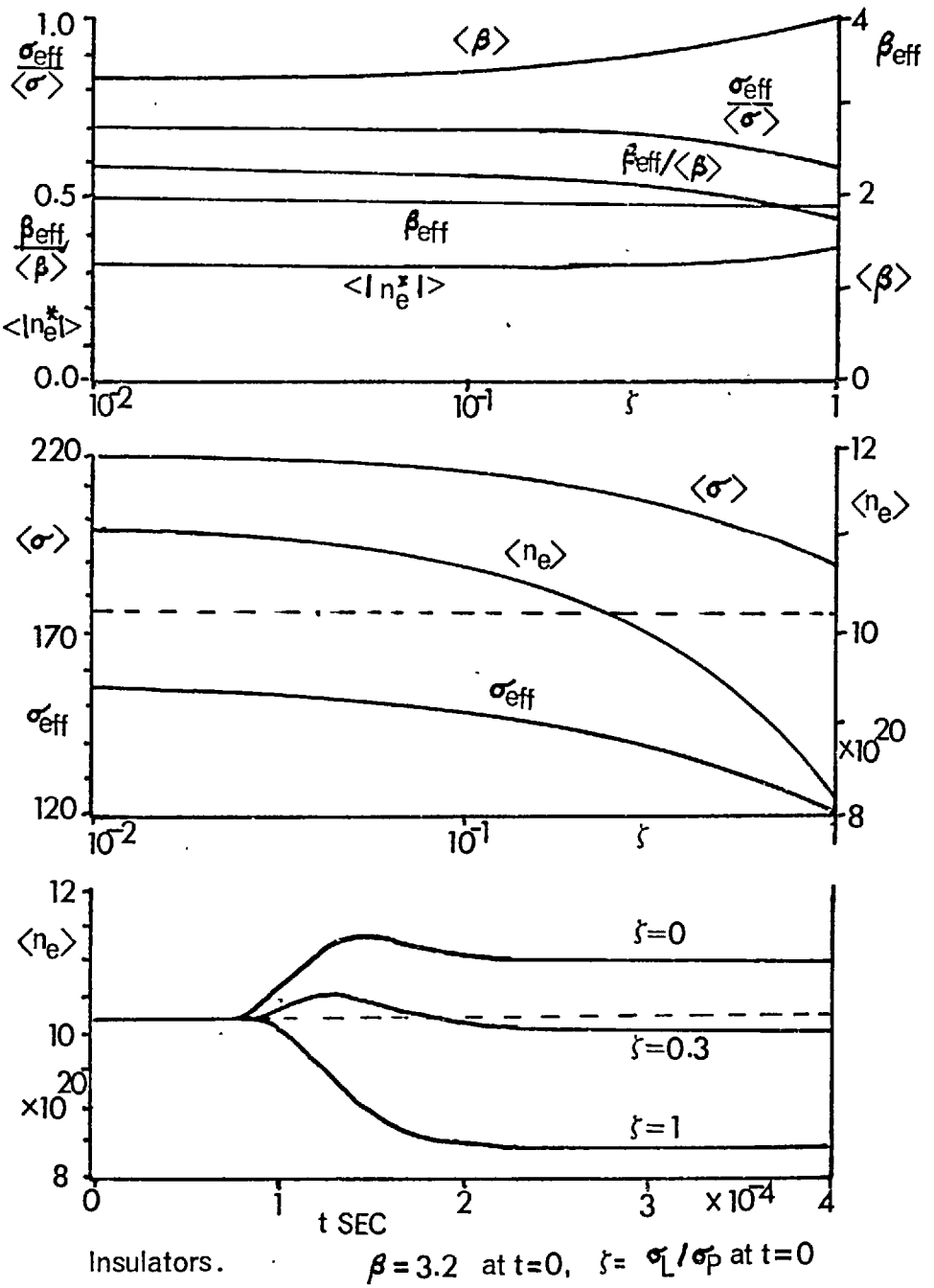

Insulators. $\beta = 3.2$ at t=0, $\zeta = \sigma_L/\sigma_P$ at t=0

(1) Figure 6.18: Averaged parameters against ζ . All units MKS

(2) Figure 6.19: As above

(3) Figure 6.20: Temporal development of average density (m^{-3}) for several ζ

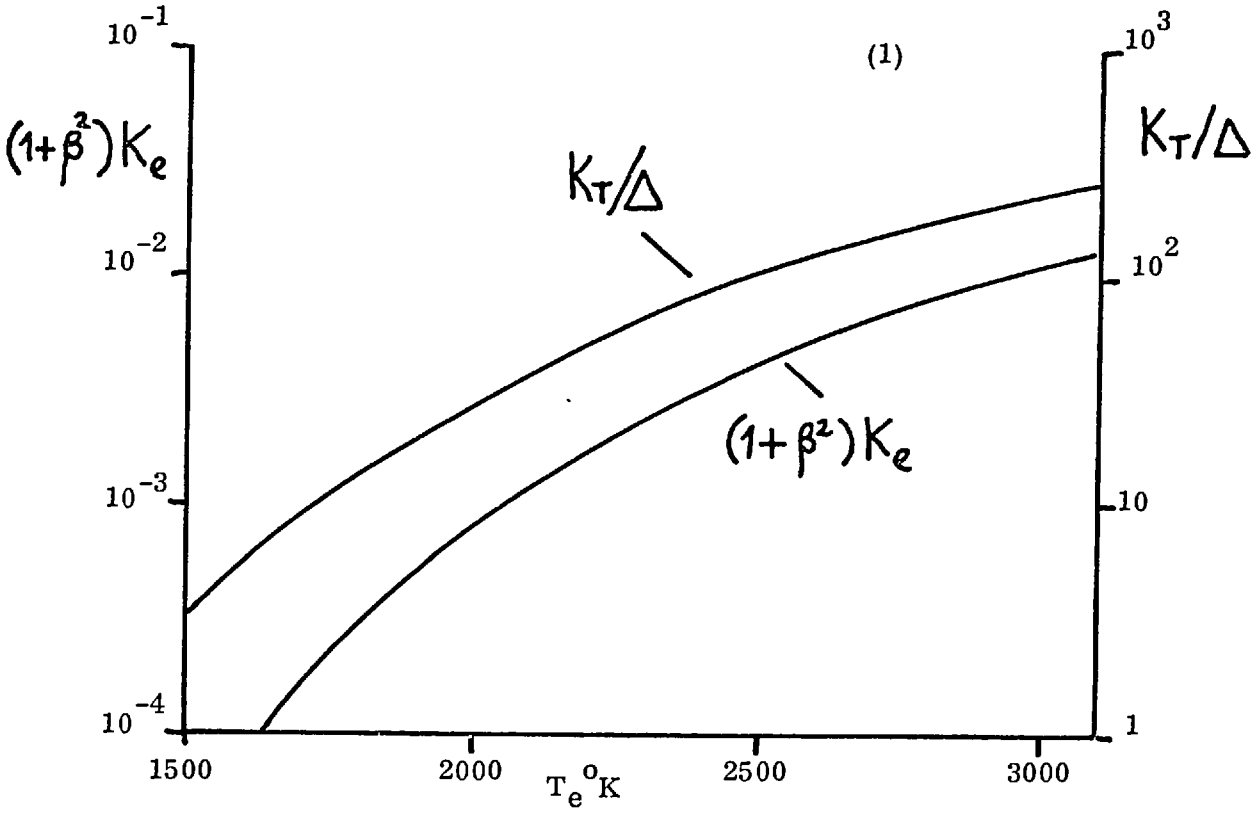

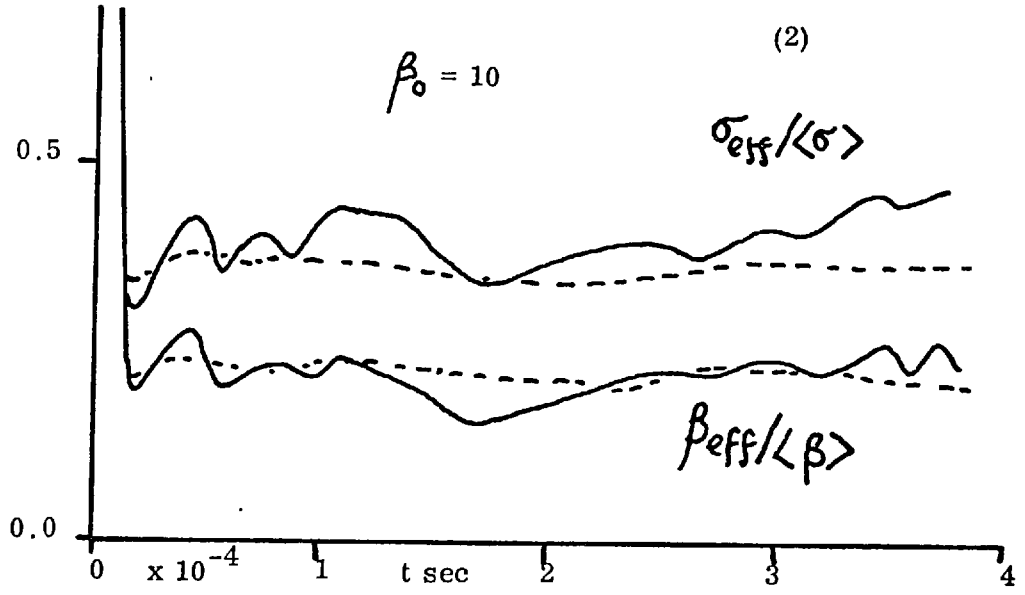

(1) Figure 6.21: k_T/Δ and $(1+\beta^2)\,k_e$ against T_e

(2) Figure 6.22: $\sigma_{eff}/\langle\sigma\rangle$, $\beta_{eff}/\langle\beta\rangle$ against time with radiation conduction -----, and without _____ for $\beta_o = 10$

(1)

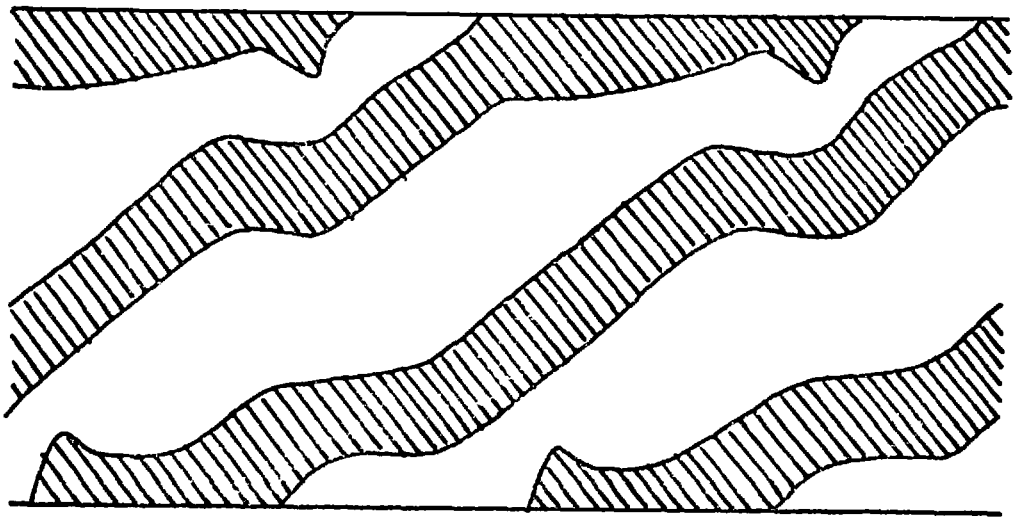

(2)

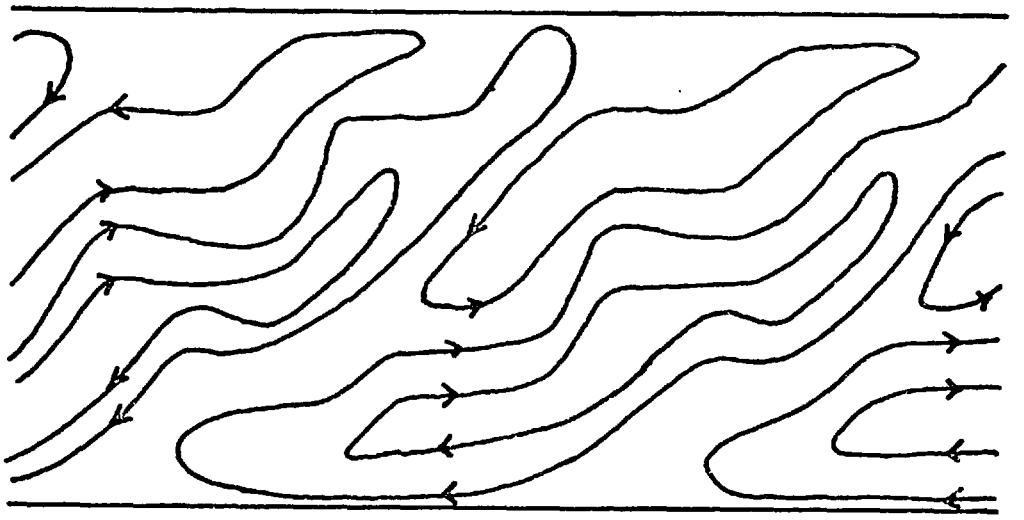

(1) Figure 6.23: Electron density distribution for $\beta_0 = 10$ in quasi-stationary state and with radiation "conductivity". (13 x 13) mesh.

(2) Figure 6.24: Eddy current flow corresponding to the above case.

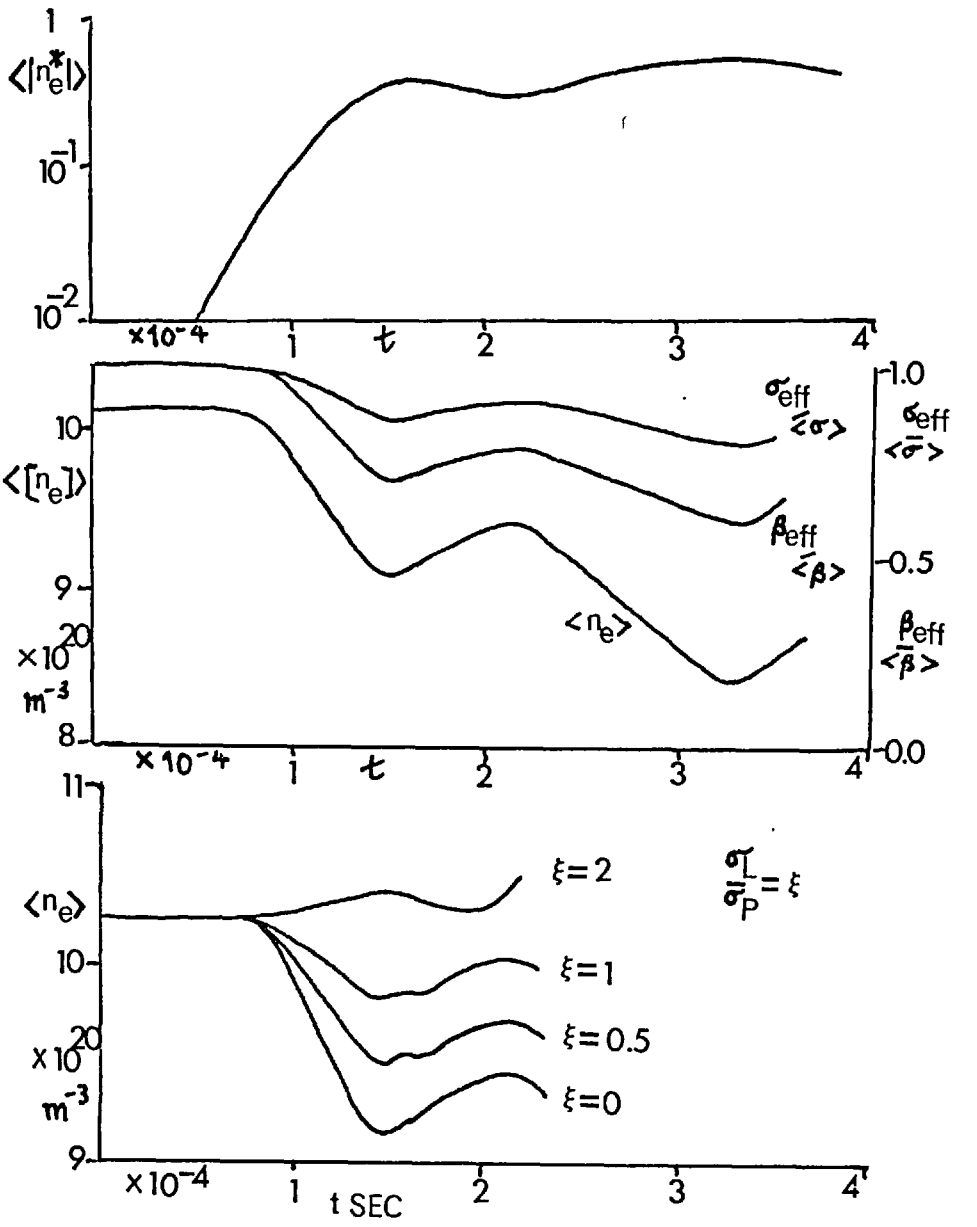

(1)

(2)

(3)

Continuous electrodes $\beta = 3.2$ at $t = 0$

(1) Figure 6.25: Average non-uniformity against time

(2) Figure 6.26: Averaged parameters against time

(3) Figure 6.27: Average density against time for several values of ξ

(1)

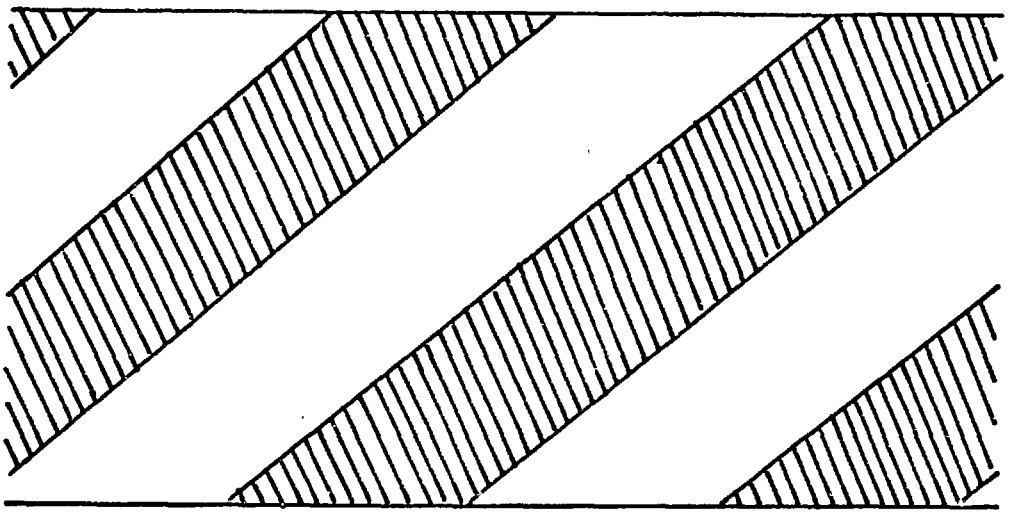

(2)

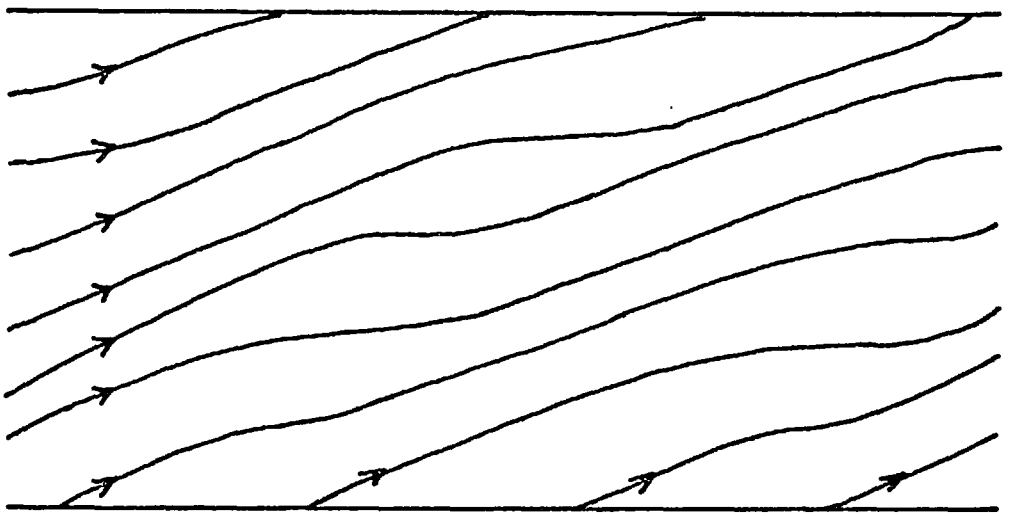

(1) Figure 6.28: Electron density distribution, n_e^*, for continuous electrodes at $\tau = 10$, $\beta_0 = 3.2$, $\sigma_L/\sigma_P \ll 1$.

(2) Figure 6.29: Current distribution ψ corresponding to above case.

(1)

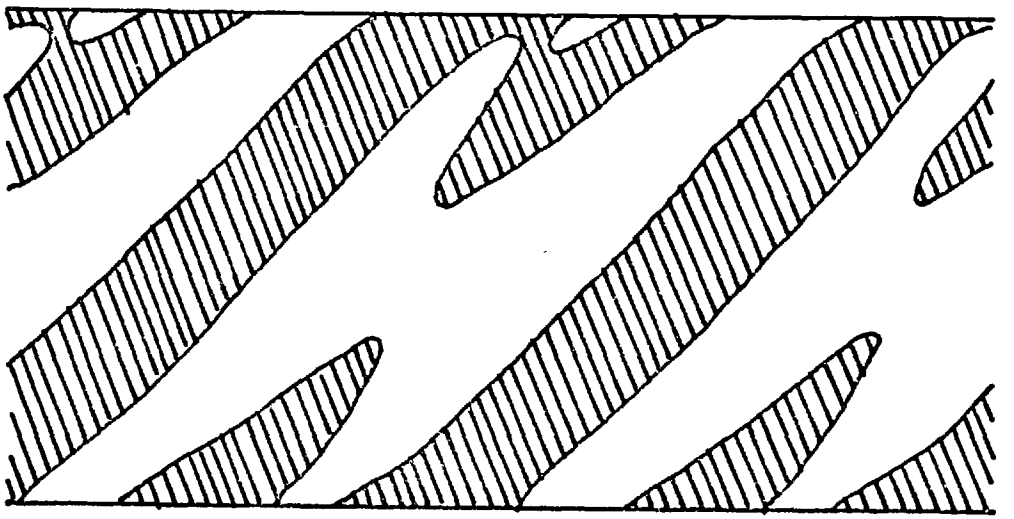

(2)

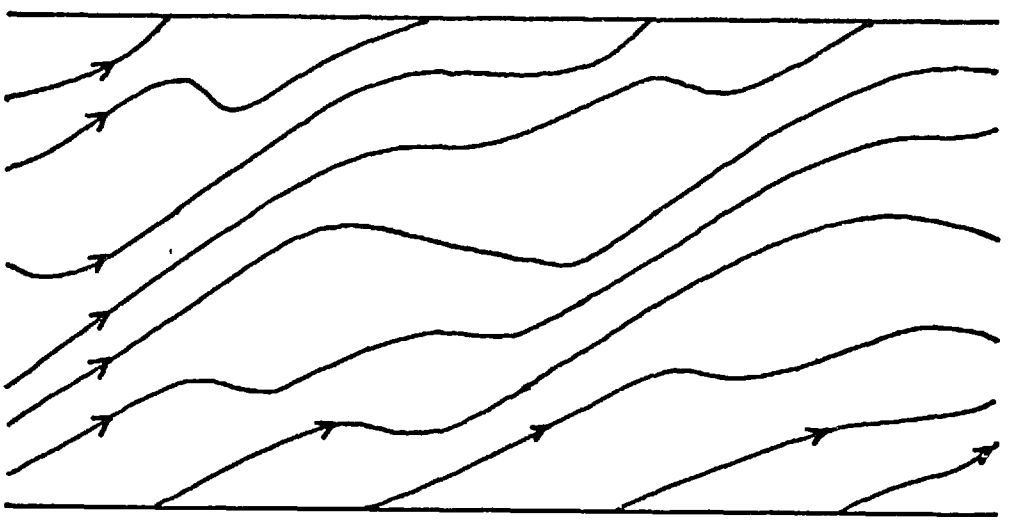

(1) Figure 6.30: Electron density distribution, n_e^*, for continuous electrodes at $\tau = 25$. $\beta_o = 3.2$, $\sigma_L/\sigma_P << 1$

(2) Figure 6.31: Current distribution ψ corresponding to above case

CHAPTER VII

CURRENT AND DENSITY DISTRIBUTIONS IN A SEGMENTED ELECTRODE GENERATOR

7.1 Introduction

The presence of the Hall effect in segmented electrode generators leads to non-uniform current flow. The one-dimensional theory of this configuration, in which j_x = constant and $j_y = 0$, assumes the ideal case of infinitely segmented electrodes. In practice, the electrodes have finite dimensions and a two-dimensional theory must be applied.

In an open cycle generator the non-uniform current flow leads to an increased impedance of the device compared with one-dimensional theory. The plasma parameters are otherwise unaffected by this non-uniformity, and the current flow is determined by $\nabla^2\psi = 0$. Analytic solutions to this problem have been obtained by Hurwitz et al (1961), Witalis (1965) and Haines (1967). Numerical solutions have been provided by Crown (1961) and Celinski et al (1966). The main feature of these analyses is the prediction of large current concentrations occurring on the downstream edge of the cathode, and the upstream edge of the anode of a given electrode pair.

In the closed cycle generator the non-uniform current flow and Ohmic heating lead to non-uniformities in the plasma parameters. The determination of the electron density and current profiles therefore requires the solution of equations (2.1)-(2.8) as discussed in Chapter V. Numerical solutions have been obtained in the stable regime, $\beta < \beta_{crit}$, by Lengyel (1969, 1971), Kim (1969) and Oliver et al (1966). The latter two references use the approximations outlined in Chapter II, section 2.4(e), and Lengyel retains only those spatial gradient terms in the electron energy equation which depend on heavy particle motion. Similar calculations have been reported by Argyropoulos (1967, 1969) at large β and assuming steady state, again only those spatial gradient terms depending on heavy particle motion were considered in the energy equation.

In this Chapter the temporal developments of the current and density distributions in a segmented electrode duct are followed. The current distribution is solved consistently with the external conditions of the problem; Saha equilibrium is assumed, and a complete electron energy equation including thermal conduction and radiation transport, as discussed in Chapter VI, is solved.

The method of solution is as follows: for $t < 0$ the plasma is assumed to be uniform with $T_e = 3000^{o}K$, $T = 1500^{o}K$ and $n_e = S(T_e)$ everywhere. This state is considered to be maintained by a uniform discharge along the duct. At $t = 0$ this discharge is removed, and external voltage sources applied to each electrode pair activated. The voltage sources are chosen to provide an average current density approximately equal to that sustaining the original non-equilibrium state.

The load resistance is taken to be much greater than the plasma resistance, in order that the ensuing changes in plasma resistance do not perturb the average heating greatly. The relaxation of the plasma to a state consistent with the external circuitry, and its own non-uniformity, is then followed numerically.

In section 7.2 the uniform segmented electrode generator is briefly discussed as a basis for comparison with the non-equilibrium generator, and previous theoretical work, and the remaining sections are concerned with the non-equilibrium distributions.

7.2 The Uniform Generator

In this case the current distribution is defined by equation (5.6) with P = Q = R = 0, ie: $\nabla^2\psi = 0$, together with the boundary conditions specified in Chapter V, section 5.7(b). The geometry of the system is shown in figure 5.2. Since the total current flow in the axial 'y' direction is constrained to be zero between neighbouring electrode pairs, σ_{eff} and β_{eff} are defined here according to

$$\sigma_{eff} = H/R_p WL$$

and

$$\beta_{eff} = H\langle E_y\rangle/IR_p$$

where $IR_p = v_s + vBH - IR_L$, and $\langle E_y\rangle$ is obtained by integration of the Ohms law.

(a) Effective Conductivity and Hall Parameter

Plots of σ_{eff} and β_{eff} for the uniform generator are shown in figures 7.1 and 7.2 respectively. For each plot the ratio of electrode length to insulator length for a given periodic segment, c/s, is maintained

at 3.7, and the values of σ_{eff}, β_{eff} are shown for various L/H values. It is seen that the ideal values are only approached for L/H<< 1. These results are in quantitative agreement with those of Celinski et al.

(b) Electrode Leakage

The occurrence of electrode-electrode current leakage along the insulator walls separating electrodes has been discussed by Witalis (1965) in the limit L/H << 1, and in the general case by Haines (1967). The critical Hall parameter for onset of the leakage, as obtained numerically, is shown in figure 7.3 as a function of L/H. The critical value of β for leakage in the limit L/H→ 0 is in agreement with Witalis's formula $\beta = \tan[\pi s/2c]$. The presence of leakage currents is found to have a negligible effect on the development of σ_{eff} and β_{eff} with β, in the uniform case, and the current constitutes less than 1% of the total current flow.

Figure 7.4 shows the distribution of current density on the cathode for c/s = 3.7, L/H = 0.64 and β = 1.0, 4.5 and 9.0. The current concentration on the electrode edge increases with β, and for β greater than the critical value for leakage, the area of cathode carrying leakage current increases with the increasing β. For β = 9.0 the leakage current density at the cathode is of the order of 10^{-3} in the same units as those used in figure 7.4. For fixed L/H, σ_{eff} and β_{eff} are weak functions of c/s, although they exhibit maxima for c/s ~ 1, for $\beta > 1$, in accordance with Witalis's results.

Finally, comparisons of results obtained using the boundary conditions given by equations (5.10) and (5.12) are in good agreement, values of σ_{eff} agreeing to 1% for $\beta < 3$. Larger values of β lead to excessive mesh uncoupling for the second order method, which has undesirable consequences for the complete non-equilibrium solutions.

7.3 Effect of Non-Equilibrium on Conduction

In this section the following parameters are used: H = 5 cm, W = 10 cm, L = 3.2 cm, c/s = 3.7, R_L = 100 Ohms, and v = 0. The system is periodic over the length L and a (15 x 23) mesh is used. The external voltage is variable, depending on the magnitude of the initially uniform β, but is of the order of 10^4 volts; most of this voltage is dropped across R_L. The initial distribution of ψ at t = 0 satisfies $\nabla^2\psi = 0$, and the Ohmic heating at each point initiates changes in n_e and T_e which in turn alter ψ. In this way the segmentation of the device effectively acts as the initial perturbation applied in Chapter VI. The initial uniform Hall parameter, β_o, is determined by the applied magnetic field, and in general the final averaged Hall parameter is somewhat different from this.

(a) Temporal Behaviour of Averaged Parameters

Figures 7.5-7.8 show the development of β_{eff}, $\beta_{eff}/\langle\beta\rangle$ and $\sigma_{eff}/\langle\sigma\rangle$ with time for initial values of the Hall parameter, β_o, of 1.0, 2.0, 4.5 and 9.0 respectively. $\langle\beta\rangle$ and $\langle\sigma\rangle$ are functions of time also, of course, and β_{eff} at t = 0 is much less than β_o due to finite segmentation effects. The main features of the temporal development are summarised below.

(i) The solutions saturate with time for $\beta_0 \lesssim 2$. The time required to reach saturation is approximately 10^{-4} sec.

(ii) For $0 < \beta_0 \lesssim 0.3$ β_{eff}, $\beta_{eff}/\langle\beta\rangle$ initially decrease with time and $\sigma_{eff}/\langle\sigma\rangle$ initially increases until saturation is reached.

(iii) For $0.3 < \beta_0 \lesssim 1.6$ β_{eff}, $\beta_{eff}/\langle\beta\rangle$ and $\sigma_{eff}/\langle\sigma\rangle$ decrease with time until saturation, as in figure 7.5.

(iv) For $2 \gtrsim \beta_0 > 1.6$ β_{eff}, $\beta_{eff}/\langle\beta\rangle$ decrease with time until saturation. $\sigma_{eff}/\langle\sigma\rangle$ initially decreases with time, experiences a minimum and then undergoes a period of adjustment, as in figure 7.6, until saturation.

(v) For $\beta_0 > 2$ small amplitude oscillations occur in the solutions, as is shown in figures 7.7 and 7.8. The fractional amplitudes of the oscillations vary from approximately 1% to 15% as β_0 varies from 3.5 to 9.0, and the periods vary from approximately 10^{-4} sec to 3×10^{-5} sec over the same range.

(vi) For $\beta_0 \gtrsim 2.5$, β_{eff} and $\beta_{eff}/\langle\beta\rangle$ have final quasi-steady values which are less than their initial values; in this case $\sigma_{eff}/\langle\sigma\rangle$ initially decreases with time, reaches a minimum, and finally achieves a quasi-steady state which exceeds the initial value. The time for which $\sigma_{eff}/\langle\sigma\rangle$ reaches its first minimum varies from approximately 3×10^{-6} sec to 1×10^{-6} sec as β_0 varies from 3.5 to 9.0. The time requires to reach the first maximum varies from approximately 9×10^{-5} sec to 2×10^{-5} sec as β_0 varies from 3.5 to 9.0.

(b) Quasi-Steady State

The results shown in figures 7.9-7.13 represent the final averaged parameters obtained in the calculations as functions of $\langle\beta\rangle$, the averaged Hall parameter for the final solutions. For $\beta_o > 2$ the time averaged values of the space averaged parameters are plotted.

The variation of β_{eff} with $\langle\beta\rangle$ is shown in figure 7.9; also shown are the curves representing the uniform segmented generator, and the ideal one-dimensional generator for which $\beta_{eff} = \langle\beta\rangle$. For the uniform generator $\beta = \langle\beta\rangle$ = constant, $\sigma = \langle\sigma\rangle$ = constant within the plasma, and β_{eff} is much less than $\langle\beta\rangle$ at large $\langle\beta\rangle$ due to finite segmentation effects. The non-equilibrium generator always possesses a lower β_{eff} than the uniform generator. A maximum value for β_{eff} is attained at $\langle\beta\rangle = 1.8$, β_{eff} then decreases somewhat over the range $2 < \langle\beta\rangle < 10$. This result is similar to the result $\beta_{eff} \approx \beta_{crit}$ for $\langle\beta\rangle > \beta_{crit}$ obtained for the insulator wall configuration in Chapter VI.

The corresponding values of $\sigma_{eff}/\langle\sigma\rangle$ are shown in figure 7.10. For $0.3 \lesssim \langle\beta\rangle \lesssim 2.5$ the system demonstrates the expected result that the non-equilibrium generator possesses lower values of $\sigma_{eff}/\langle\sigma\rangle$ than the uniform generator. For $\langle\beta\rangle \gtrsim 2.5$ and $\langle\beta\rangle \lesssim 0.3$ the reverse is true. At $\langle\beta\rangle = 10$. for example, $\sigma_{eff}/\langle\sigma\rangle$ for the non-equilibrium generator is approximately twice that of the uniform generator. This new and important result may be of use in the optimization of non-equilibrium, high Hall parameter generator ducts.

The averaged plasma non-uniformity $\langle|n_e^*|\rangle$, as defined in Chapter VI, section 6.4, is shown in figure 7.11. The non-uniformities result from segmentation effects, and instabilities when present. The values of $\langle|n_e^*|\rangle$ are therefore larger than those obtained in Chapter VI.

For reference the values of $\beta_{eff}/\langle\beta\rangle$ and β_o as functions of $\langle\beta\rangle$ are shown in figure 7.12; β_o against $\langle\beta\rangle$ expresses the uniform Hall parameter at t = 0 for a particular simulation, as a function of the averaged Hall parameter at the end of the simulation. $\langle\sigma\rangle$, $\langle n_e\rangle$ and σ_{eff} as functions of $\langle\beta\rangle$ are shown in figure 7.13; $\langle\sigma\rangle$ and $\langle n_e\rangle$ increase with $\langle\beta\rangle$, whilst σ_{eff} decreases. The values of $\langle\sigma\rangle$, $\langle n_e\rangle$ and $\langle\beta\rangle$ depend, of course, on the applied voltage, and for this reason the fractional effective values, $\sigma_{eff}/\langle\sigma\rangle$ for example, are a more useful indication of the effects of segmentation and instabilities.

The current and density distributions, as they are at the end of the previously described calculations, are shown for various $\langle\beta\rangle$ in figures 7.15-7.19. For comparison the current distributions pertaining to the uniform plasma generator at β = 1.0 and β = 9.0 are shown in figure 7.14 a and b.

Figure 7.15 a and b shows the lines n_e^* = constant and ψ = constant for β_o = 1.0. The value of n_e^* on a contour numbered 'a' is given by

$$n_e^* = (a - 0.05)(n_{e\,max}^* - n_{e\,min}^*) + n_{e\,min}^*$$

A similar relationship applies for the ψ contours, although it is only the orientation and relative separation of the contours, representing the direction of current flow and current density respectively, which are of significance. Similarly, figures 7.16-7.19 show the distributions for β_o = 2, 3.5, 6.5 and 9.0 respectively. For $\beta_o > 2$ the maximum n_e^* contour is taken to be n_e^* = 2.5, and regions of greater density are hatched.

The current distributions have the following main features.

(i) The current concentrations at the electrode edges increase with increasing Hall effect, ie: $\langle\beta\rangle$.

(ii) The direction of current flow in the duct centre, ie: the region directly between opposite electrodes, becomes more axial with increasing $\langle\beta\rangle$, and more transverse between opposite insulators.

(iii) The distributions show an asymmetry between cathode and anode conduction which increases with $\langle\beta\rangle$.

(iv) For $\beta_o \geq 2$ the main current flow exists in the form of streamers which flow in the transverse 'x' direction in the regions of greatest current density between oppositely situation insulators. The streamers become more pronounced with increasing $\langle\beta\rangle$.

(v) With increasing $\langle\beta\rangle$ the current lines in the duct follow more complicated paths.

The main features of the density distribution are summarized below.

(i) The strongest gradients in electron density occur at the current concentration points on the electrode edges. The density at these points increases with $\langle\beta\rangle$, and the seed achieves 99% ionization for $\beta_o = 9.0$ at the edges. These regions are extremely stable in the sense that n_e is relatively insensitive to T_e, regardless of the value of the local Hall parameter.

(ii) The electron density in the duct centre, the region between electrodes, decreases with increasing $\langle\beta\rangle$.

(iii) The electron density at the anode is rather more uniform than that at the cathode. The concentration point is hotter on the cathode than the anode. The asymmetry increases with $\langle\beta\rangle$.

(iv) For $\beta_0 \gtrsim 2$ the regions of highest density exist in the form of filaments. The filaments extend from the region of current concentration on the cathode to the region of concentration on the anode of the neighbouring electrode pair. The density in the filaments increases with $\langle\beta\rangle$.

(v) Striations exist in the duct centre for $\beta_0 \gtrsim 2$. The alignment of the striations with respect to the local current flow is similar to that expected for electrothermal instabilities.

Electrode leakage currents occur for the uniform plasma when $\beta_0 > 1.1$; in the final non-equilibrium state these currents are not present

The density distribution along the centre axis of the duct, the line x = H/2, is shown in figure 7.20 for several values of β_0. The non-uniformity increases with $\langle\beta\rangle$.

(c) Discussion of Results

The above results demonstrate that the behaviour of the non-equilibrium plasma can be discussed in terms of the two regimes $\beta_0 < \beta_{crit}$ and $\beta_0 > \beta_{crit}$. An estimate of β_{crit} is difficult to make for the above geometry, owing to the effects of finite segmentation; however, the preceeding discussions would indicate that β_{crit} lies between 1.6 and 2.5, ie: approximately 2.

For $\beta_0 < \beta_{crit}$ the plasma relaxes to a non-uniform stationary state. That this state is achieved in approximately 10^{-4} sec, for all $\beta_0 < \beta_{crit}$, indicates that the relaxation is determined by the average heating rather than localized non-uniformities.

Increasing β_0 leads to an increase in the current concentration at the electrodes; the current available for the remaining area of an electrode is diminished, and this leads to reduced heating and low ionization over the bulk of the electrode. This effect produces low density, high resistance regions close to the electrodes, which tends to 'expel' the current lines from these regions.

The local Hall parameter can deviate markedly from the average value, and in the low density regions can satisfy $\beta > \beta_{crit}$ although $\langle\beta\rangle < \beta_{crit}$. This is found not to affect the overall stability of the system, and it appears that $\langle\beta\rangle$ is a better guide to the stability. The local Hall parameter in the regions of electrode current concentration can become much less than $\langle\beta\rangle$, for example, for $\beta_0 = 2$, $\langle\beta\rangle \approx 2$, β in these regions is approximately 0.6; for this reason the axial component of current flow at the electrodes for these points is much reduced compared with the uniform generator. This follows from the condition $E_y = 0$ at the electrodes, which leads to the boundary constraint $j_y = \beta j_x$ when thermal diffusion is neglected.

The asymmetry which is present in the distributions between anode and cathode conduction can be understood qualitatively in terms of electron thermal diffusion in the Ohms law, and electron compression in the energy equation. Evaluation of the Ohmic heating on the electrodes

gives

$$\frac{j^2}{\sigma} \approx \frac{j_x^2}{\sigma}(1+\beta^2) + \sigma\frac{k_B^2 T_e^2}{e^2}\left(\frac{\partial \ln n_e}{\partial y}\right)^2 + 2\beta\frac{k_B T_e}{e} j_x \frac{\partial \ln n_e}{\partial y}$$

for $\nabla \ln n_e \gg \nabla \ln T_e$. On the cathode $j_x > 0, \frac{\partial \ln n_e}{\partial y} > 0$, whilst on the anode $j_x > 0$, $\frac{\partial \ln n_e}{\partial y} < 0$. Thus, the current concentration region on the cathode tends to become hotter, and more conducting than that of the anode. For this reason, the current distribution is rather more uniform on the anode, it is carrying less current at the hot edge. Writing the energy equation explicitly for the first order gradient terms and using the above value for the heating one obtains,

$$\partial \epsilon_e / \partial t \approx \frac{k_B T_e}{e} j_x \left[\beta \partial \ln n_e / \partial y - \partial \ln n_e / \partial x\right] + \cdots$$

for $\nabla \ln n_e \gg \nabla \ln T_e$. At early times the cathode current concentration edge heats more rapidly, the effect increasing with β_0. A similar asymmetry has been observed in the experiments of Zauderer (1966).

The above effects are accentuated with increasing β_0, and for $\beta_0 > \beta_{crit}$ new phenomena are present. Electrothermal instabilities and current streamers occur. Since the current streamers develop rapidly with β_0 for $\beta_0 > \beta_{crit}$, it can be concluded that they are electrothermal instabilities which are initially derived from segmentation induced non-uniformities.

The current streamers represent a part of the total current flow of neighbouring electrode pairs. An individual current streamline leaves the anode and, in general, passes through the relatively resistive plasma in the duct centre before joining the streamer. Having reached the streamer, it then flows along the region of high electron density to join the cathode.

The streamers have an important influence on the average properties of the system. For $\langle\beta\rangle \gtrsim 2.5$ $\sigma_{eff}/\langle\sigma\rangle$ rises above the uniform plasma generator value; this is due to the presence of the streamers. The non-uniformities cause the flow to be much more one-dimensional, and transverse, than it would be in their absence. The high density, high conductivity plasma in the streamer provides a low resistance path between electrodes. Moreover, because this effect becomes more pronounced with increasing $\langle\beta\rangle$ the resistance of the device becomes less sensitive to $\langle\beta\rangle$ than the uniform plasma generator.

It is seen from the plots of the averaged parameters against time that the behaviour of these quantities is similar for all $\beta_0 > \beta_{crit}$. The sequence of events within the plasma can be understood in the following way. At t = 0 the voltage source supplies a power I^2R_p per segment to the plasma, where R_p is the resistance of the uniform plasma generator. This is, in general, greater than the power required to maintain the uniform plasma; at t = 0 the net power supplied to the electrons is

$$\langle j^2/\sigma\rangle - \langle L\rangle = I^2R_p/WHL - j_0^2/\sigma_0$$

where j_0 is the current density required to maintain the uniform discharge for $t < 0$, and $I \approx j_0 wL$ from $R_L >> R_p$. This gives the net power gain to electrons at t = 0 as approximately $\frac{j_0^2}{\sigma_0}\left[\frac{\sigma_0}{\sigma_{eff}} - 1\right] > 0$, since $\sigma_{eff} < \sigma_0$ for the uniform generator from figure 7.1. The plasma therefore heats, regardless of the configuration. While the overall heating is occurring, non-uniformities occur in the electron density

around the current concentration points, this process is very rapid owing to the large current densities at these points. The presence of localized boundary non-uniformities affects the behaviour of the current flow in the duct and leads to a reduction in $\sigma_{eff}/\langle\sigma\rangle$. Non-uniformities in the plasma centre develop more slowly, as determined by the applied power and the local current density, until streamers begin to grow and permit $\sigma_{eff}/\langle\sigma\rangle$ to increase; this behaviour is clearly shown in figures 7.7 and 7.8. The reduced R_p resulting from the growth of streamers therefore reduces the heating in the plasma, I^2R_p, for $R_L >> R_p$, and $\partial\langle n_e\rangle/\partial t$ decreases. When the streamer first ceases to grow, $\partial\langle n_e\rangle/\partial t$ is non-zero, the streamer adjusts to the changes and the process continues. One would therefore expect the oscillation amplitudes to increase with $\langle\beta\rangle$ since the conduction properties of the non-equilibrium generator deviate further from those of the uniform generator as $\langle\beta\rangle$ increases.

That the time required to reach the first maximum in $\sigma_{eff}/\langle\sigma\rangle$ should decrease with $\langle\beta\rangle$, and that the period of the oscillations should also decrease, is consistent with the increased power supplied to the plasma and the increased growth rates associated with electrothermal instabilities at large $\langle\beta\rangle$.

The improved conduction properties of the non-equilibrium generator for $\beta_o \lesssim 0.3$ is due to the smallness of the Hall effect. The slight current concentrations which occur on both edges of each electrode, to satisfy $\nabla \times \underline{E} = 0$, result in increased conductivity at these points for the non-equilibrium plasma.

Finally, the striations in the duct centre have small amplitudes compared with the streamers. In figures 7.18a and 7.19a the striations consist of two approximately one-dimensional density ridges lying NW, one near each electrode and separated by a density trough. Similarly, in figure 7.17a the striations consist of a single density ridge in the duct centre lying NE, banked by density troughs and terminated at its ends by streamers. The latter well-defined non-uniformity does not occur for $\beta_0 < \beta_{crit}$ and is an essential feature of the transition $\beta_0 < \beta_{crit}$ to $\beta_0 > \beta_{crit}$; one may therefore conclude that their formation is a result of this transition. The main effect of the striations is to complicate the pattern of streamlines in the duct centre. They appear in the solutions at times varying from 1.6×10^{-4} sec to 6×10^{-5} sec as β_0 varies from 3.5 to 9.0.

(d) Velocity Effects

It is of interest to see how heavy particle motion affects the previous results, because of the possibility of convection or convective diffusion of the streamers. In small scale experiments, flow velocities are typically of the order of 100-200 m sec^{-1}, and the following calculation is a repeat of the previous $\beta_0 = 3.5 > \beta_{crit}$ calculation with v = 170 m sec^{-1}.

The results can be seen in figure 7.21, which shows $\sigma_{eff}/\langle\sigma\rangle$, $\beta_{eff}/\langle\beta\rangle$ and β_{eff} as functions of time, and figure 7.22a and b, which shows n_e^* and ψ contours. The development of the averaged parameters is essentially the same as the v = 0 case. The average non-uniformity, $\langle |n_e^*| \rangle$, is approximately 0.5 in this case compared with 0.6 for v = 0.

The effect of the motion is to displace the streamer downstream, and with it the current distribution. The streamer is a more diffuse object and attains a smaller peak value with finite gas flow. The effect of the increased length and lower density of the streamer is to increase the resistance of the device compared with the v = 0 case.

In the final state leakage currents flow from cathode to cathode along the insulator wall. These constitute less than 4% of the total current flow and result from the downstream convection of highly conducting plasma from the electrode edge. They are too small in magnitude to show up on the ten contour diagram shown.

It is found that in the contrasting case of $\langle\beta\rangle < \beta_{crit}$, and for v 200 m sec^{-1}, the distributions are little affected by flow effects. Downstream displacements of the discharge over distances comparable with the discharge width require streamers, ie: large plasma gradients. For example, from figure 7.20 it is seen that the ratio of $\partial \ln n_e/\partial y$ for $\beta_o = 3.5$, to $\partial \ln n_e/\partial y$ for $\beta_o = 1.0$ is approximately 20 when maximum values for these terms are used.

(e) Effect of Reducing L/H

The above results relate to a specific duct geometry. It is of interest to see how the non-uniformities develop in a more nearly one-dimensional system. For the following calculation L/H = 0.2, c/s = 1.7, H = 5 cm, W = 10 cm, v = 0, $\beta_o = 3.5 > \beta_{crit}$, and other conditions correspond to the previous calculation.

Figure 7.23 shows β_{eff}, $\beta_{eff}/\langle\beta\rangle$ and $\sigma_{eff}/\langle\sigma\rangle$ as functions of time. The main differences from the previous case are the absence of oscillations in the solutions, and $\sigma_{eff}/\langle\sigma\rangle$ tending to saturate at a lower value than its t = 0 value.

Distributions for this case are shown in figures 7.24-7.27, contours exceeding 0.5 have been shaded for clarity. Two periodic sections are shown for the ψ distributions. At t = 0, figure 7.24, the current distribution is relatively uniform within the bulk of the plasma, the main current non-uniformities existing near the cathode and anode boundaries. At $t = 2 \times 10^{-5}$ sec, figure 7.25, electron density non-uniformities have developed close to the boundaries. The regions of highest density are at the boundaries and large leakage currents flow from cathode to cathode, much smaller ones from anode to anode, and the current is tending to flow axially in the centre of the duct. The large cathode leakage currents are probably due to thermal diffusion. At the insulators $j_x = 0$ and

$$j_y = \sigma E_y + \sigma/n_e e \cdot \partial P_e/\partial y$$

Along the cathode and anode wall insulators $\partial P_e/\partial y < 0$ and $\partial P_e/\partial y > 0$ respectively for $t > 0$. Since small leakage currents flow in the -'y' direction along the insulators at t = 0, this term will increase the flow at the cathode wall and reduce it at the anode wall. The leakage currents also depend on E_y, which will be determined by the total current flow in the duct. At $t = 5 \times 10^{-5}$ sec, figure 7.26, the non-uniformities have 'propagated' into the centre of the duct and the current flow is significantly perturbed. At $t = 1.5 \times 10^{-4}$ sec, figure 7.27, the main feature of the

density distribution is the presence of an approximately plane wave streamer, the current flow is mainly transverse in the peaks of the streamer and axial in the troughs. Leakage currents are still present but are a small fraction of the total flow.

From figure 7.27 it is seen that the effect of the boundaries on the current flow non-uniformities is only apparent within a small distance, of order L, of the boundaries. However, segmentation effects near the boundaries perturb the plasma, and for $\langle\beta\rangle > \beta_{crit}$ form the streamers which dominate the system. The orientation of the streamers is determined initially by the requirement $\underline{j} \times \underline{k} \cdot \underline{B} \approx \underline{j} \cdot \underline{k} |\underline{B}|$. In the non-linear phase the current tends to flow along the streamers. The ultimate effect of the streamers is to increase the path length, compared with the uniform plasma generator, of an individual current streamline as it passes from anode to cathode through the peaks and troughs of the non-uniformities.

The behaviour of the plasma for $\langle\beta\rangle > \beta_{crit}$ is therefore sensitive to whether L/H is of the order of, or much less than, unity. For $L/H \ll 1$ the growth of instabilities in the duct centre is similar to that expected from the infinite plasma theory; whereas for $L/H \sim 1$ the interaction between boundary and instability is dominant, and the presence of instabilities can have a mitigating effect on conduction with strong Hall effect. The absence of oscillations from the solution is a result of the reduction of $\sigma_{eff}/\langle\sigma\rangle$ with time; in this case the external circuits heat the plasma for $t \gtrsim 0$, and the growth of instabilities also heats the plasma, $I^2 R_p$ increases, so that circuit and instability effects can keep in step.

7.4 Multisegment Systems

In practice, conditions are seldom truly periodic. In this section the results of calculations will be given which demonstrate that the essential physical phenomena are not sensitive to this assumption. The conditions are H = 5 cm, W = 10 cm, L (the total length of the duct) 9.7 cm, β_o = 9.0 and v = 170 m sec^{-1}. There are four segments, each with R_L = 100 Ohms; each electrode is of length 1.4 cm and the interspacing insulators 0.6 cm in length. A (19 x 36) node mesh is used.

The current distribution at t = 5 x 10^{-5} sec is shown in figure 7.28. The calculation was not taken to its final quasi-steady state, but nevertheless demonstrates the important features of the distribution. The current flow is similar to that of the periodic β_o = 9.0 case discussed earlier, but with a downstream displacement of the streamers due to heavy particle flow. The value of L/H for the two inner electrode pairs is 0.4, and $\sigma_{eff}/\langle\sigma\rangle$ for the system at t = 5 x 10^{-5} sec is 50% greater than its t = 0 value. This improvement should also be maintained in the final state. It is apparent that streamers will be a dominant feature of non-equilibrium, low velocity, segmented electrode generators at high Hall parameter.

The results of the same calculation repeated with v = 2000 m sec^{-1} are shown in figure 7.29. In this case the distribution is dominated by convection effects. It is likely that the close proximity of the upstream and downstream 'infinities' to the first and last electrode pair, and the diffusion properties of the convective term truncation error corrupt the physical values somewhat. Nevertheless, the current distribution

does give some indication of the phenomena at large flow velocities, and the results are similar to those obtained by Argyropoulos (1969).

The downstream sweeping of the current lines is apparent. The intense streamers obtained with v = 170 m sec^{-1} are not present although some streaming does occur. For $t < 3 \times 10^{-6}$ sec the main leakage currents occur at the cathode boundary, at later times the anode boundary carries the main leakage current. It is interesting to note that $\sigma_{eff}/\langle\sigma\rangle$ for this case is less than the t = 0 value; ie: the smoothing effect of the heavy particle convection destroys the mitigating effect of the streamers.

7.5 Conclusions and Comparison with Experiment

The results presented here demonstrate that the non-equilibrium segmented electrode generator has, broadly speaking, the two regimes of operation, $\langle\beta\rangle > \beta_{crit}$ and $\langle\beta\rangle < \beta_{crit}$.

For $\langle\beta\rangle < \beta_{crit}$ a relatively uniform conduction mode is possible, the main non-uniformities occurring at the current concentration electrode edges. In particular, for $L/H \ll 1$ the main segmentation effects are restricted to boundary layers of depth roughly L.

For $\langle\beta\rangle \gg \beta_{crit}$ the current flow is dominated by the presence of streamers. The streamers are approximately one-dimensional, regardless of the order of L/H (less than or equal to unity) The effect of the streamers on the system depends on L/H. For $L/H \ll 1$ the orientation of the streamers is such that the path length of an individual current line

as it passes from anode to cathode through the peaks and troughs of non-uniformities, is increased compared with the uniform generator. The internal resistance of the non-equilibrium generator is therefore increased. For L/H~1 a current line may treat a streamer as a 'short-circuit' between anode and cathode, thereby reducing the internal impedance of the device compared with the uniform generator. For $\langle\beta\rangle > \beta_{crit}$, β_{eff} becomes insensitive to $\langle\beta\rangle$.

With heavy particle flow the streamers 'bend' downstream and become diffuse. Streamer formation occurs for $\langle\beta\rangle > \beta_{crit}$ regardless of whether periodicity is assumed or not, and the effects of heavy particle motion are similar in both cases.

From a practical viewpoint, the most important results are those which can be related to generator performance. It has been shown for the two cases L/H = 0.4 and L/H = 0.64, that streamers have a beneficial influence on plasma conduction. For L/H = 0.2 the reverse is true, and a critical value of L/H must exist. Since the induced fields in a practical generator are proportional to $|\underline{B}|$, and therefore $\langle\beta\rangle$, it is possible, with optimization of L/H that the most useful regime for MHD power production will be at large $\langle\beta\rangle$, in which the plasma is dominated by streamers. That β_{eff} does not increase with $\langle\beta\rangle$ for $\langle\beta\rangle > \beta_{crit}$ would seem to be of no consequence for current conduction in this regime.

For heavy particle velocities as great as 2000 m sec^{-1}, the streamers are smoothed out in these calculations and their beneficial

influence is largely absent. However, the important feature is that electrothermal instabilities need not be a limiting factor in MHD power production.

A detailed comparison of all the results in this Chapter with experiments is not possible. However, certain features repeatedly observed in experiments using simulated segmented electrode generators can be correlated with the above findings.

Golubev et al (1969) observed approximately one-dimensional streamers for $\langle\beta\rangle \approx 5$; the streamers were oriented in the transverse direction and contained a fine structure. Similarly, Zinko et al (1970) reported discharge photographs which showed that streamers occurred, and that they were 'blown' in the flow direction. These authors concluded that the streamers were not electrothermal instabilities because the non-uniformities approximately coincided with the current direction; it has been demonstrated in this thesis, however, that such streaming phenomena are a non-linear feature of the wave-current interaction. Gilpin et al (1969) observed transverse streamers at large magnetic fields, which they termed 'the normal mode of operation' of their apparatus, when the ionization relaxation length became less than the wavelength of the stationary streamers. In the calculations presented here the ionization relaxation length is zero, owing to the assumption of Saha equilibrium. Brederlow et al (1971) observed that for $\beta < 2$, $L/H \ll 1$, a uniform discharge filled their duct; for $\beta > 2$ streamers and striations appeared. They also found that the streamers were of

greater extent in the $\underline{B}$ direction than in the perpendicular planes, and that the streamers contained fine structure. Fluctuation frequencies up to 50 KHz were measured in the plasma. Zauderer (1966) observed streamers at large magnetic fields and also an additional heating along the anode wall.

Although no mention of streamers was made by Brederlow et al (1969), saturation of β_{eff} was observed in the range $3 < \beta < 14$, together with cathode leakage currents. Also, Burger et al (1970) recorded saturation of β_{eff} at large magnetic field strengths, and concluded that this was due to electrothermal instabilities.

Flow velocities for these experiments were of the order of 10^2 m sec^{-1}, except in Zauderer's case for which $v = 10^3$ m sec^{-1}, and L/H varied from approximately 0.5 to 0.1.

The existence of streamers is therefore a well established fact, both experimentally and theoretically. Fine structure in the streamers has not been observed in the calculations, but this is possibly due to the practical limitations imposed on the smallness of the mesh step used.

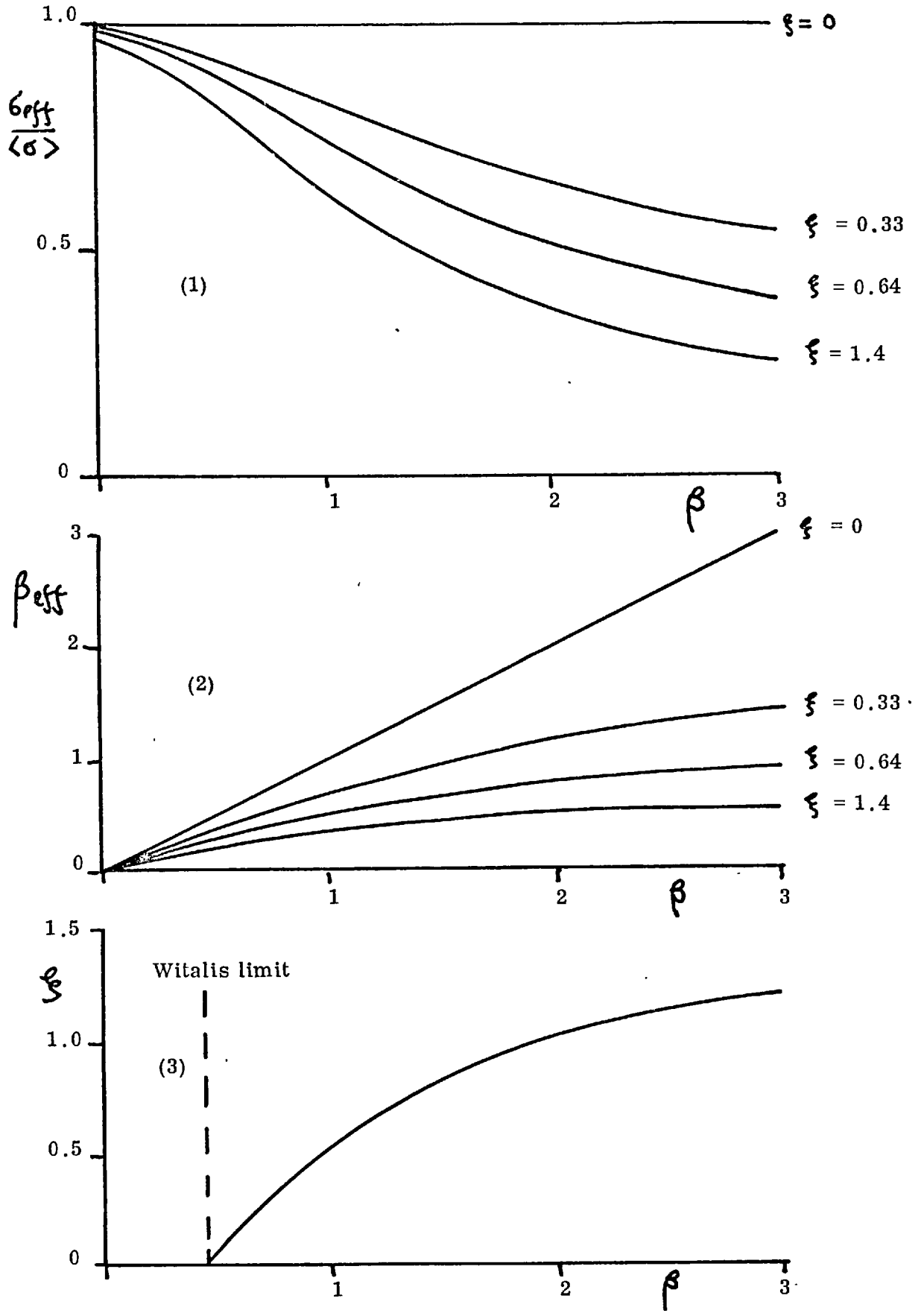

Uniform plasma generator. c/s = 3.7, ξ = L/H.

(1) Figure 7.1: σ_{eff} against β . (2) Figure 7.2: β_{eff} against β .

(3) Figure 7.3: Critical β for electrode leakage against ξ .

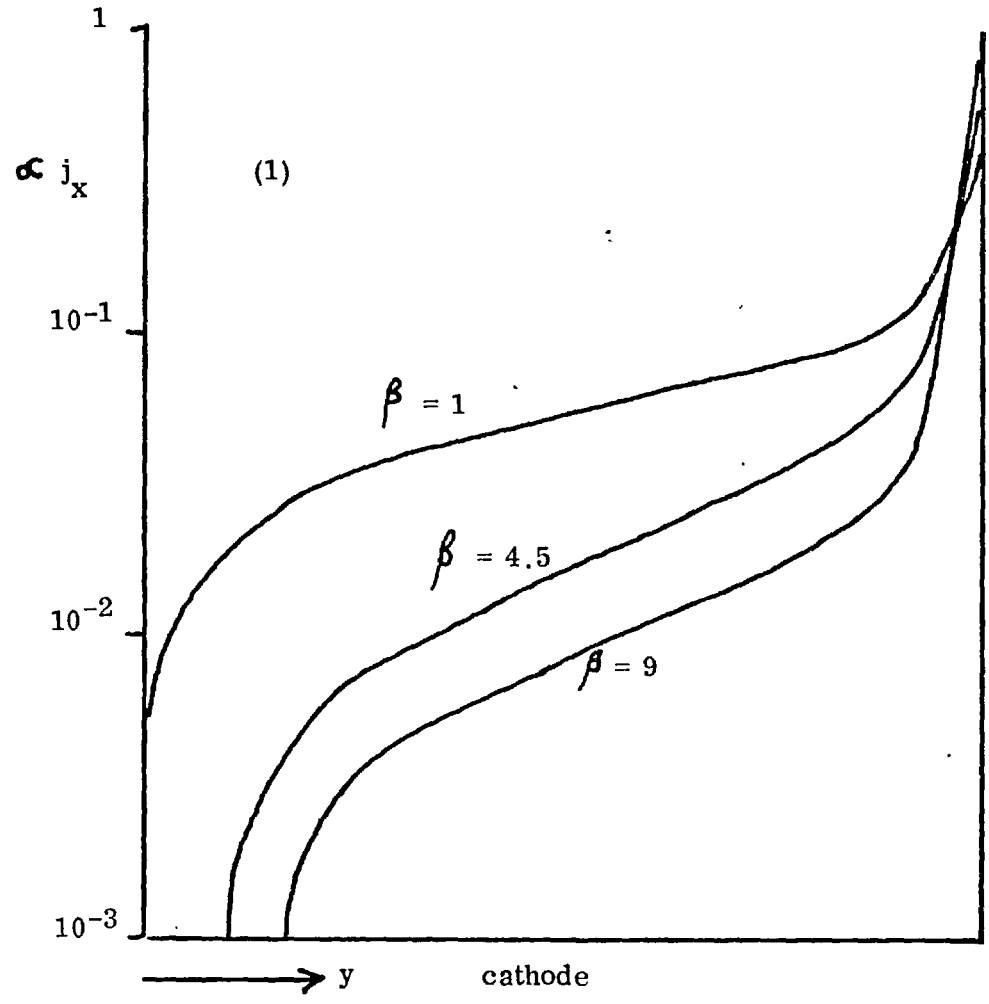

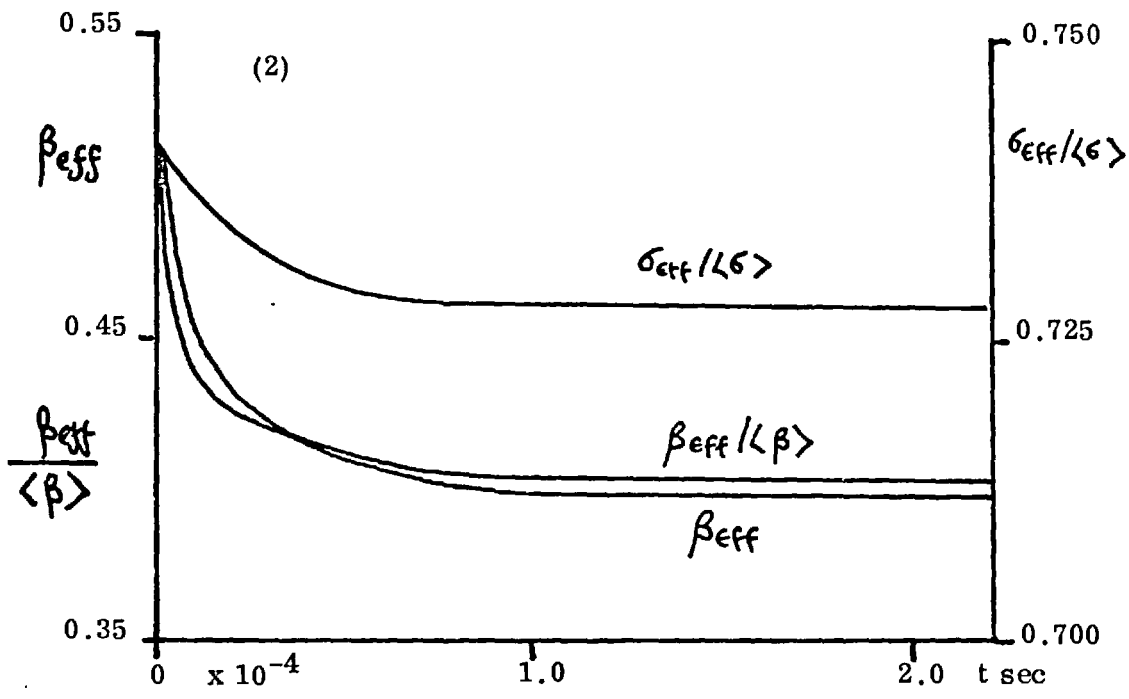

(1) Figure 7.4: j_x on cathode for $\beta = 1.0$, 4.5 and 9.0 for uniform plasma generator.

(2) Figure 7.5: $\sigma_{eff}/\langle\sigma\rangle$, $\beta_{eff}/\langle\beta\rangle$ and β_{eff} against time for $\beta_o = 1.0$.

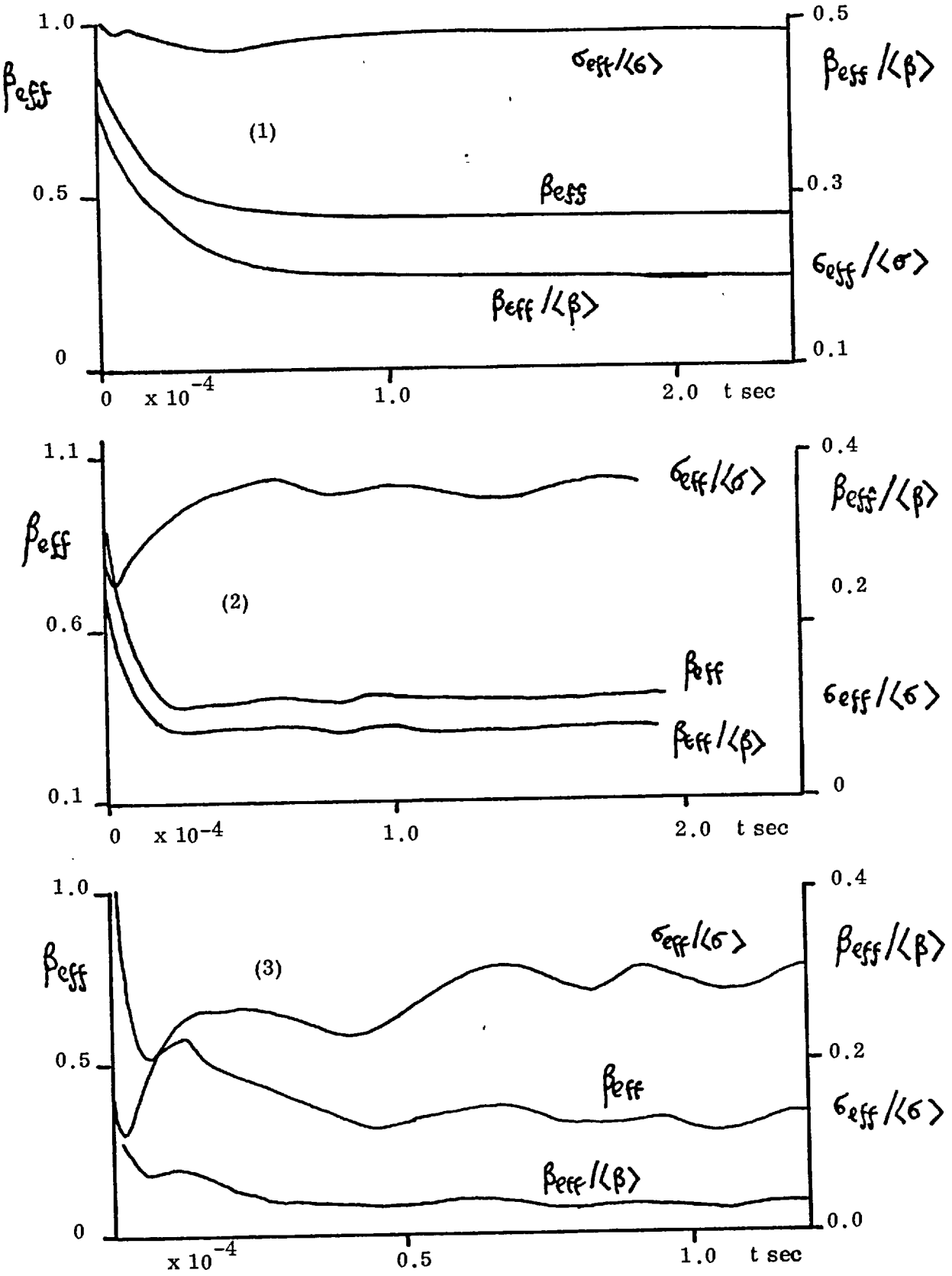

(1) Figure 7.6: $\sigma_{eff}/\langle\sigma\rangle$, $\beta_{eff}/\langle\beta\rangle$ and β_{eff} against time for $\beta_0 = 2.0$

(2) Figure 7.7: as above for $\beta_0 = 4.5$

(3) Figure 7.8: as above for $\beta_0 = 9.0$

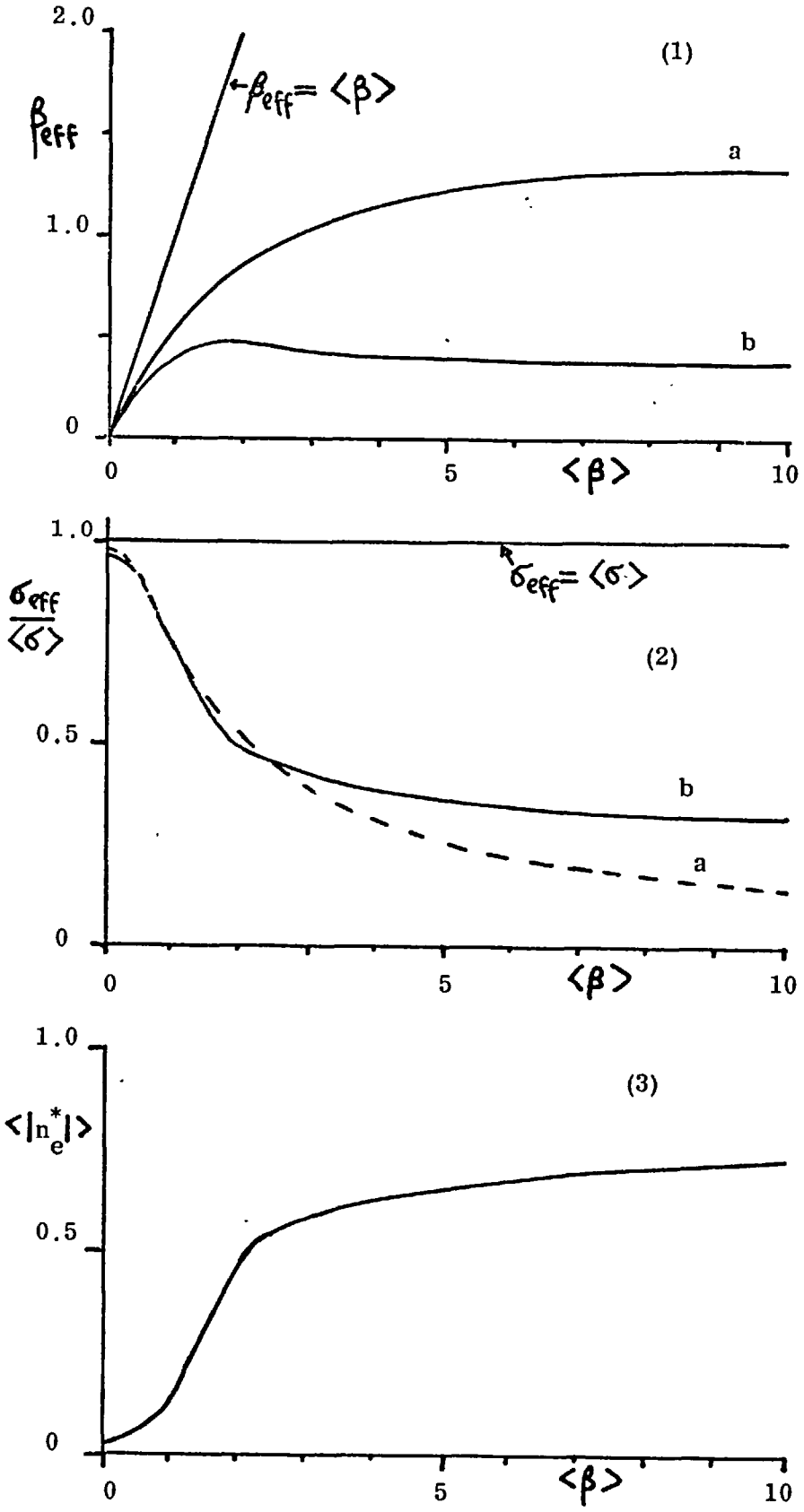

(1) Figure 7.9: β_{eff} against $\langle\beta\rangle$. (a) uniform; (b) non-equilibrium generator

(2) Figure 7.10: $\sigma_{eff}/\langle\sigma\rangle$ against $\langle\beta\rangle$. (a) uniform; (b) non-equilibrium generator

(3) Figure 7.11: $\langle|n_e^*|\rangle$ against $\langle\beta\rangle$.

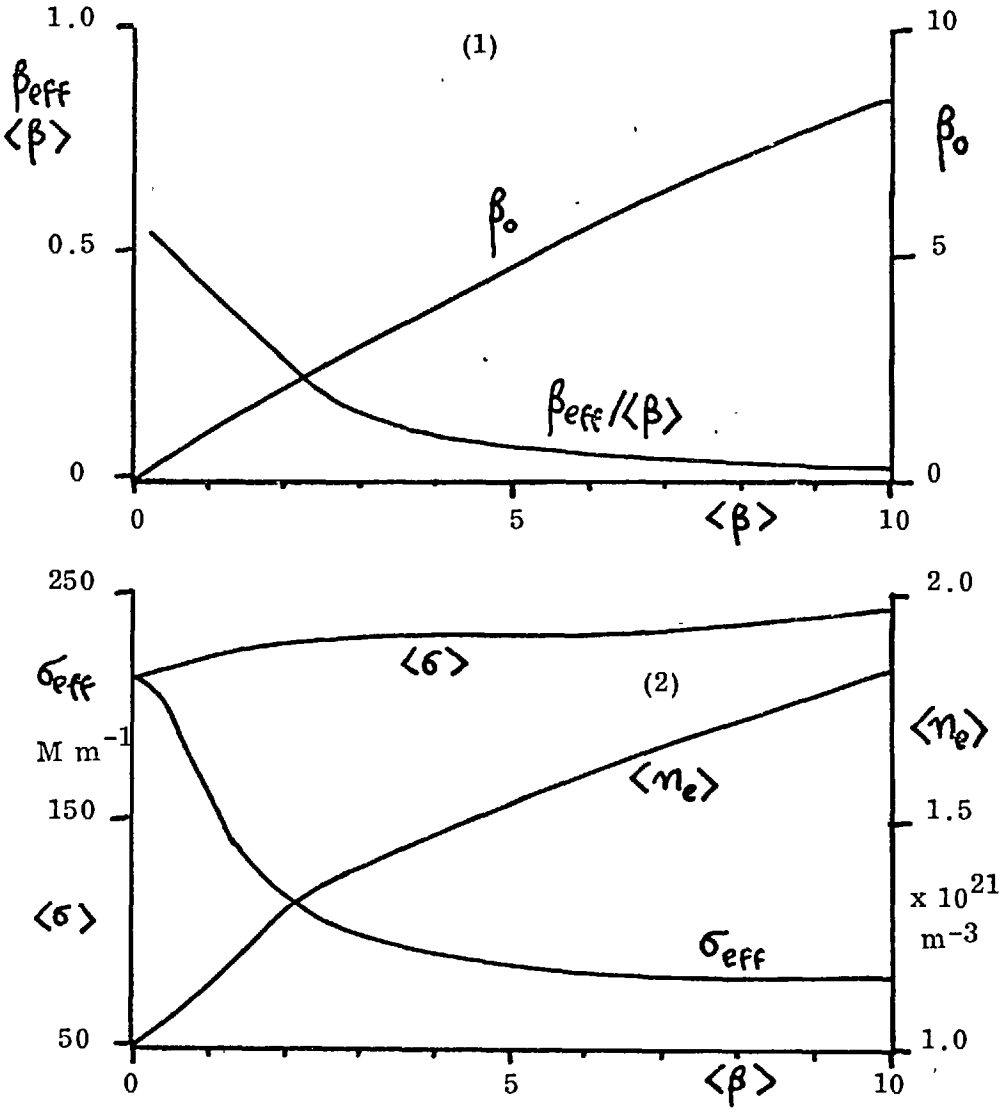

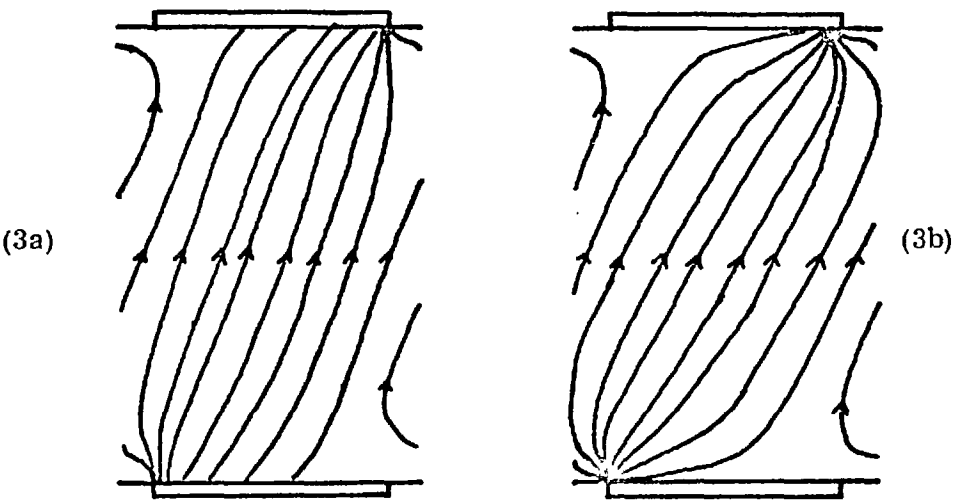

(1) Figure 7.12: β_0 and $\beta_{eff}/\langle\beta\rangle$ against $\langle\beta\rangle$.

(2) Figure 7.13: $\langle\sigma\rangle$, $\langle n_e\rangle$, σ_{eff} against $\langle\beta\rangle$.

(3) Figure 7.14: ψ for the uniform plasma generator, (a) $\beta_0 = 1.0$, (b) $\beta_0 = 9.0$.

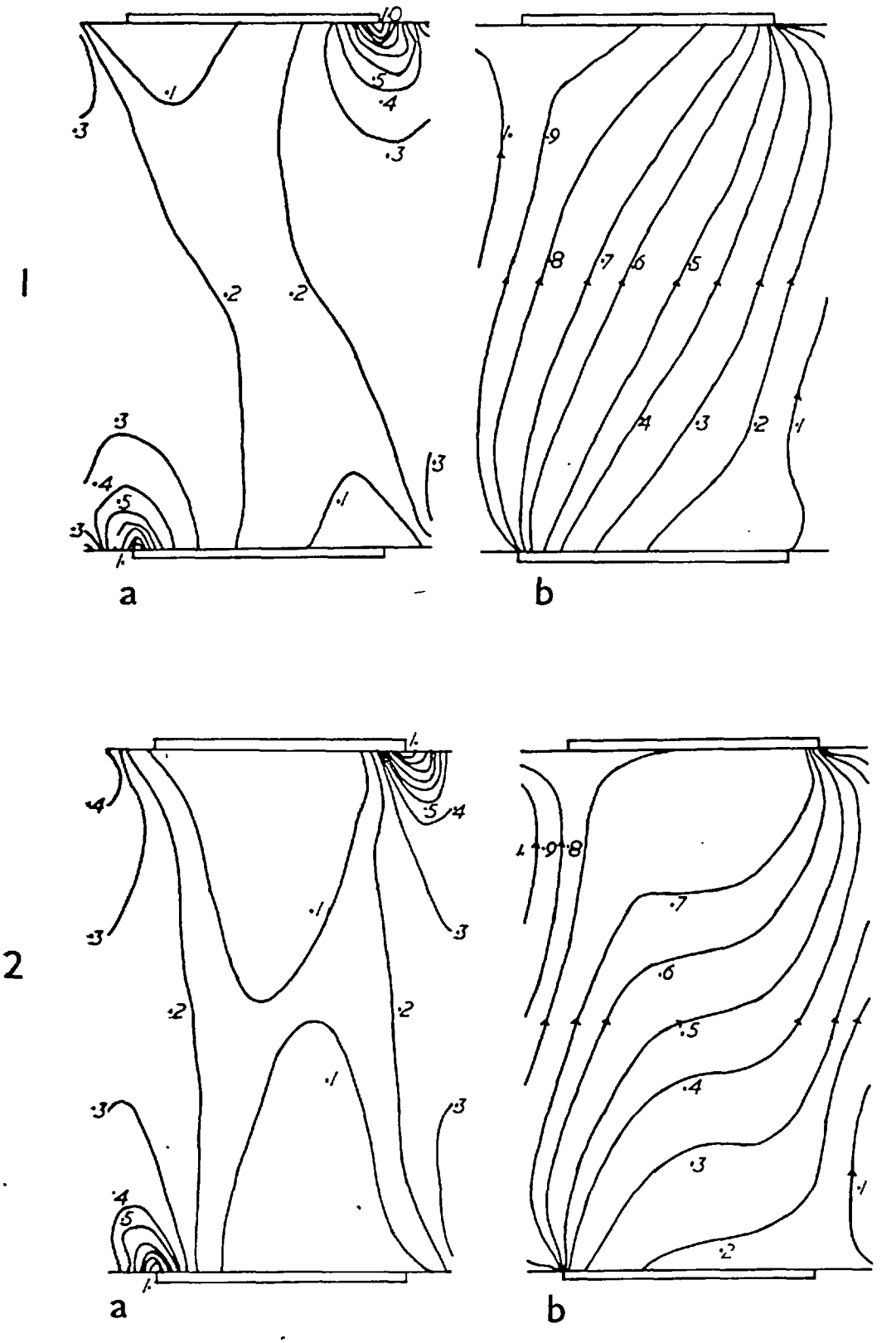

c/s = 3.7, L/H = 0.64, v = 0 steady distributions

(1) Figure 7.15: $\beta_0 = 1$. (a) n_e^*, $n_{e\max}^* = 3.23$, $n_{e\min}^* = -0.85$; (b) current distribution

(2) Figure 7.16: $\beta_0 = 2$. (a) n_e^*, $n_{e\max}^* = 4.03$, $n_{e\min}^* = -0.84$; (b) current distribution

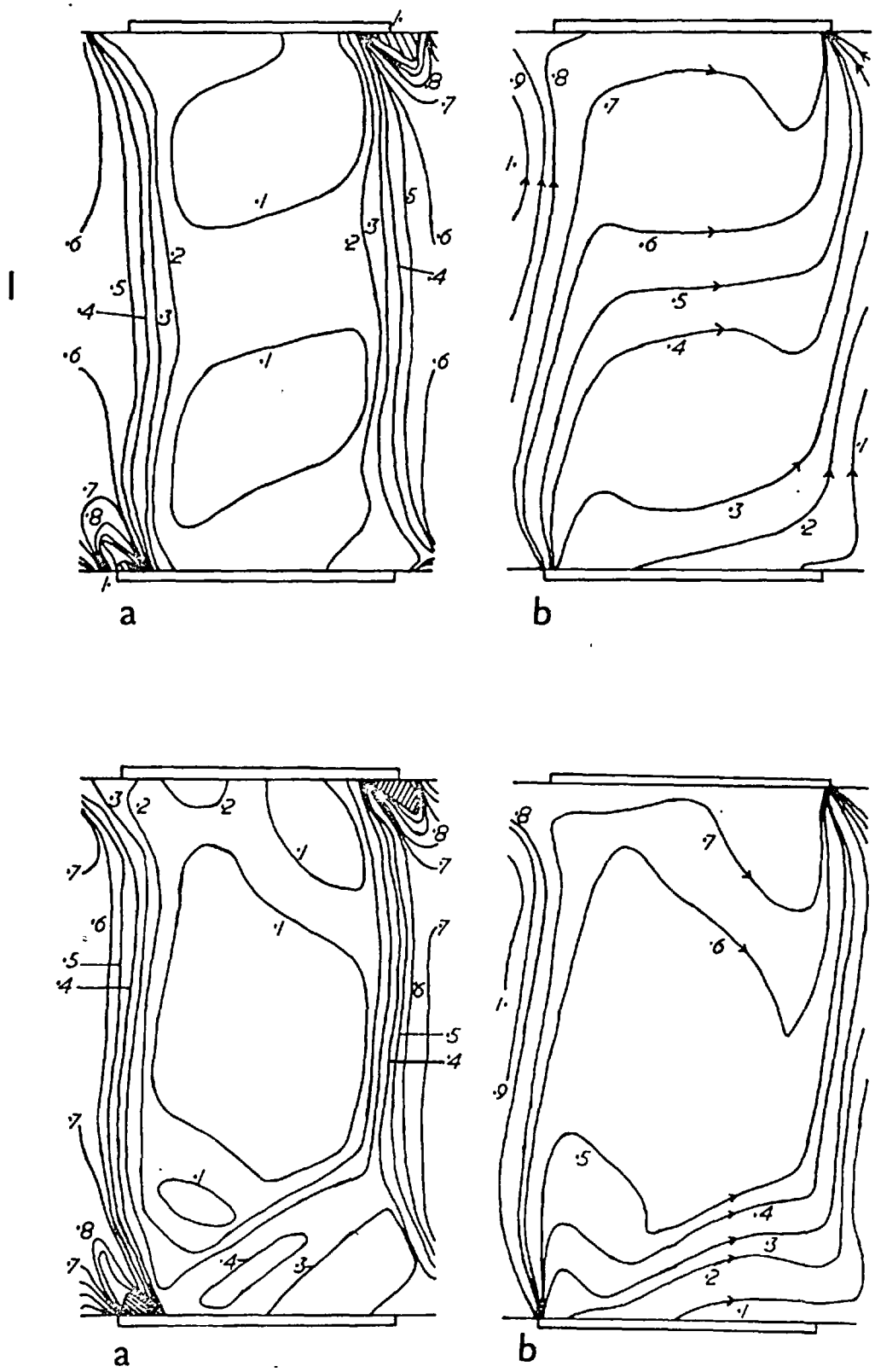

c/s = 3.7, L/H = 0.64, v = 0 steady distributions.

(1) Figure 7.17: $\beta_0 = 3.5$. (a) n_e^*, $n_{e\max}^* = 2.5$, $n_{e\min}^* = -0.88$; (b) current distribution

(2) Figure 7.18: $\beta_0 = 6.5$. (a) n_e^*, $n_{e\max}^* = 2.5$, $n_{e\min}^* = -0.94$; (b) current distribution

1

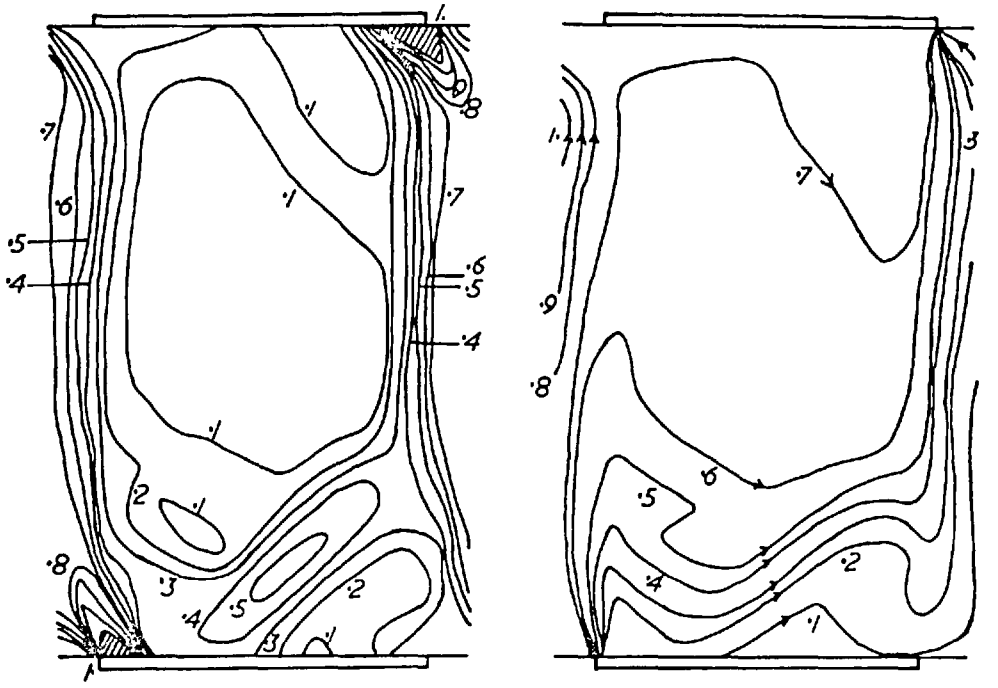

2

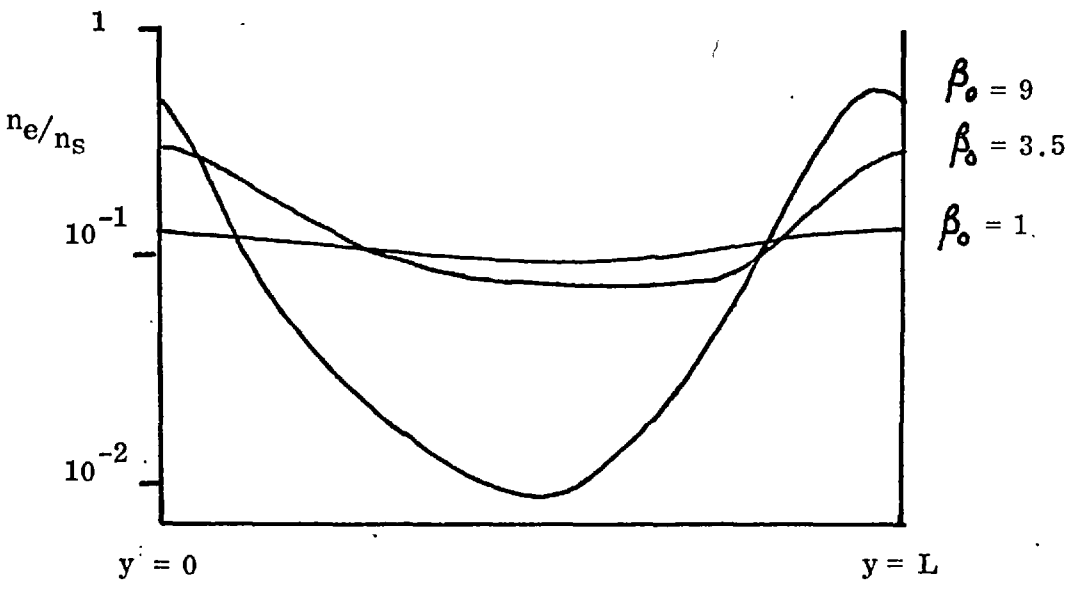

(1) Figure 7.19: c/s = 3.7, L/H = 0.64, v = 0, steady distributions. $\beta_0 = 9$. (a) n_e^*, $n^*_{e\,max} = 2.5$, $n^*_{e\,min} = -0.95$; (b) current distribution.

(2) Figure 7.20: n_e/n_s along x = H/2 for steady distributions at $\beta_0 = 1$, 3.5, 9.

1

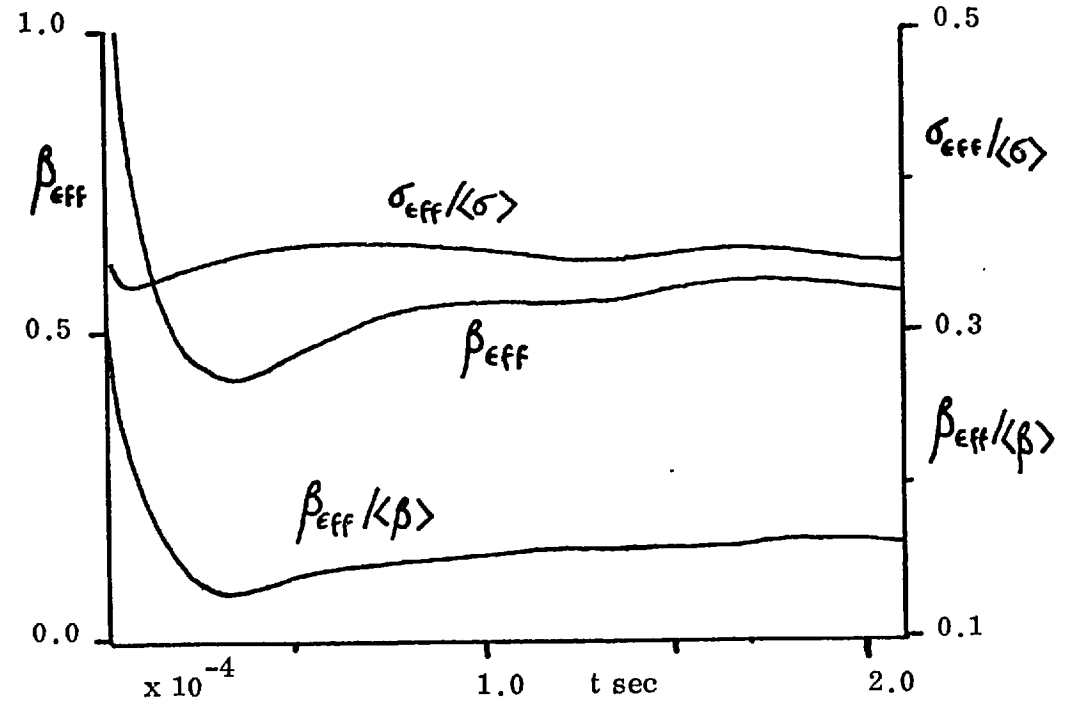

2

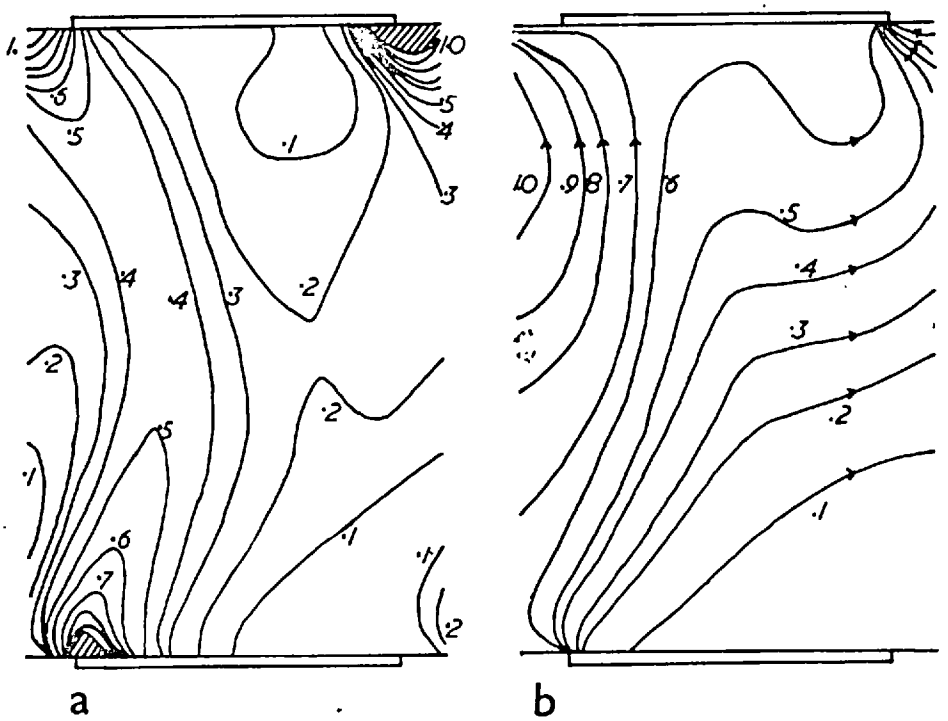

(1) Figure 7.21: averaged parameters against time for v = 170 m sec^{-1}, β_o = 3.5

(2) Figure 7.22: final distributions for above case. (a) n_e^*, $n_{e\,max}^*$ = 2.5, $n_{e\,min}^*$ = - 0.88; (b) current distribution

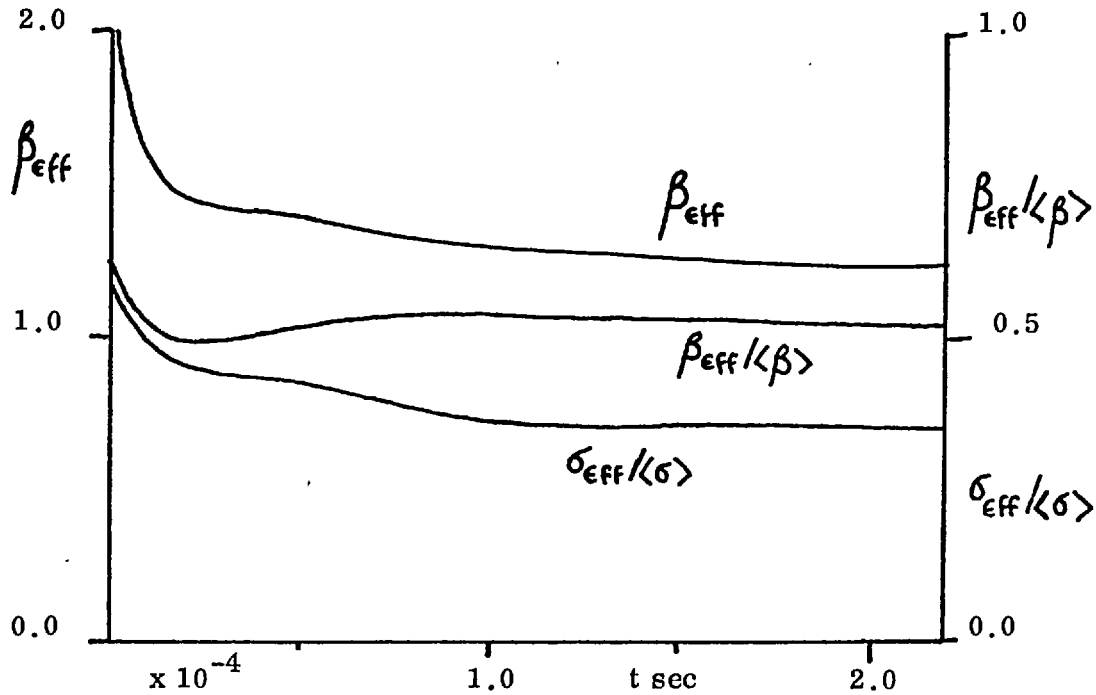

c/s = 1.7, L/H = 0.2, v = 0, β_o = 3.5

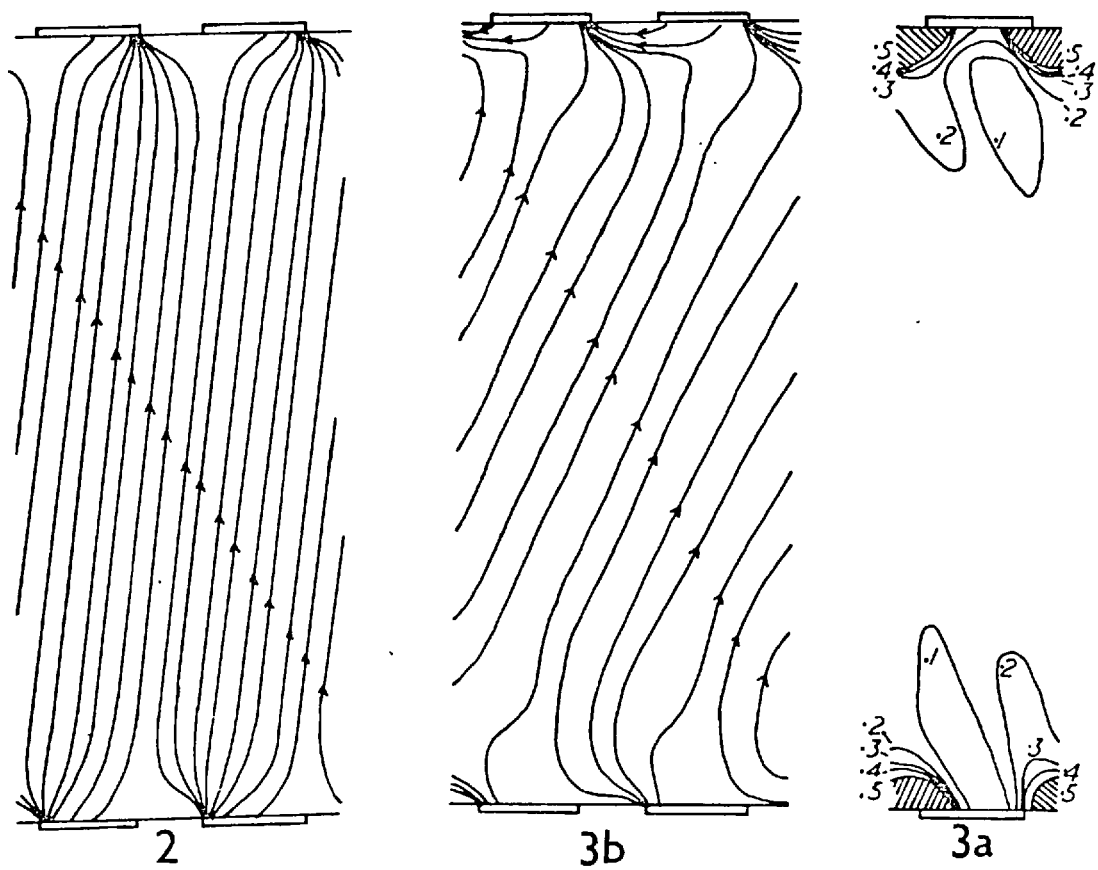

(1) Figure 7.23: averaged parameters against time, v = 0, β_o = 3.5

(2) Figure 7.24: current distribution ψ at t = 0

(3) Figure 7.25: distributions at t = 2 x 10^{-5} sec. (a) n_e^*, $n^*_{e\,max}$ = 2.5, $n^*_{e\,min}$ = - 0.54. (b) ψ .

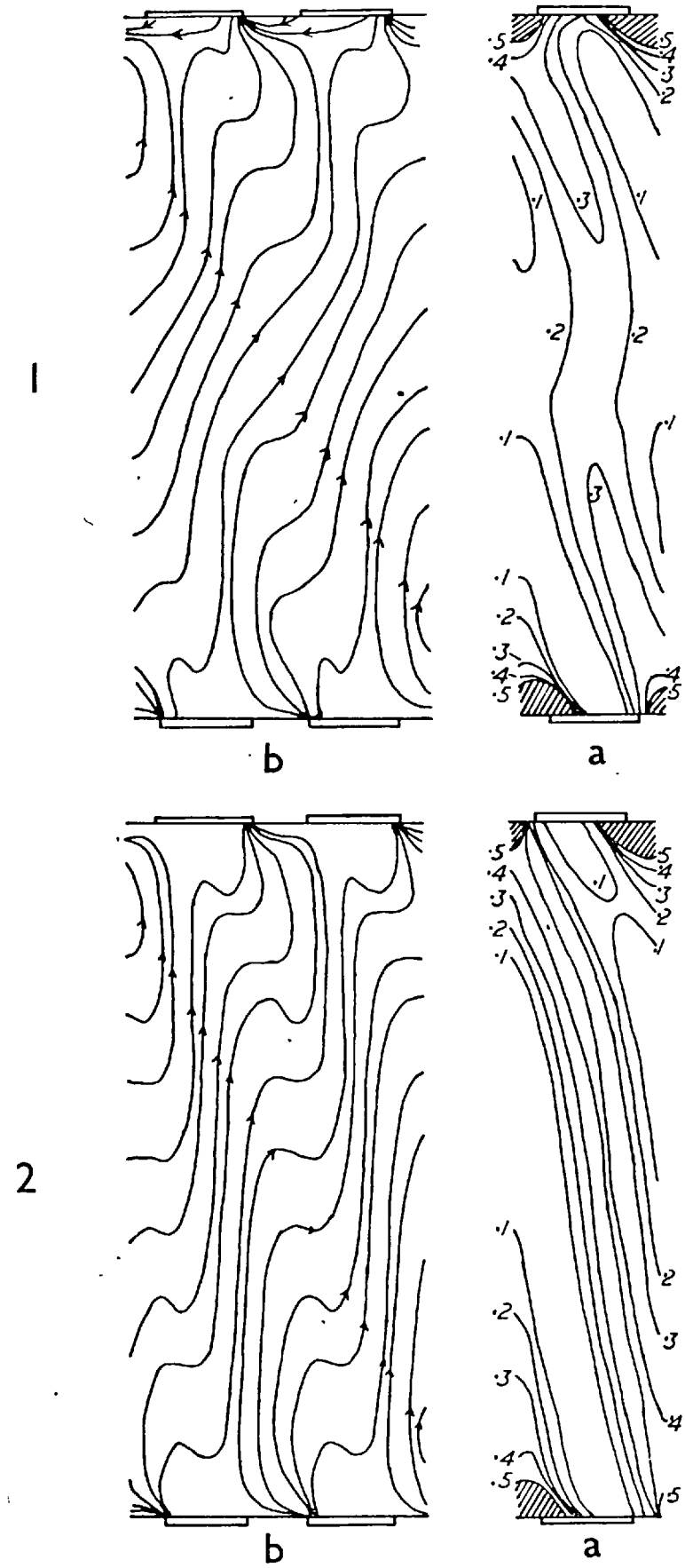

(1) Figure 7.26: Distributions at $t = 5 \times 10^{-5}$ sec. (a) n_e^*, $n_{e\,max}^* = 2.5$, $n_{e\,min}^* = -0.62$. (b) ψ .

(2) Figure 7.27: Distributions at $t = 1.5 \times 10^{-4}$ sec. (a) n_e^*, $n_{e\,max}^* = 2.5$, $n_{e\,min}^* = -0.66$; (b) ψ .

1

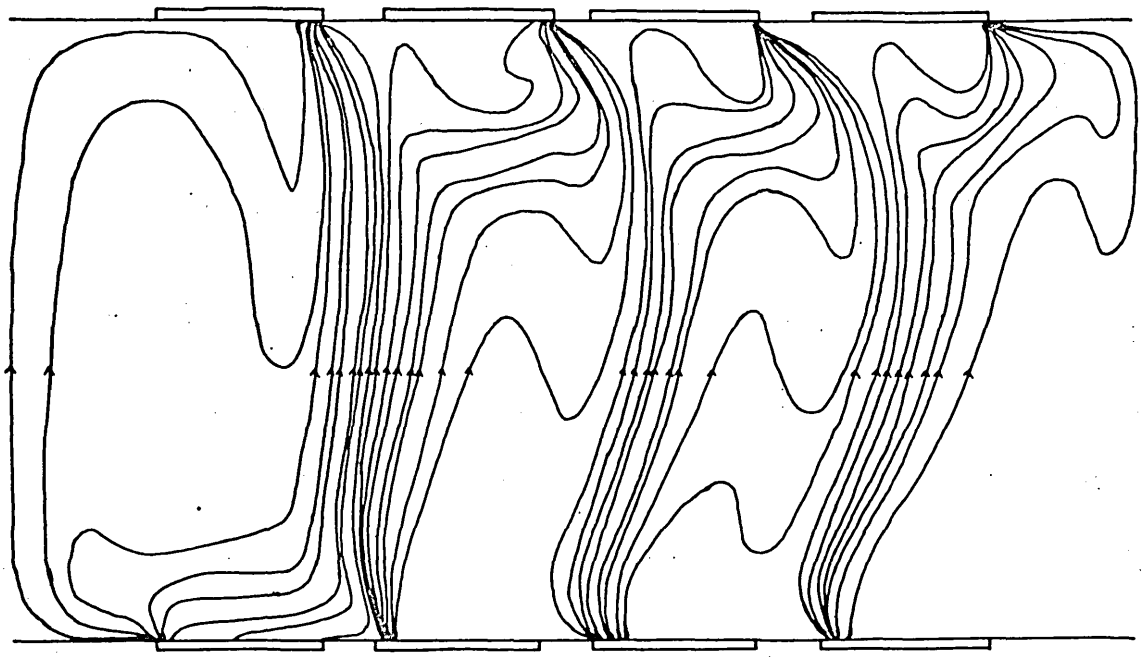

2

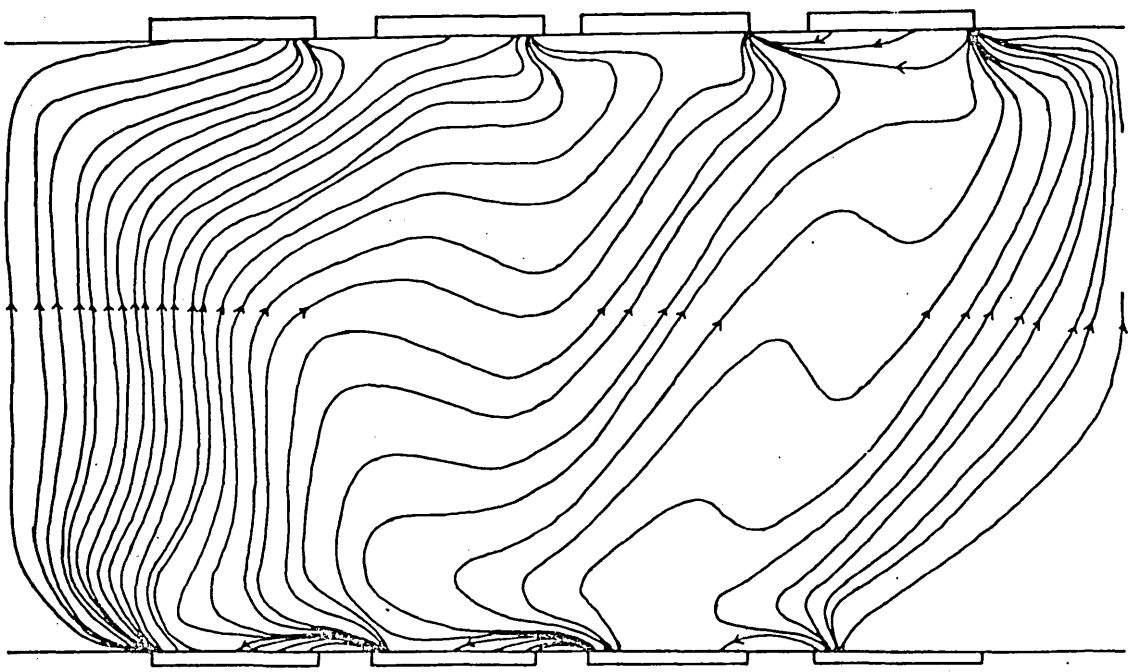

Multisegment systems. H = 5 cm, W = 10 cm, L = 9.7 cm, $\beta_0 = 9$.

(1) Figure 7.28: current distribution at $t = 5 \times 10^{-5}$ sec, $v = 170$ m sec^{-1}

(2) Figure 7.29: as above for $v = 2000$ m sec^{-1}.

SUMMARY

This summary is a brief re-statement of the most important results obtained from this work.

A numerical simulation of the basic theoretical model of the electrothermal system is capable of reproducing the main features observed in experiments involving highly magnetized, partially ionized plasmas. Quantitative data for electrothermal instabilities, their amplitudes, structure and motion, is in accord with experiment.

The maximum value of the Hall parameter used in the work is 10. The main restriction on the magnitude of the Hall parameter is the slower convergence rate for the current distribution at large Hall parameter.

An investigation of the effects on instability growth of increasing the plasma to load resistance ratio, R_p/R_L, maintaining the same degree of non-equilibrium ionization, for the insulator walls configuration shows that the amplitudes of the instability, and its effect on the plasma is not significantly altered by increasing R_p/R_L from zero to unity.

The behaviour of plasma in a segmented electrode duct is of great interest in MHD power generation research. It has been shown here that this behaviour depends on the stability of the plasma to electrothermal instabilities, and the ratio of segmentation length to electrode pair separation L/H.

In the stable regime a relatively uniform conduction mode is possible, the main non-uniformities existing near the boundaries. In particular, for L/H much less than unity the main segmentation non-uniformities are restricted to boundary layers of depth roughly L.

In the unstable regime the current flow is dominated by the presence of streamers, which are approximately one-dimensional. With heavy particle motion the streamers 'bend' downstream and become diffuse. These conclusions are independent of whether or not the assumption of periodicity over a segmentation length is made.

For L/H of order unity the streamers have a beneficial influence on current conduction; ie: the non-equilibrium generator possesses a lower internal resistance than the uniform open cycle generator for the same average conductivity, Hall parameter and duct dimensions. For L/H much less than unity the reverse is true. However, in this case it seems likely that the instability can be removed using the method suggested in Chapter IV.

Since the conduction properties of the non-equilibrium generator deviate further from those of the uniform generator as the magnetic field is increased, and because the induced electric fields are proportional to the magnetic field, with careful choice of L/H the presence of streamers may turn out to be of benefit to MHD power production. In this regime the performance of an experimental configuration should be discussed in terms of the internal resistance of the device, rather than the magnitude of the effective Hall parameter which tends to saturate with increasing magnetic field.

For heavy particle velocities as great as 2000 m sec^{-1} the numerical model predicts that the streamers are largely smoothed out. However, the important result is the suggestion that electrothermal instabilities, streamers,need not be a limiting factor in MHD power production.

A Note on Nomenclature

Standard MHD plasma physics notation has been used throughout this thesis. The partially ionized nature of the fluid introduces the quantity $I_p = k_B T_p$, the ionization energy of the seed. The elastic collision losses have been denoted by L, which has also been used to denote duct length. This should not cause confusion except possibly on page 150, in which elastic collision losses and segmentation length appear on the right and left hand side respectively of the energy balance equation. Boltzmann's constant, instability wavenumber and thermal conductivity are denoted by k_B, k and k_e.

REFERENCES

Ames W F, 1969, 'Numerical Methods for Partial Differential Equations' (Nelson)

Arakawa A, 1966, J Comp Phys 1, 119-143

Arakawa A, 1970, Proc Symp in App Maths (1968), Am Maths Soc

Argyropoulos G S, Demetriades S T, Kendig A P, 1967, Proc AIAA Conf on Elec Propulsion and Plasma-dynamics, Colorado

Argyropoulos G S, Casteel M A, Demetriades S T, 1969, 10th Symp MHD

Brederlow G, Zinko H, 1969, Proc 10th Symp Eng Aspects MHD, p 179

Brederlow G, Zinko Z, Witte K-J, 1971, Proc 5th Int Conf on MHD Elec Power Generation, Munich, 223-225

Brogan T R, 1968, Adv in Plasma Phys, Vol 1, pp 227-331, (Ed: A Simon, W B Thompson, Interscience Publishers)

Burger J, Brederlow G, 1970, Proc 11th Symp Eng Aspects MHD

Celinski Z N, Fischer F W, 1966, AIAA J, Vol 4, 3, 421

Cool T A, Zukoski E E, 1968, Phys of Fluids, Vol 9, 4, 780-796

Courant R, Hilbert D, 1962, 'Methods of Mathematical Physics', Vol 2, (Interscience Publishers)

Crown J C, 1961, Report R-1852-2, United Aircraft Corp, Research Labs, East Hartford, Conn, AD No: 294697

De Groot S R, Mazur P, 1963, 'Non-Equilibrium Thermodynamics' (North-Holland Publishing Co, Amsterdam)

Dodel G, 1970, Plasma Phys, Vol 12, 273-292

Evans R M, Louis J F, Mitchner M, Kruger C H, 1970, Proc 11th Symp Eng Aspects MHD, p 190

Fischer F W, 1966, Proc Symp Elec from MHD, Salzburg, 197-205

Gilpin R R, Zukoski E E, 1969, AIAA J, Vol 7 , 8, 1438

Golubev V S, Malikov M M, Nedospasov A V, 1969, Proc 10th Symp Eng Aspects MHD, 177-178

Haines M G, 1967, Phil Trans Roy Soc London A, vol 261, 440-454

Haines M G, McNab I, 1968, AIAA J, vol 6, 9, 1679-1684

Hinnov E, Hirschberg J G, 1962, Phys Rev 3, 795-801

Hiramoto T, 1970, Phys Fluids, vol 13, 6, 1492

Hoffman M A, 1968, AIAA J, vol 6, 9, 1667-1673

Hurwitz H, Kilb R W, 1961, J Ap Phys, vol 32, 2, 205-216

Karlovitz B, Halasz D, 1962, Proc 3rd Symp Eng Aspects MHD (N Mather, G Sutton - editors; Gordon & Breach, New York)

Kerrebrock J L, 1964, AIAA J, vol 2, 6, 1072-1087

Kerrebrock J L, 1966, AIAA J, vol 4, 11, 1938-1947

Kerrebrock J L, Dethlefsen R, 1968, AIAA J, vol 6, 11, 2115

Kim C S, 1969, UTIAS Technical Note No: 143

Kolb G, 1971, Proc 5th Int Conf on MHD Elec Power Generation, 175-190

Lengyel L L, 1969, Energy Conversion, vol 9, 13-23

Lengyel L L, 1970, Proc 11th Symp Eng Aspects MHD, p 193

Lengyel L L, 1971, Proc 5th Int Conf on MHD Elec Power Generation, 207-223

Lengyel L L, 1971, AIAA J, vol 9, 4, 745-747

Lilly D K, 1965, Monthly Weather Review , vol 93, 1, 11-26

Lutz M A, 1967, AIAA J vol 5, 8, 1416

Nedospasov A V 1968, 'Striations', Soviet Physics Uspekhi, vol 11, 2, 174-185

Nelson A H, 1969, PhD Thesis, University of London

Nelson A H, 1971, Energy Conversion, vol 11, 11-15

Nelson A H , Haines M G, 1969, Plasma Phys, vol 11, 811-837

Oliver D A, Mitchner M, 1967, AIAA J, vol 5, 8, 1424

Ovcharienko V, 1969, High Temperature Institute, Moscow, private communication

Richtmyer R D, Morton K W, 1967, 'Difference Methods for Initial Value Problems' (Interscience, Wiley, New York)

Riedmüller W, 1968, Proc Symp Elec from MHD, vol 1, p 519

Riedmüller W, 1970, Proc 11th Symp Eng Aspects MHD, p 199

Roberts K V, Potter D E, 1970, Methods in Computational Physics, vol 9, (ed: B Alder, S Fernbach, M Rotenberg; Academic Press)

Rosa R J, 1962, Phys Fluids 5, 1081

Shipuk I, Pashkin S, 1968, 'Plasma Ionization Instability in Crossed Fields' (Soviet Physics-Doklady), vol 12, No: 10, pp 959-961

Smith M G, 1967, 'Introduction to the Theory of Partial Differential Equations' (D Van Nostrand Co Ltd, London)

Solbes A 1968, Proc Symp Elec from MHD, vol 1, p 499

Spitzer L, 1961, 'Physics of Fully Ionized Gases', 2nd edition (Interscience)

Velikhov E P, Degterev L M, Samarskii A A, Favorskii A P, 1969 Proc 10th Symp Eng Aspects MHD

Velikhov E P, Degtyarev L M, Favorskii A P, 1971, Proc 5th Int Conf on MHD Elec Power Generation, 307-324

Witalis E A, 1965, Plasma Physics (J Nucl En, part C), vol 7, 235-244

Young J A, 1968, Monthly Weather Review, vol 96, 6, 357-364.

Zampaglione V, 1972, Plasma Phys (to be published)

Zauderer B, 1966, Proc Symp Elec from MHD, vol II, 597-611

Zauderer B, 1968, AIAA J, vol 6, 4, 701-707

Zinko H, Brederlow G, 1970, Proc 11th Symp Eng Aspects MHD, p 90